6. RESULTS AND DISCUSSION

6.1 SMEDDS

SMEDDS are very well reported in literature as a drug delivery system used for enhancement of solubility of lipophilic drugs. Self-emulsifying preconcentrate is made of oil, surfactant, co-surfactant and drug. Surfactant and cosurfactant get preferentially adsorbed at the interface, reducing the interfacial energy and provides mechanical barrier against coalescence. The decrease in the free energy required for emulsification consequently improves the thermodynamic stability of the microemulsion formulation [1]. On dispersion in water it forms <100 nm sized droplets. Based on characteristics of oil, it is directly disseminated to the systemic circulation or absorbed via the lymphatic pathway. Oil-surfactant-cosurfactant driven very high solubility, nano-size and permeability results in significant rise in bioavailability. The spontaneous formation of nanosized emulsion droplets generates enormously high surface area for drug to diffuse in the lumen and get absorbed rapidly [2].

6.2 ILO SMEDDS – Formulation development

ILO, being a BCS class II drug, has solubility issues. Getting water insoluble APIs into solution to promote improved absorption for the intended therapy is a challenge for the formulator. SMEDDS is a lipid based drug delivery system used to improve solubility of such drugs.

6.2.1 Solubility Study

The core part of emulsion is composed of oil, in which the drug is solubilized. Hence, it is very much essential to choose the oil having high solubility for drug [3]. Hence, various types of oil were screened including fatty acids, medium chain mono/di/tri glycerides, propylene mono/di glycerides and long chain triglycerides.

Captex 200 (Propylene glycol dicaprylate/dicaprate), Captex 300 (Medium chain triglycerides – Caprylic and capric triglycerides) and Peceol (Glyceryl Monooleate) showed minimal solubility of ILO while other glyceryl derivative of Medium chain triglycerides i.e. Capmul MCM C8 (Glyceryl Caprylate), Isopropyl myristate etc. showed moderate solubility of ILO (Figure 6.1). Oleic acid showed significantly highest solubility of ILO (124.45 ± 9.65 mg/g).

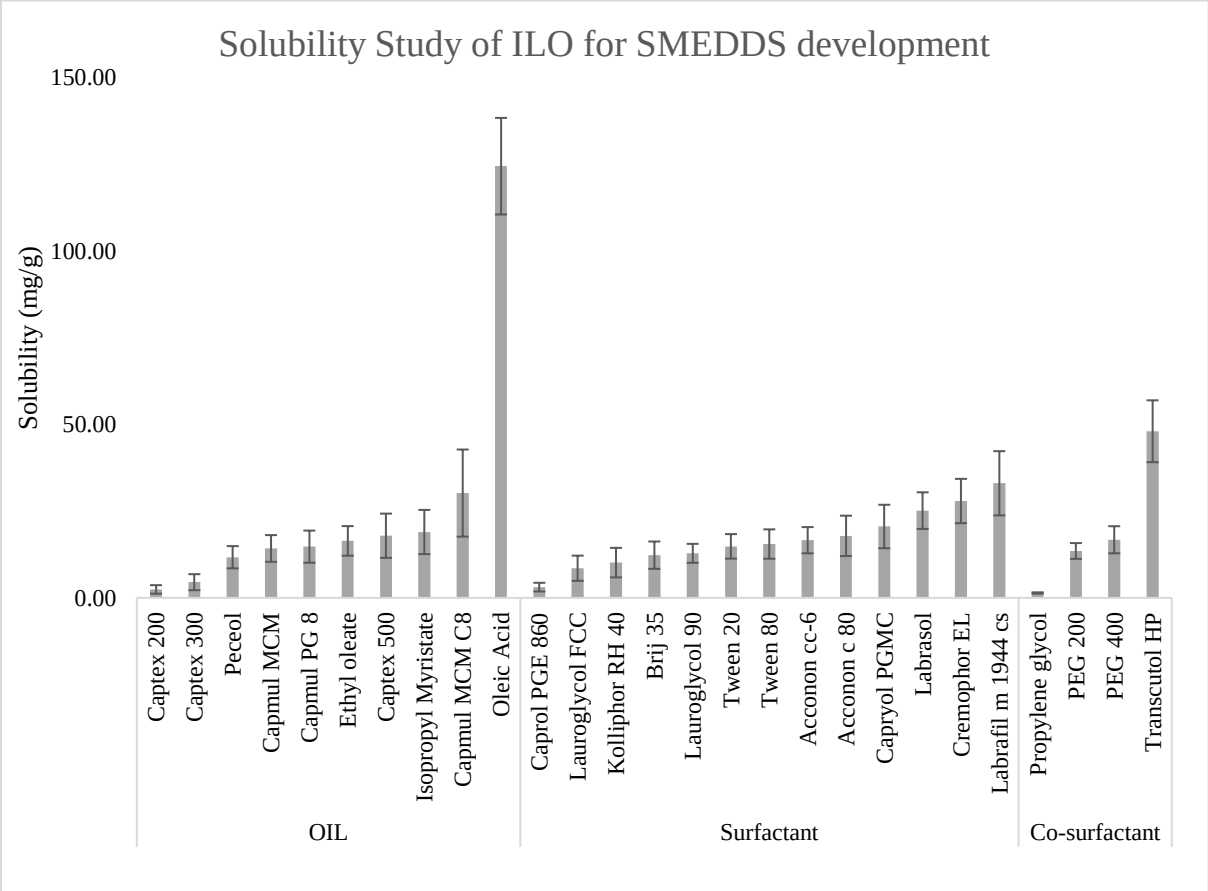

Figure 6.1 Solubility Study of ILO for SMEDDS development

However, upon dilution, the system consisting of oleic acid, surfactant and co-surfactant was opaque in nature. Hence, combination of oils was chosen. For this, Capmul MCM C8 was taken along with oleic acid as it showed the second highest solubility. Herein, we tried different ratio of Capmul MCM C8 and oleic acid to get transparent microemulsion upon dilution. Ratio of Capmul MCM C8 : Oleic acid was varied from 1:1 to 1:3. The ratio of 1:1 and 1:2, when diluted with water up to 100 times, produced transparent microemulsion. Whereas, 1:3 ratio of Capmul MCM C8 : Oleic acid produced opaque emulsion. Hence, 1:3 ratio was not used.

Further, in **1:2** ratio of **Capmul MCM C8: Oleic acid**, amount of oleic acid was more. As the solubility of ILO is more in oleic acid, internal oil ratio of 1:2 was used.

6.2.2 Screening of surfactant

Selection of suitable surfactant is very crucial part for SMEDDS development especially when translucent nanosized emulsion is required [4]. Surfactant was selected on the basis of two criterions: saturation solubility of ILO and its micro-emulsification efficiency for ILO+Capmul MCM C8+Oleic acid (drug+oil).

Amongst available surfactants, only non-ionic surfactants were used for screening due to their non-toxic nature [5]. Different non-ionic surfactants (polysorbates, PEG fatty acid ester, polyoxyethylene surfactants) were screened for solubility of ILO (Figure 6.1). Negligible solubility was found in Caprol PGE 860 (mono/diester of oleic acid and glycerin polymer of ten units), Lauroglycol FCC (propylene glycol monolaureate), Kolliphor RH 40 (polyoxyl 40 hydrogenated castor oil) and Brij 35 (polyoxyethlene surfactant). Polysorbate series of surfactants (Tween 20 and Tween 80) showed comparative higher solubility. Whereas, there was significant increase solubility in coconut oil derived surfactants (Acconon CC-6 (glyceride derivative) and Acconon C 80 (polyoxyethylene 30 derivative)). Highest solubility was observed in Labrasol (Caprylocaproyl macrogol-8 glycerides), Cremophor EL (polyoxyl 35 hydrogenated castor oil) and Labrafil m 1944 CS (Oleyl macrogol-6 glycerides).

From the solubility pattern in various surfactants, it was found that compared to glycerin or propylene glycol derivatives, ILO was more soluble in macrogol (PEG) derivatives (Acconon C 80 > Acconon CC 6). Another contributing factor was chain length of the surfactant molecule. ILO was more soluble in surfactants having longer chain length (Cremophor EL > Acconon C 80). [Chemically, Cremophor is castor oil derivative having major component of ricinoleic acid (C-18) and Acconon is coconut oil derivative having major component of lauric acid (C-12)] Here, saturation does not seem to have played a role as majority of the surfactants are either saturated chains or they have been hydrogenated.

Based on the solubility study, Labrafil M 1944 CS was chosen as the surfactant. However, it did not show proper emulsification as the final system remained hazy upon dilution. Hence, Labrafil M 1944 CS was rejected, despite highest solubility due to its poor micro-emulsification property for ILO+ Oleic acid+ Capmul MCM C8 system (Figure 6.2).

Cremophor EL showed highest %transmittance amongst all surfactants. Hence, **Cremophor EL** was selected as surfactant.

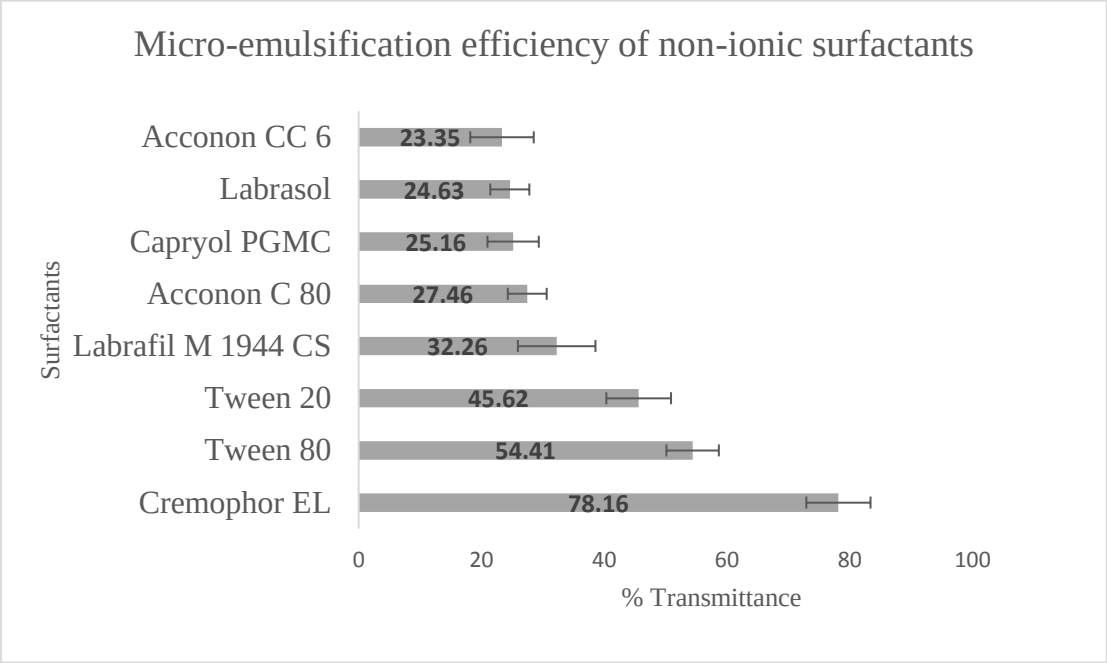

Figure 6.2 Micro-Emulsification efficiency of non-ionic surfactants

6.2.3 Screening of co-surfactant

All the cosurfactants, increased the spontaneity of the micro-emulsion formation (emulsification time decreases) when the formulation was diluted with water [6]. This was owing to alignment of co-surfactant with its hydroxyl group lying between the polar group of surfactant and nearby water molecules and its hydrocarbon groups amongst the apolar chain of surfactant molecule. Thus, co-surfactant molecules reside at the interfacial region between oil and water [7].

Moreover, all the cosurfactants appeared to be equivalent in improving micro-emulsification ability of oil + surfactant mix based on % transmittance data (table 6.1). Hence, appearance upon dilution and emulsification time were taken into consideration [8]. According to this, Transcutol HP (diethylene glycol monoethyl ether) was used as co-surfactant.

Table 6.1 Selection of co-surfactant

Co-surfactant	% Transmittance	Emulsification time (sec)	Appearance
Propylene glycol	89.14 ± 1.92	39 ± 5	Clear system
PEG 200	92.72 ± 2.31	42 ± 4	Clear system
PEG 400	93.82 ± 1.53	45 ± 6	Clear system
Transcutol HP	96.24 ± 2.40	38 ± 4	Clear system

6.2.4 Pseudo Ternary Phase Diagrams

After screening of oil, based on its solubilization capacity of the drug; surfactant and co-surfactant were screened based on emulsification efficiency measured in terms of %Transmittance. Capmul MCM C8 : Oleic acid (1:2) were selected as oil phase and Cremophor EL and Transcutol HP were selected as surfactant and co-surfactant respectively. Pseudo-ternary phase diagrams were constructed using different proportions of oil to surfactant/co-surfactant ratio (Smix) at room temperature [9]. For the given weight ratio, the total of oil, Smix and water always added to 100%. The weight ratio of oil: Smix was varied from 1:9 to 9:1. Internal ratio of Smix (Surfactant:Co-surfactant) was varied from 1:1 to 3:1. 200 mg of each weight ratio was titrated slowly with distilled water to allow equilibrium to produce fine emulsion.

As seen from the ternary plots (Figure 6.3), 3:1 Smix ratio gave highest microemulsion region. (The filled region of Pseudoternary diagram is considered as the area of microemulsion formation [9].) Hence, 3:1 ratio of Smix was considered for further optimization.

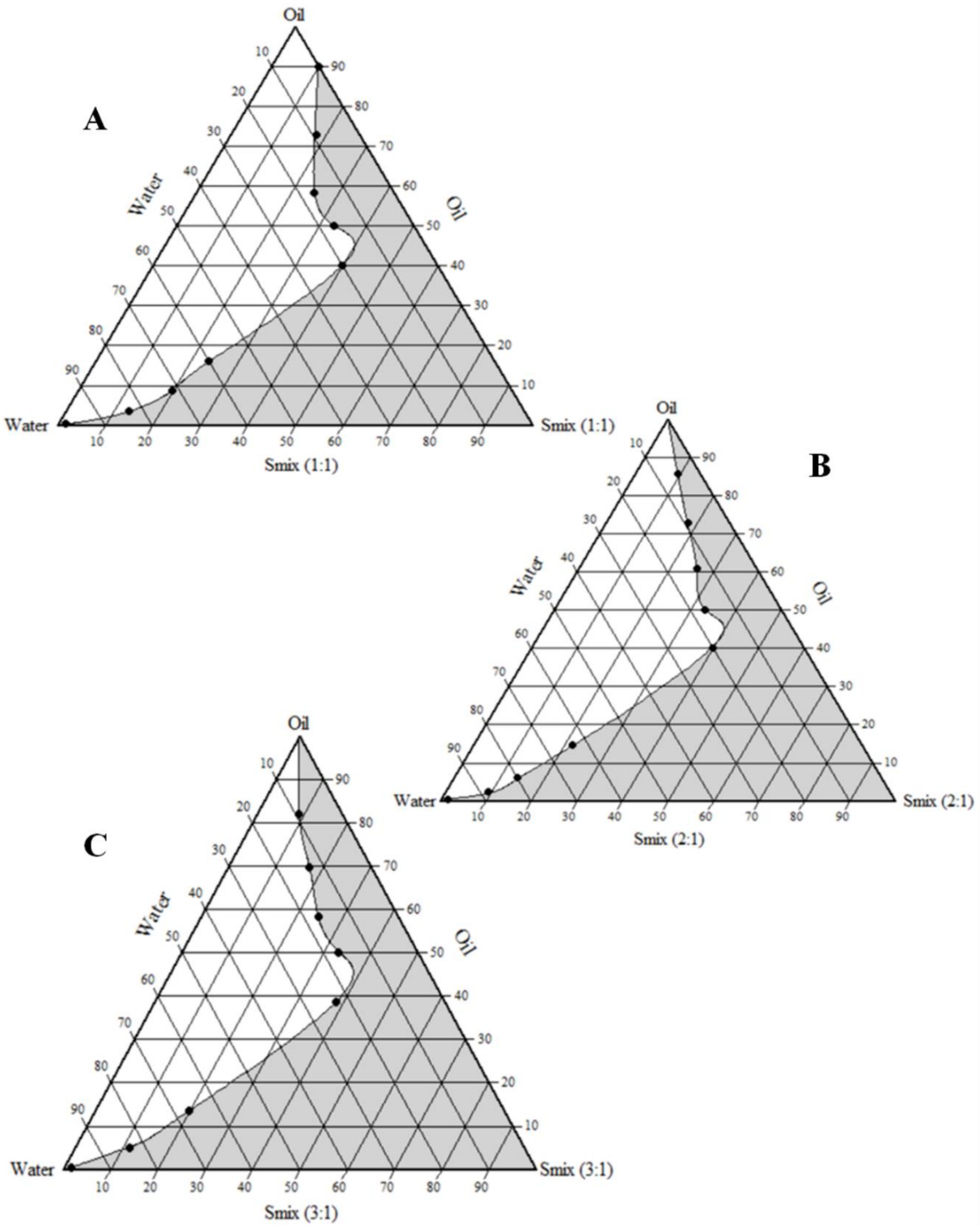

Figure 6. 3 Pseudo-ternary phase diagram for ILO SMEDDS for oil (1:2 Capmul MCM C8: Oleic Acid) + Smix (Cremophor EL + Transcutol HP) titrated against water
A: For Smix 1:1 Ratio, B: For Smix 2:1 Ratio and C: For Smix 3:1 Ratio

6.3 ILO SMEDDS – Formulation optimization

6.3.1 Batch preparation as per I-optimal design

In this computer generated I-optimal design, 16 batches were prepared as generated by design expert 10.0.0 software. Being a mixture design, the total of the mixture was 100% i.e. the fractions of each component A, B and C summed up to 1 in the final formulation. The response in terms of size (nm) has been given in table 6.2.

Table 6.2 Three Component I-optimal design for optimization of ILO SMEDDS

Run	Space type	Component A Oil (mg)	Component B Surfactant (mg)	Component C Co-surfactant (mg)	Response Size (nm) ± SD
1	Interior	11.0322	62.1051	26.8627	118.70 ± 4.12
2	Edge	13.725	56	30.275	194.30 ± 3.93
3	Edge	8	64.707	27.293	24.33 ± 2.14
4	Interior	11.0621	59.6453	29.2926	127.60 ± 3.01
5	Edge	8	62.363	29.637	33.26 ± 4.18
6	Interior	11.0621	59.6453	29.2926	126.50 ± 3.90
7	Vertex	10	65	25	99.91 ± 4.74
8	Vertex	9	56	35	69.09 ± 4.61
9	Interior	10.8247	57.1891	31.9681	133.70 ± 2.56
10	Vertex	14	61	25	174.30 ± 3.63
11	Edge	14	58.3932	27.6068	195.90 ± 4.39
12	Vertex	9	56	35	60.93 ± 5.33
13	Edge	8	59.5448	32.4552	12.34 ± 4.66
14	Vertex	10	65	25	92.95 ± 5.48
15	Interior	11.0621	59.6453	29.2926	124.10 ± 3.53
16	Edge	13.725	56	30.275	194.90 ± 5.37

6.3.2 Analysis of mixture design

The space type of the design matrix was generated by the computer-based mixture design algorithm as shown in table 6.2. For each run, build type was also generated. Build type

indicates whether the run is model point, lack of fit point or replicate point from the generated matrix [10]. The model points are used for estimation of all coefficients, lack of fit points test how well model represents the actual behavior and the replicate points estimate pure error.

The condition number of this matrix was 175.677. This value indicates moderate to strong multicollinearity. i.e. the predicted variable (size) in the multiple regression model (quadratic model) is highly correlated with the predictor variables (Component A, B and C) [11].

Fraction of design space (FDS) graph was generated at process sigma, s = 1 and α risk level of 0.05 as shown in figure 6.4. It displays the area/volume of the design space having a mean standard error less than or equal to a specified value. The ratio of the area/volume to total area/volume is the fraction of design space. This graph as shown in figure 6.4 indicates that 50% of design space had a relative standard error of less than 0.5 suggesting that predictability using this design space is very less [10].

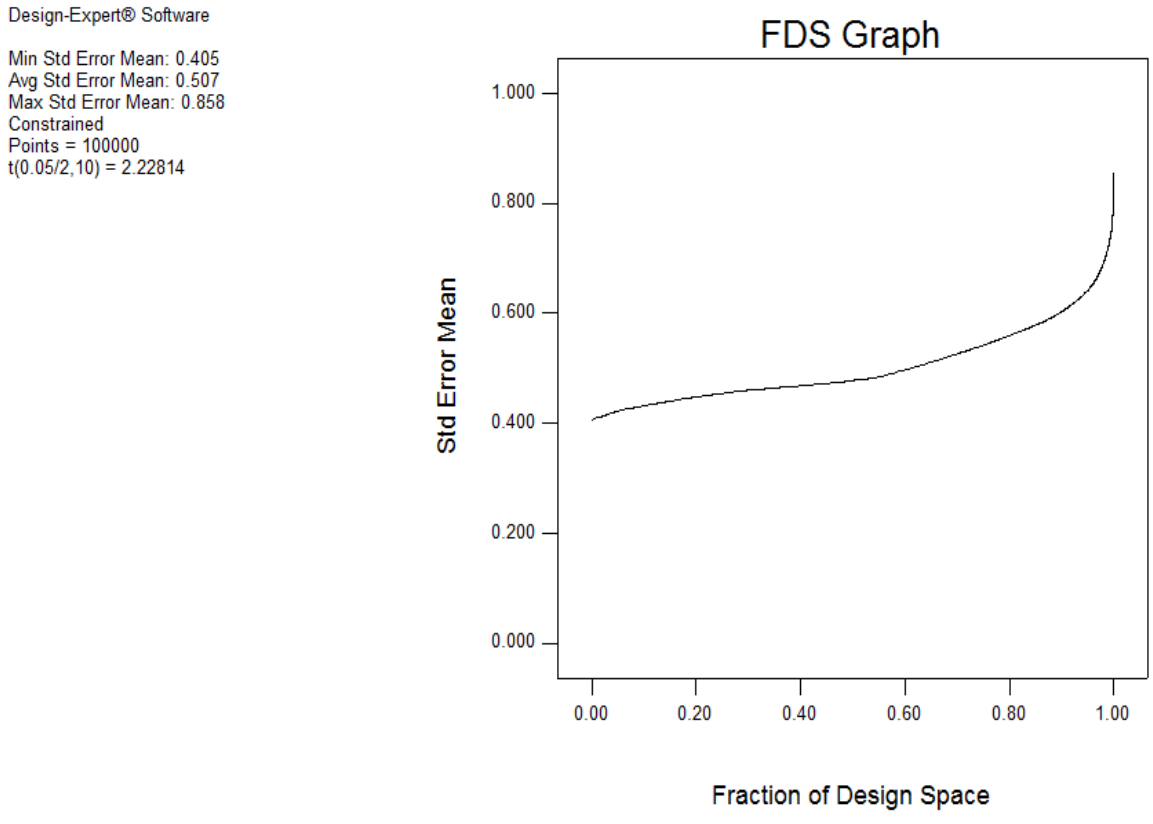

Figure 6.4 Fraction of Design Space (FDS) graph

Based on the statistical analysis of ANOVA, models were generated for interpretation of size from I-optimal design as shown in table 6.3.

Table 6.3 Model selection based on R^2 value for I optimal design

Model	Adjusted R^2 value	Predicted R^2	PRESS value	
Linear	0.9583	0.9422	3144.85	
Quadratic	0.9893	0.9810	1033.04	Suggested
Special cubic	0.9885	0.9709	1586.77	
Cubic	0.9960	-11.2189	6.654E+05	Suggested
Special quartic	0.9909	0.8494	8202.30	
Quartic	0.9965		-	Aliased

Based on the highest adjusted R^2 value, quadratic model was chosen for interpretation of size. Due to lack of orthogonality, even though the adjusted R^2 values were high for quartic model, it was aliased. The PRESS (predicted residual error sum of squares) statistics also indicated that the selected model, quadratic was best fit. This can also be confirmed from the graph of predicted vs. actual as shown in figure 6.5. as the best fit straight line passes nearly through all points and there are no any outliers. The MSE for the quadratic model was 48.94 indicating low predictability using this model.

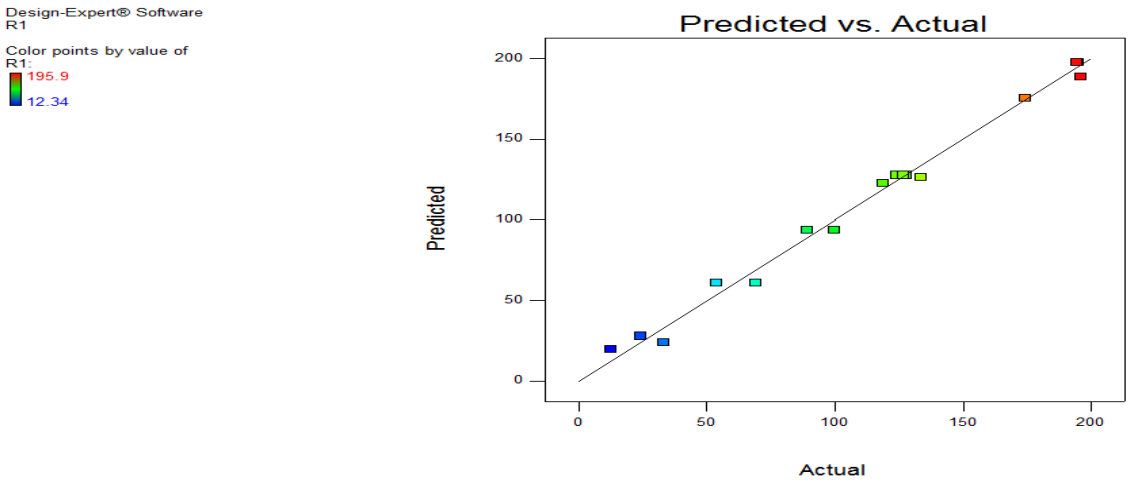

Figure 6.5 Predicted Graph for Response - Size (nm)

6.3.3.1 Fitting of the model and analysis

The relationship between experimentally obtained globule size and formulation variables was determined in terms of actual components used as input variables.

Globule size (nm) = – 136.61*A + 1.13*B – 2.97*C + 1.66*AB + 2.73*AC – 0.18*BC……..Equation 6.1

The effect on size due to different proportion of components could be explained by equation 6.1 Based on the calculated model for mean droplet size, the contour plot is shown in figure 6.6.

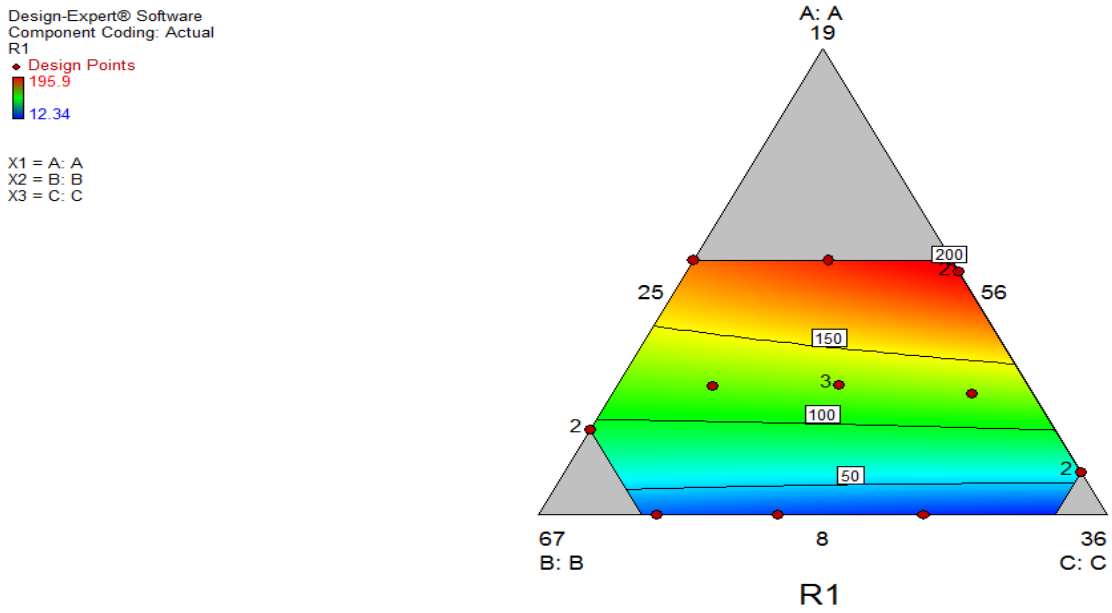

Figure 6.6 2D contour plot for droplet size

From the quadratic equation, it can be concluded that there was complex interdependency between all components on size.

6.3.3.2 Optimized formulation by desirability function

The optimized formulation, having least globule size, was selected based on the desirability value from the suggested results. Due to applied constrains on input variables and output variables, the highest desirability value was 0.458. Removing the constraints increases desirability value but the obtained formulation in such cases does not meet the quality target product profile. Hence, the formulation composition having highest desirability of 0.458 was formulated in triplicate and the globule size was measured (Table 6.4). Figure 6.7 shows

globule size of the optimized formulation. The Polydispersity Index (PDI) was found to be 0.285. PDI is calculated from cumulant analysis of measured intensity. This is autocorrelation function which describes width of the Gaussian distribution of the size [12]. PDI ranges from 0 to 1. Lesser value of PDI indicates mono-dispersed formulation. The value of 0.285 for PDI indicates monodispersed globules.

Table 6. 4 Optimized formulation composition

	Component A (Oil)	Component B (Surfactant)	Component C (Cosurfactant)	Size (nm)	Desirability
Suggested	11.147	63.853	25.000	122.377	0.458
Prepared	11.147	63.853	25.000	118.2 ± 2.3	-

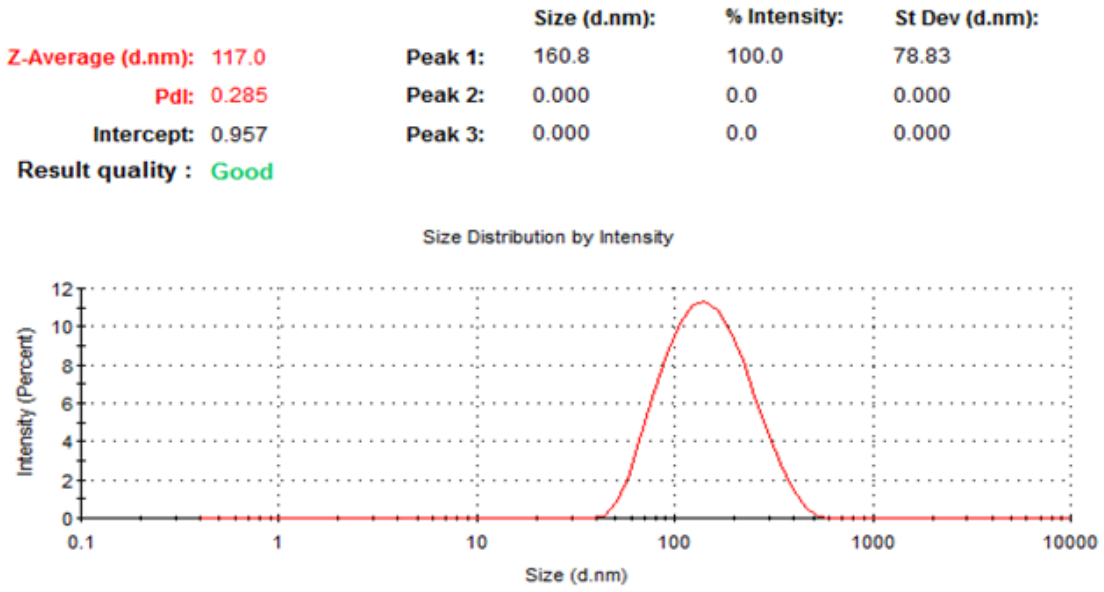

Figure 6.7 Globule size of optimized formulation

6.3.3 Artificial neural network

6.3.3.1 Structure of ANN

ANN feed forward back propagation framework was fitted to data of I-optimal design. The data set was divided into training (12 sets), validation (2 sets) and testing data (2 sets). The training

of the network by Levenberg-Marquardt topology minimized the error sum of square for the training dataset to give high R value. During training, the weights and biases of the network were adjusted iteratively to minimize the network performance function. Learning function was gradient descent with momentum (learngdm), because the momentum allows the network to ignore small features in the error surface. The number of training cycles were on the basis of MSE of the validation dataset [13,14]. Figure 6.8 shows the architecture of ANN.

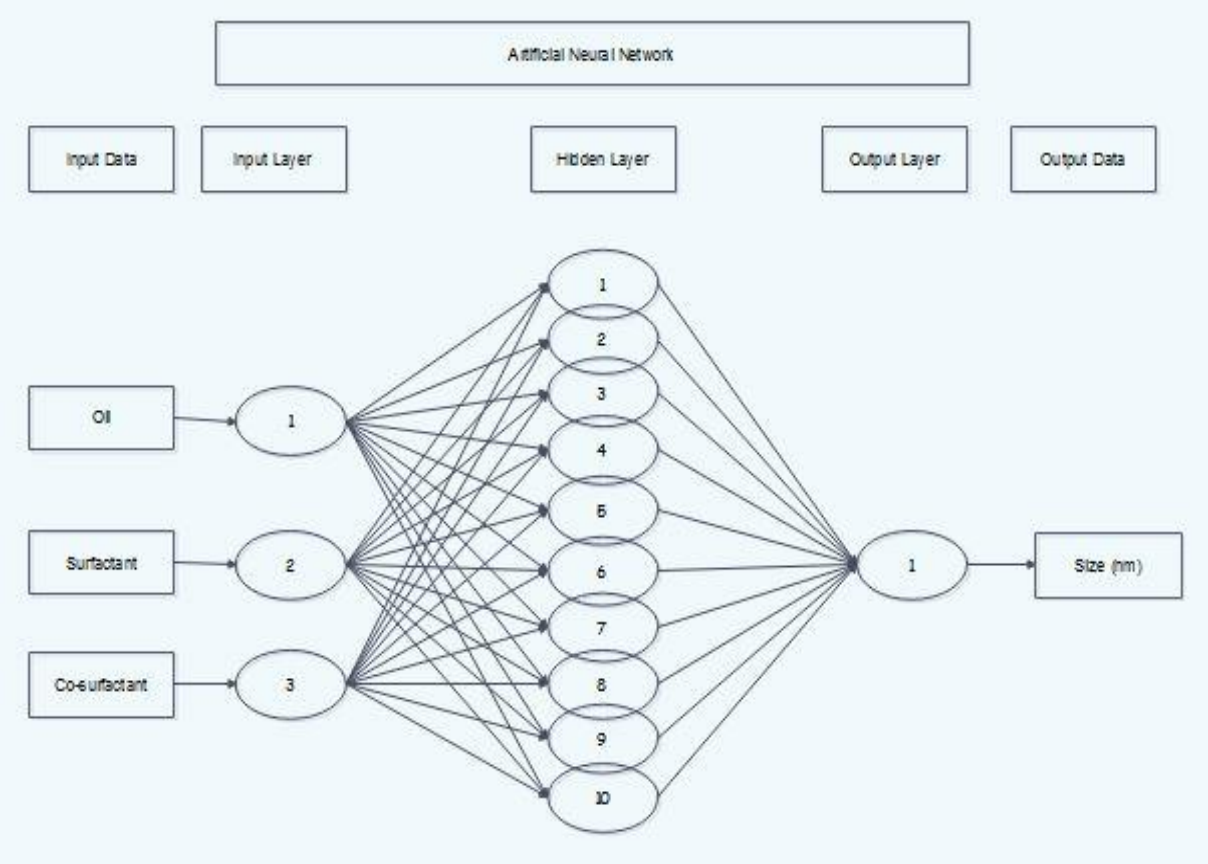

Figure 6.8 Architecture of Artificial neural network for optimization of globule size

6.3.3.2 Regression

Regression of the neural network dataset showed high R value. Overall value of the regression coefficient was found to be 0.99548 (Figure 6.9) and the MSE of the ANN model was 0.014 for the training dataset. As the value of MSE was near to zero it indicated that ANN had very good predictability to measure the quality of estimator i.e. size [15].

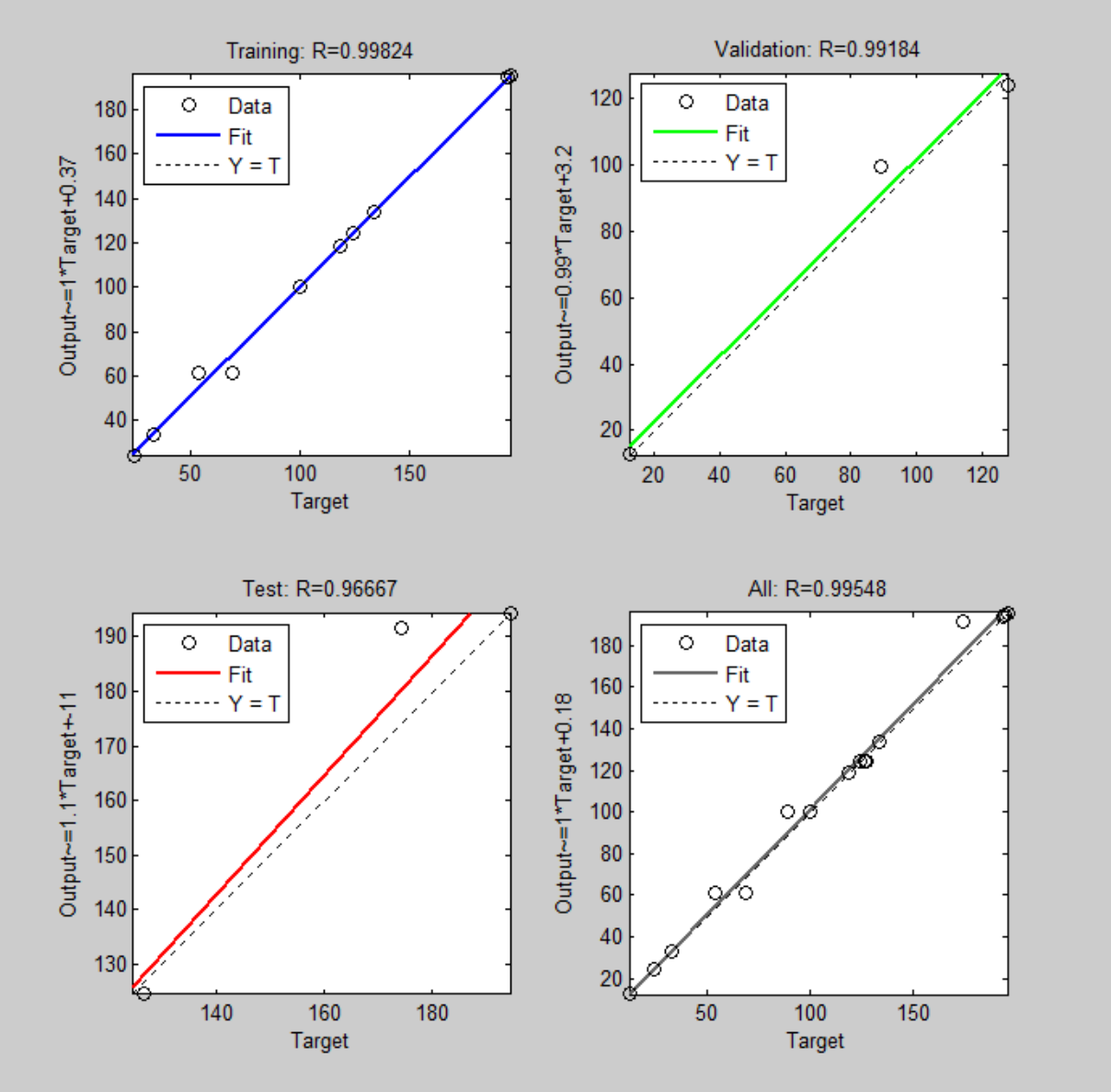

Figure 6.9 Regression of dataset using MATLAB for measuring size of globules of ILO SMEDDS

The 3D surface plots for the three input data against the output are shown in figure 6.10. The 3D graphs suggest that by increasing oil content, the size increases whereas by increasing the concentration of surfactant and co-surfactant, the size decreases. The relative contributory effect of each input on the output is shown in figure 6.11. It also shows that the output (size) is majorly dependent on the level of oil, with 54% relative contribution whereas surfactant and co-surfactant had equal contribution of 23% each.

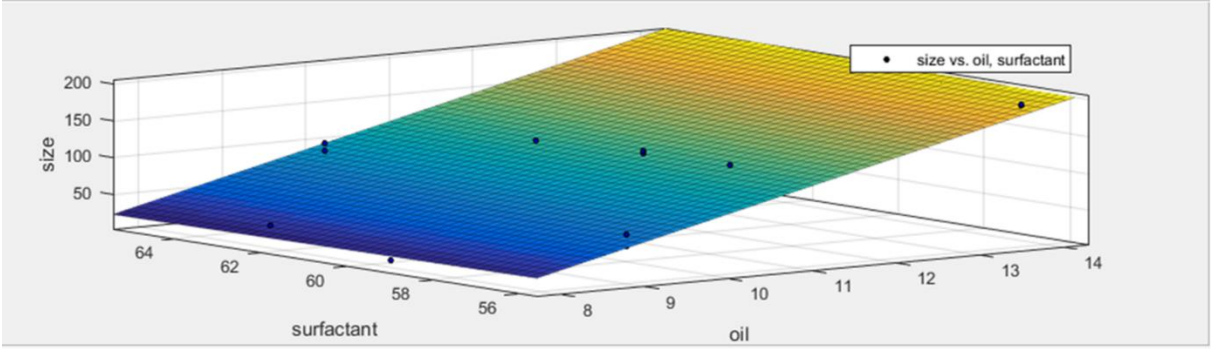

A : Effect of oil and surfactant on size

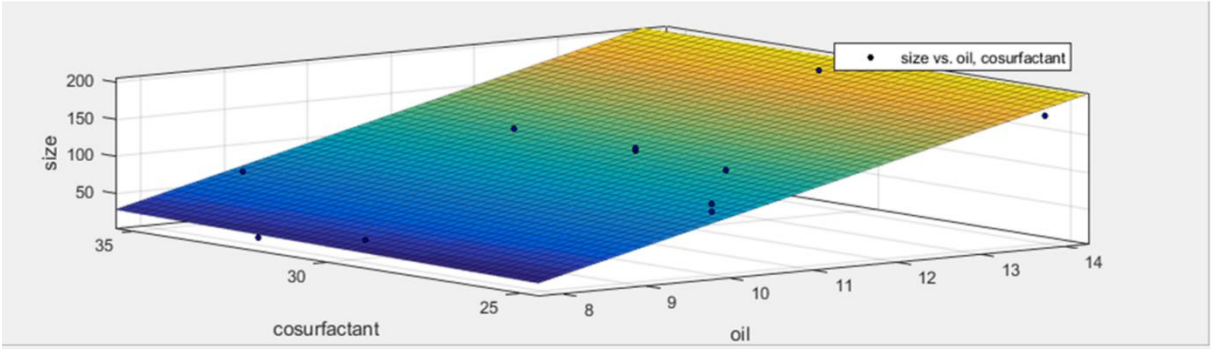

B : Effect of oil and cosurfactant on size

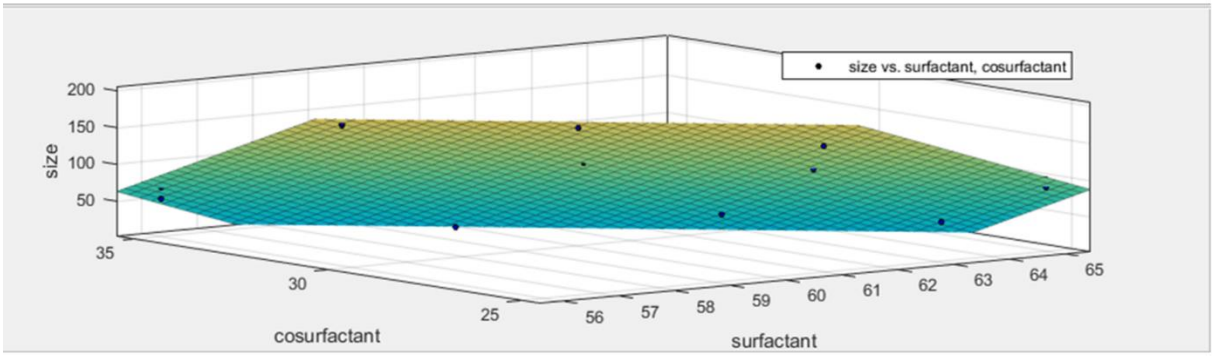

C: Effect of surfactant and cosurfactant on size

Figure 6.10 Effect of input variables on output

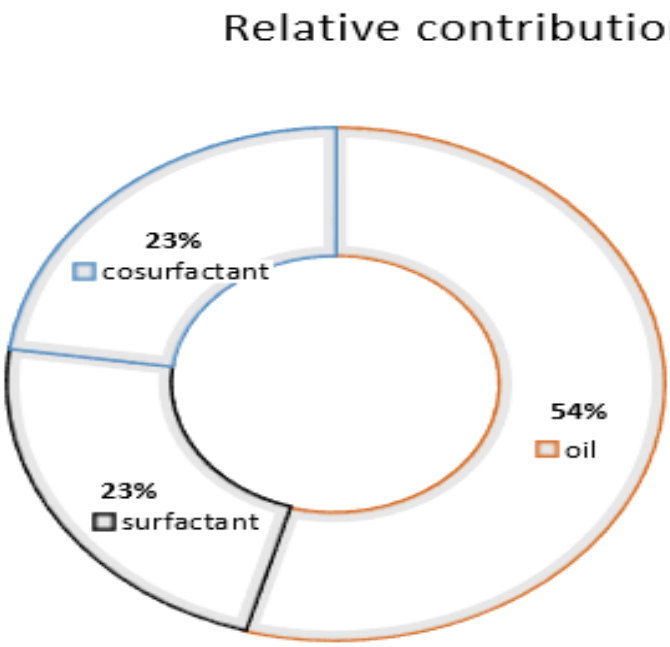

Figure 6.11 Relative contribution of each ingredient on size

6.3.3.3 Simulation of the ANN network

For the simulation of the generated network, the new dataset same as the one suggested by the I – optimal design was used as input for ANN [16]. The amount of oil, surfactant and co-surfactant was 11.147, 63.859 and 25.000 mg respectively. The output generated for the simulation dataset was 119.6783 nm. The batch prepared using same composition gave the actual size of 118.2 ± 2.3 nm.

6.3.3.4 Comparison of I-optimal design and ANN

The R value for the I-optimal design based quadratic model was 0.9867 whereas for ANN it was 0.99548. The MSE for quadratic model was 48.94 whereas for ANN it was only 0.014. The error for ANN was less as compared to I-optimal design, indicating better accuracy in prediction of the size. The size predicted by the I-optimal design was 122.377 nm, whereas by ANN it was 119.6783 nm. The actual size was found to be 118.2 ± 2.3 nm. This indicates better predictability power of the ANN over I-optimal design [17].

Thus, in this study, ILO SMEDDS were prepared and optimized by I-optimal design and ANN approaches. The developed ANN model showed higher predictability as compared to I-optimal design based quadratic model as the MSE value was low and R value was high. Contour plot and 3D graphs generated by I-optimal design and ANN respectively, showed interaction between input and output data. The relative contribution of each ingredient on size generated by the ANN indicated that oil showed the highest effect on the output.

6.4 ILO SMEDDS – Characterization

6.4.1 Globule size

Size of reconstituted ILO SMEDDS was determined by both DLS and SANS techniques. The average size obtained by DLS was found to be 118.2 nm. DLS yields D_h, which is supposed to be the oil core with stronger-bounded surfactant film and perhaps may contain some solvent molecules too around it [18]. As a consequence, the size as measured by DLS (118.2 nm) was higher than SANS (10.6 nm) for the reconstituted ILO SMEDDS.

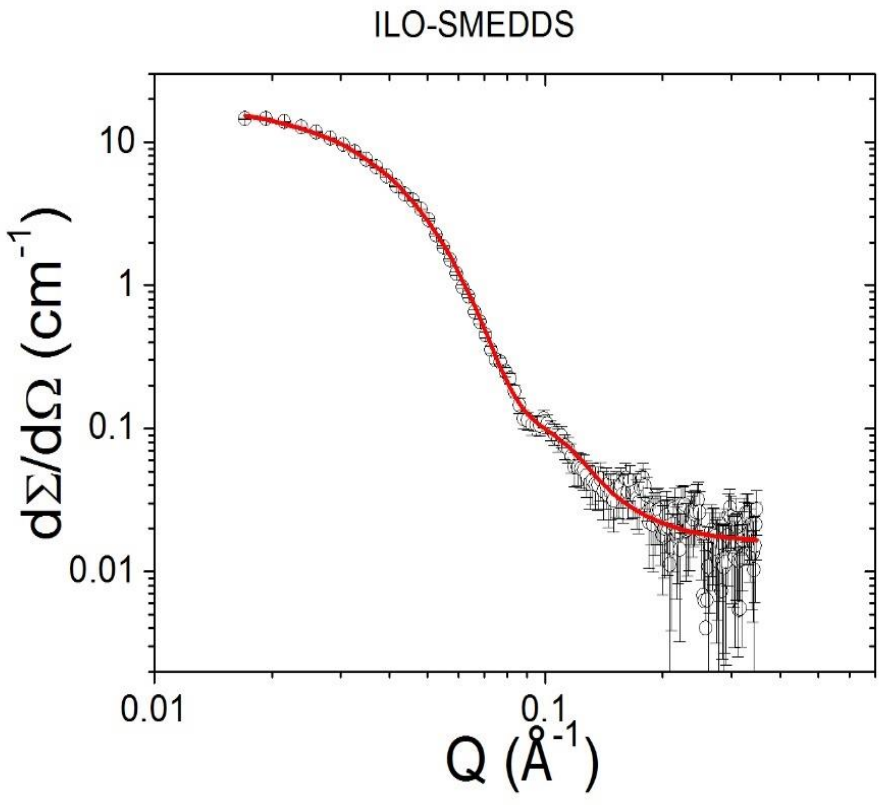

Figure 6.12 Scattered intensity as observed by SANS for ILO SMEDDS

For the scattered intensity of neutrons for ILO SMEDDS formulation, as shown in figure 6.12, model fitting was applied. Applying the model fitting for this curve, it was found that ILO SMEDDS followed polydisperse core-shell hard sphere model. The increase in oscillations at higher Q values indicates polydispersity [19]. The model fitting was carried out using open access SASfit software (Version: 0.94.8, developed by Joachim Kohlbrecher for Paul Scherrer Institute, Laboratory for Neutron Scattering and Imaging, Switzerland).

In SANS experiment, the magnitude of neutron scattering, I(Q), depends on square of difference between average scattering length densities of the particle and the medium ($\Delta\rho^2$) (equation 6.2).

$$I(Q) \propto \Delta\rho^2 \quad \text{……. Equation 6.2}$$

As the scattering length is negative (-0.372×10^{-12} cm) for hydrogen and positive (0.667×10^{-12} cm) for deuterium, SANS is ideally suited for studying the structural aspects in hydrogenous materials [20]. Deuterating either the particle or the medium will easily enhance the contrast between the particle and the medium. According to this theory of contrast between sample particle and media, the ILO SMEDDS were diluted using D_2O and scattering intensity of neutron was measured. Contrast matching by D_2O makes only oil to be 'visible' to neutrons. So, the results as obtained after data treatment for model fitting gives information on size of oil core only.

Size of ILO SMEDDS was found to be 10.6 nm by SANS, which is actually much smaller than the size obtained by DLS.

6.4.2 Zeta potential

Zeta potential of ILO loaded SMEDDS was -11.42 ± 3.26 mV.

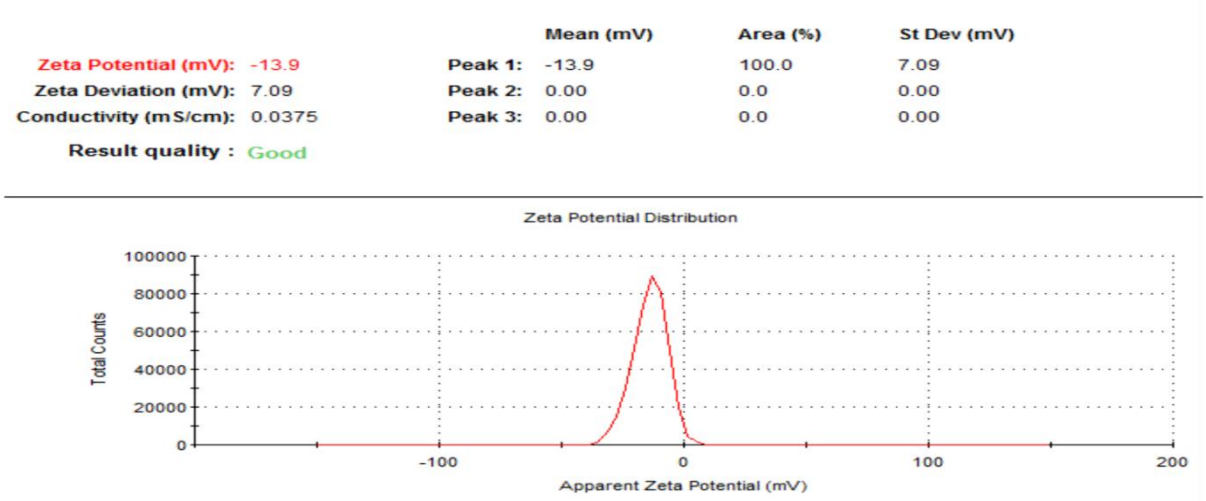

Figure 6.13 Zeta potential of diluted ILO SMEDDS

6.4.3 Spectroscopic characterization for optical clarity

The % transmittance was found to be 97.72±2.72% for reconstituted ILO SMEDDS. High values of % transmittance are related with small size. The result of % transmittance are in accordance with the globule size of diluted SMEDDS.

6.4.4 Morphology Study

The morphology of SMEDDS was assessed by cryo-TEM after dilution with water. The images in figure 6.14 shows tiny droplets of diluted SMEDDS sample. There is freeze fractured boundary of water seen in the image in uneven shape [21]. The cryo-TEM micrographs show presence of discrete droplets of oil in water microemulsion of few nanometers mean diameter size.

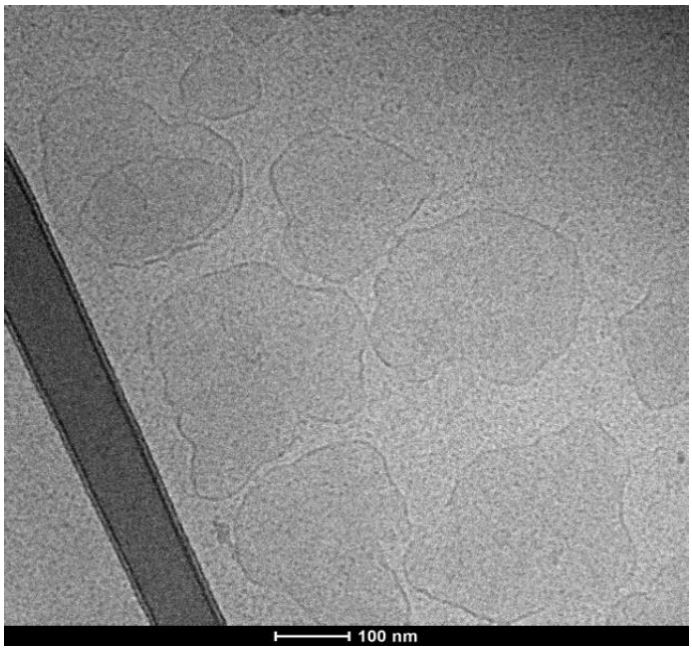

Figure 6.14 Cryo-TEM of ILO SMEDDS

Thus, the size of ILO SMEDDS obtained by SANS and Cryo-TEM was found to be similar. Hence, merely relying on intensity weighed mean diameter obtained by DLS may be a bit misleading in case when presence of surfactant leads to larger hydrodynamic diameter than the actual core size.

6.4.5 Thermodynamic Stability

The objective of thermodynamic stability study was to evaluate the phase separation and effect of temperature variation on SMEDDS formulations so as to avoid formation of metastable formulations [22]. The ILO SMEDDS did not show any signs of phase separation, cracking or creaming when subjected to centrifugation, heating – cooling cycle and freeze thaw cycle stress tests which indicated thermodynamic stability of the developed system.

6.4.6 Rheology Study

SMEDDS formulated as liquid dosage form are generally filled in soft gelatin capsules. In such circumstances, the rheological parameters play an important role while adjusting the machine parameters. Low viscosity fills are prone to leakage whereas anything more viscous is difficult

to encapsulate due to pourability issues. So, rheology study such as viscosity, Newtonian or non-Newtonian behavior were carried out. The viscosity was found to be 109.9 ± 16.94 mPa.s which fitted into the ideal range of 100 to 1000 mPa.s for capsule filling [23]. Viscosity depends on the component mixture. The major component contributing the viscosity herein is Cremophor EL surfactant due to presence of ricinoleic acid. Rheogram for ILO SMEDDS yielded a nearly straight line indicating Newtonian system as shown in figure 6.15 [24]. This indicates that even if there is any variation in shear stress there will be no change in viscosity, which is a required property during soft gelatin capsule machine filling operation.

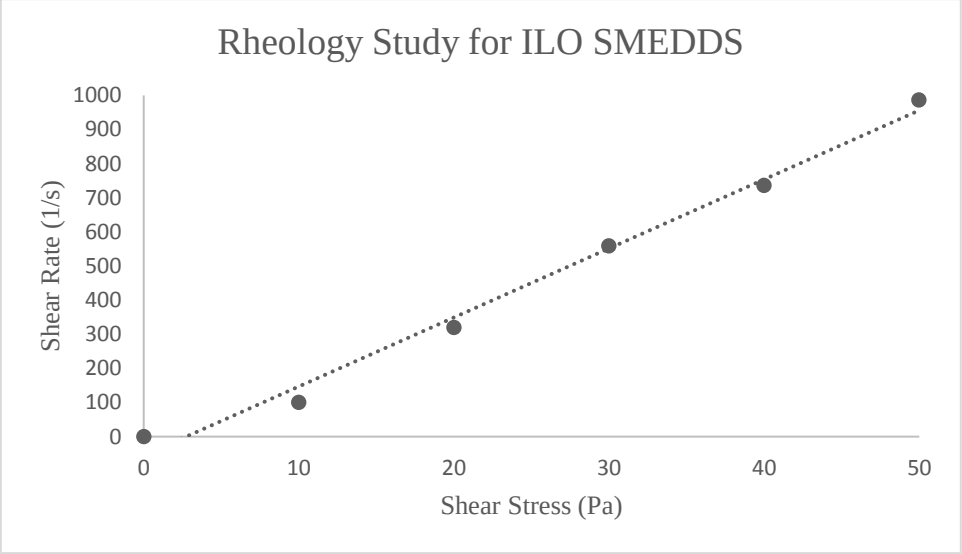

Figure 6.15 Rheology study of ILO SMEDDS

6.4.7 Cloud Point (Tc) measurement

Tc is a crucial factor in SMEDDS containing non-ionic surfactants as it is responsible for the successful formation of a stable emulsion. The temperature above which a clear formulation turns cloudy is known as the Tc. At temperatures higher than the Tc, an irreversible phase separation occurs due to dehydration of its ingredients, which may affect the drug absorption. To avoid this phenomenon in vivo, the Tc for SMEDDS should be above 37°C (body temperature) [25]. Tc was 80°C for ILO SMEDDS. As the Tc was substantially higher than 37°C, it indicated that the micro-emulsion will remain stable at physiological temperature. The higher Tc is due to polyoxyethylene content of the surfactant Cremophor EL. Further, the

branching in the hydrophobic part of the surfactants may affect Tc. In Cremophor EL, there is a network of branched alkyl chains. As a result, the Cremophor EL containing ILO SMEDDS showed 80°C Tc.

6.4.8 Dispersibility Study

As per the requirement for a promising SMEDDS, its dispersibility should be grade A or grade B (Table 5.3). All the samples passed the dispersibility test. Moreover, there was no observed drug precipitation upon dilution due to the solubilization capacity of the surfactant and co-surfactant.

6.5 Drug release

6.5.1 *In vitro* drug release

The dissolution profile of ILO from SMEDDS and suspension is presented in Figure 6.16. The SMEDDS dispersed instantaneously after dissolution of the capsule shell indicating the high self-microemulsion efficiency of the developed SMEDDS formulation. ILO SMEDDS showed rapid dissolution of the drug (>85% drug released in 15 min) as compared to the drug suspension (Less than 25% at the end of 45 min) due to enhanced solubilization. This clearly demonstrates the superior performance of the developed SMEDDS as compared to the drug. The SMEDDS, as expected, quickly presented ILO in solubilized form in the dissolution media leading to enhanced dissolution rate [26].

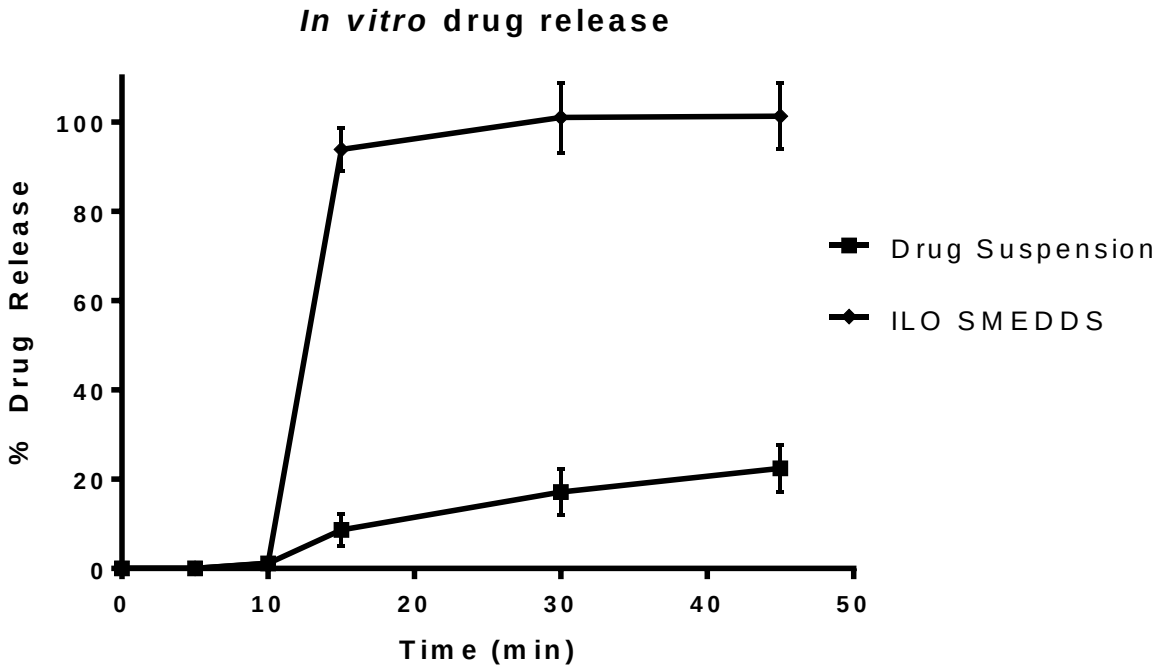

Figure 6.16 *In vitro* drug release of ILO SMEDDS

6.5.2 *Ex vivo* drug release

The core mechanisms of SMEDDS permeation across the GIT can be interpreted by ex vivo study. Diffusion mechanisms depend on the physicochemical properties of formulation, chemical nature of the drug, the lipid/water partition coefficient and the degree of ionisation of molecule across the varied pH range [27]. Drug absorption through the intestinal tissue occurs via versatile mechanisms similar to that of biological membranes, and the main diffusion mechanisms are passive or active. Passive diffusion includes a transcellular route through the cell membranes, a paracellular route through the intercellular fluid and tight junctions [28]. Whereas, active mechanisms generate gradients across the barriers, which are ATP dependent. From *ex vivo* diffusion study across the intestinal barrier, it was observed that drug diffusion from the SMEDDS was faster than drug suspension. Reasonably, it can be attributed to solubilization of the drug in the SMEDDS formulation. Within 5 h, 54.58±3.74% drug diffused from ILO SMEDDS. On the other hand, only 19.06±3.59% drug diffusion was observed from

drug suspension. This may be due to the rate limiting step of dissolution of drug itself (Figure 6.17).

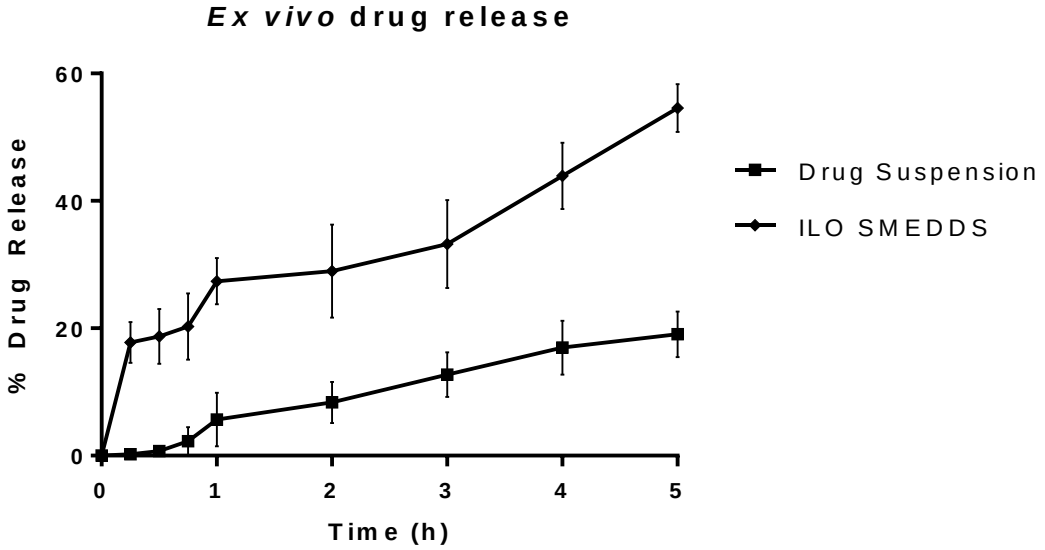

Figure 6.17 *Ex vivo* drug release of ILO SMEDDS

Enhancement ratio (Er) was found to be 2.04, clearly indicated enhancement in permeation by incorporation of ILO in SMEDDS, which is expected to enhance its absorption and bioavailability. ILO is a BCS II drug, having low solubility and high permeability. Thus, formulation as SMEDDS could significantly enhance its permeability owing to increase in solubility of drug.

6.5.3 Stability – ILO SMEDDS

Stability study of any formulation is necessary as it reflects whether the desirable properties of the formulation are retained on storage. The desirable properties for SMEDDS include clarity and globule size upon dilution. Upon storage, SMEDS is susceptible to many physical changes i.e. precipitation of drug, color change, rancidity of oil which might affect clarity of SMEDDS upon dilution and may lead to increase in globule size.

As per the ICH guideline Q1A (R2) and Q1C, stability studies should be performed on a drug product intended for storage at room temperature for long term and accelerated conditions.

Hence, samples of ILO SMEDDS were stored at 25±2°C - 60±5%RH and 40±2°C - 75±5%RH conditions. After the predefined time intervals of 1, 2, 3 and 6 months, SMEDDS samples were analyzed for physico-chemical stability. The results of the evaluations carried out are shown in table 6.5. No significant change in globule size and drug content was observed at the end of 6 months stability study.

Table 6.5 Stability study results of ILO SMEDDS

Time (months)	Long term study (25±2°C - 60±5%RH)		
	Physical description	Globule size (nm)	Drug content (%)
Initial	Clear liquid	118.2±2.3	98.23±2.4
1	Clear liquid	121.8±3.5	97.37±1.5
2	Clear liquid	128.4±2.1	98.29±3.2
3	Clear liquid	109.3±4.3	95.64±2.4
6	Clear liquid	115.2±4.3	97.17±2.6
	Accelerated study (40±2°C - 75±5%RH)		
1	Clear liquid	109.3±4.3	96.38±2.7
2	Clear liquid	108.9±5.3	95.39±4.2
3	Clear liquid	112.4±2.4	97.43±2.4
6	Clear liquid	110.4±4.2	95.79±3.2

6.6 VDN SMEDDS – Formulation development

VDN is a BCS class II drug having solubility issues [29,30]. Hence, we approached the issue in a novel way to solubilize the drug in oil, surfactant and co-surfactant mixture to make SMEDDS formulation. Herein, we have compared two different SMEDDS containing two different surfactants. Based on SMEDDS's physicochemical properties and *in vivo* performance, effect of different surfactants on SMEDDS have been identified.

6.6.1 Solubility Study

The selection of the oil was based on the solubility of VDN in the oils as shown in Figure 6.18. Higher the solubility of the drug in the selected phase, drug loading potential will be increased [31]. It was observed that the solubility of VDN was more in the novel semi-synthetic medium chain derivatives than long chain derivatives.

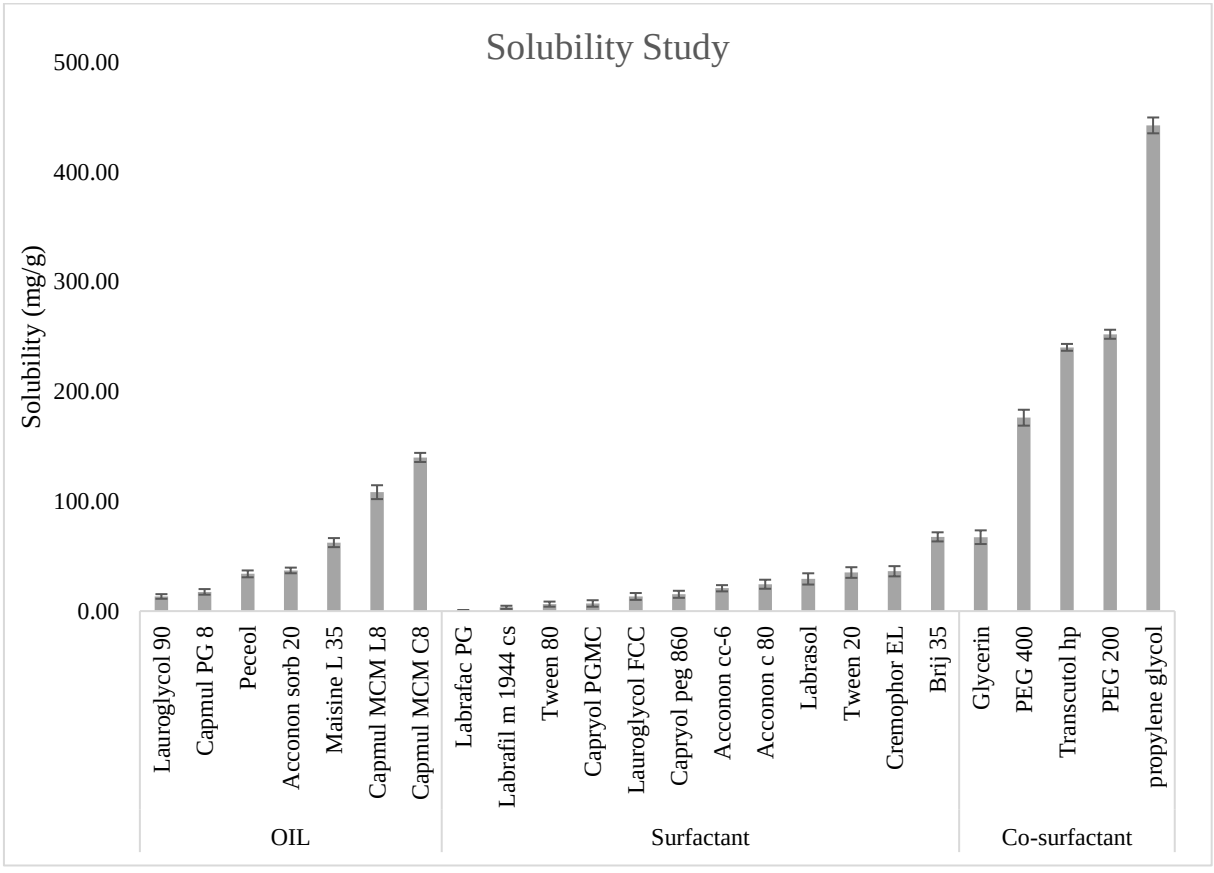

Figure 6.18 Solubility study of VDN

VDN was found to have highest solubility in **Capmul MCM C8** followed by Capmul MCM L8. As Capmul MCM C8 is also reported to have good emulsifying properties and has GRAS status, it was chosen as the oily carrier phase for formulating the VDN SMEDDS system.

6.6.2 Screening of surfactant

Selection of suitable surfactant is very crucial part for SMEDDS development, as upon dilution it requires that transparent microemulsion should be formed [32]. Surfactant was selected on the basis of two criterions: saturation solubility of VDN and its micro-emulsification efficiency for VDN+Capmul MCM C8 (drug+oil).

Different non-ionic surfactants were screened for solubility of VDN (Figure 6.19). Negligible solubility was found in Labrafac, Labrafil M 1944 CS, Capryol PGMC, Acconon CC-6 and Acconon C 80. Amongst polysorbates series of surfactants, drug showed more solubility in Tween 20 (PEG 20- Sorbitan monolaurate) than Tween 80 (PEG 20- Sorbitan monooleate). In Cremophor EL, solubility was nearly equivalent to Tween 20. Highest solubility was found in Brij 35 (Polyoxyethylene surfactant).

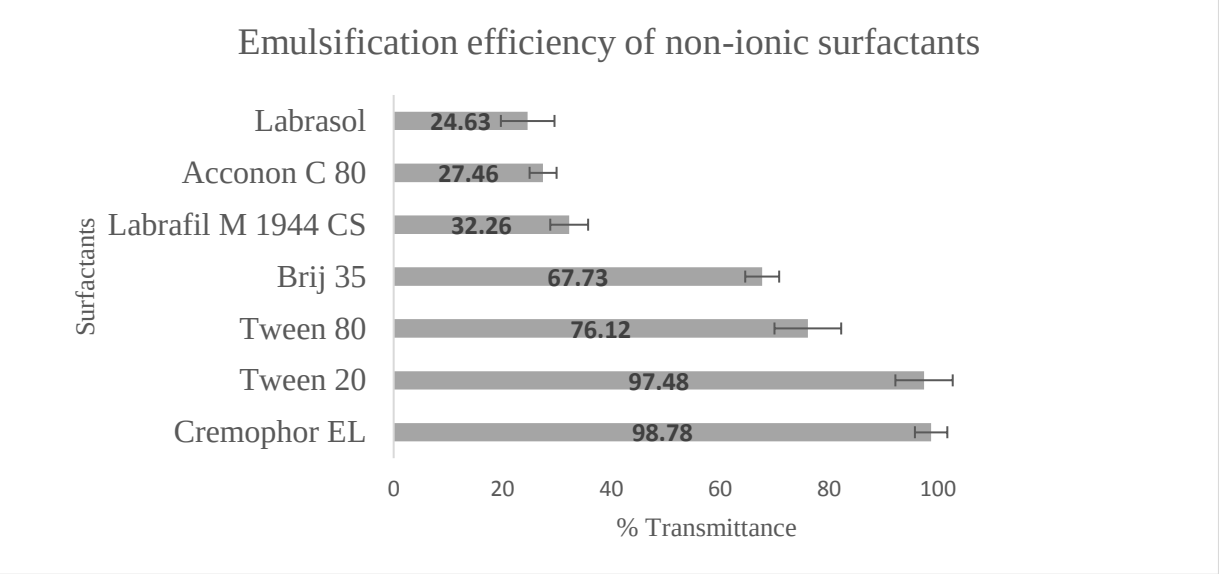

Figure 6.19 Emulsification efficiency of non-ionic surfactant

Based on the solubility study, Brij 35 can be chosen as surfactant. However, it did not show good emulsification as the final system remained hazy upon dilution and was rejected (Figure

6.19). **Cremophor EL** and **Tween 20** were found to be showing nearly equivalent emulsification ability as per % transmittance measurement. Hence, both the surfactants were chosen for further study. A comparison was made between the two systems.

6.6.3 Screening of co-surfactant

Table 6.6 Selection of co-surfactant

Co-surfactant	% Transmittance	Emulsification time (sec)	Appearance
PEG 200	99.51 ± 1.19	24 ± 5	Clear system
PEG 400	99.32 ± 2.31	31 ± 4	Clear system
Transcutol HP	98.48 ± 2.53	15 ± 6	Clear system
Propylene glycol	93.97 ± 2.17	20 ± 4	Translucent system

All the cosurfactants, upon dilution, increased spontaneity of the emulsion formation.

Here, all the co-surfactants' performance was equivalent for improving emulsification ability of oil + surfactant mix based on % transmittance data (table 6.5). Hence, appearance upon dilution and emulsification time were also taken into consideration.

Even though highest solubility of VDN was observed in propylene glycol, due to translucent microemulsion formation upon dilution, it was rejected. According to emulsification time, Transcutol HP was a favorable co-surfactant.

VDN is a BCS Class II drug, having low solubility and high first pass metabolism. The major reason behind low bioavailability is metabolism by intestinal wall enzyme CYP 340 and P-gp efflux [30]. PEG 200 is reported to inhibit intestinal wall CYP 340 enzyme and P-gp efflux inhibition as well. Hence, considering these advantages of PEG 200, we chose PEG 200 as co-surfactant.

6.6.4 Pseudo Ternary Phase Diagram

After screening of oil, based on its solubilization capacity of the drug; surfactant and co-surfactant were screened based on emulsification efficiency measured in terms of %Transmittance. Capmul MCM C8 was selected as oil phase. Cremophor EL and Tween 20, both were considered for surfactant and PEG 200 was selected as co-surfactant. Pseudo-ternary

phase diagrams were constructed using different proportions of oil to surfactant/co-surfactant ratio (Smix) at room temperature. For the given weight ratio, the total of oil, Smix and water always added to 100%. The weight ratio of oil: Smix was varied from 1:9 to 9:1. Internal ratio of Smix (Surfactant:Co-surfactant) was varied from 1:1 to 3:1. 200 mg of each weight ratio was titrated slowly with distilled water to allow equilibrium to produce fine emulsion.

As seen from the ternary plot (Figures 6.20), 2:1 ratio of Smix gave highest microemulsion region and hence, was considered for further optimization.

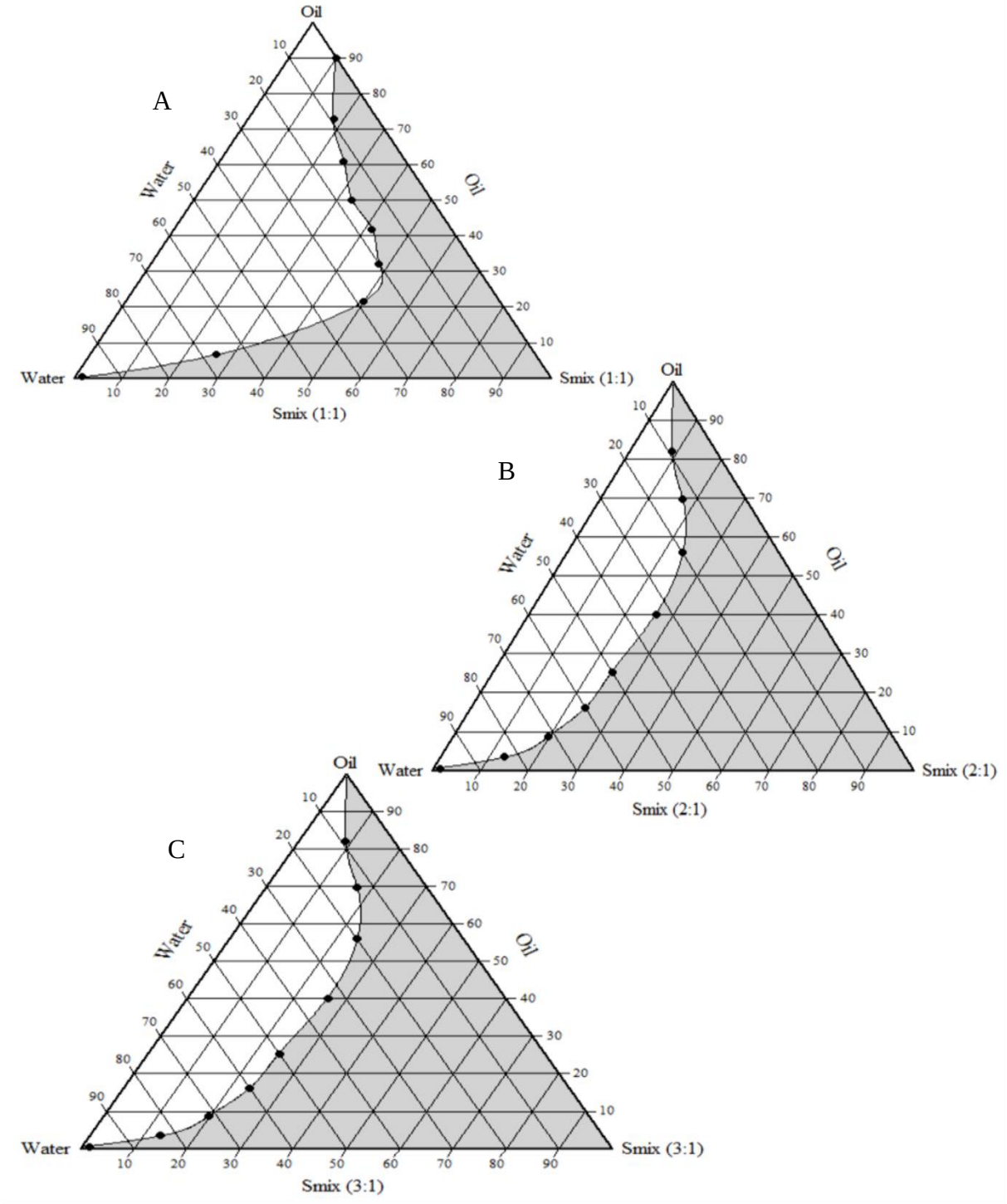

Figure 6.20 Pseudo-ternary phase diagram for VDN SMEDDS using Cremophor EL Oil (Capmul MCM C8) + Smix (Cremophor EL + PEG 200) titrated against water A: For Smix 1:1 Ratio, B: For Smix 2:1 Ratio and C: For Smix 3:1 Ratio

Similarly, for Tween 20 also, pseudo-ternary phase diagrams were plotted as shown in figure 6.21. In that also, 2:1 Smix ratio was found to be optimum.

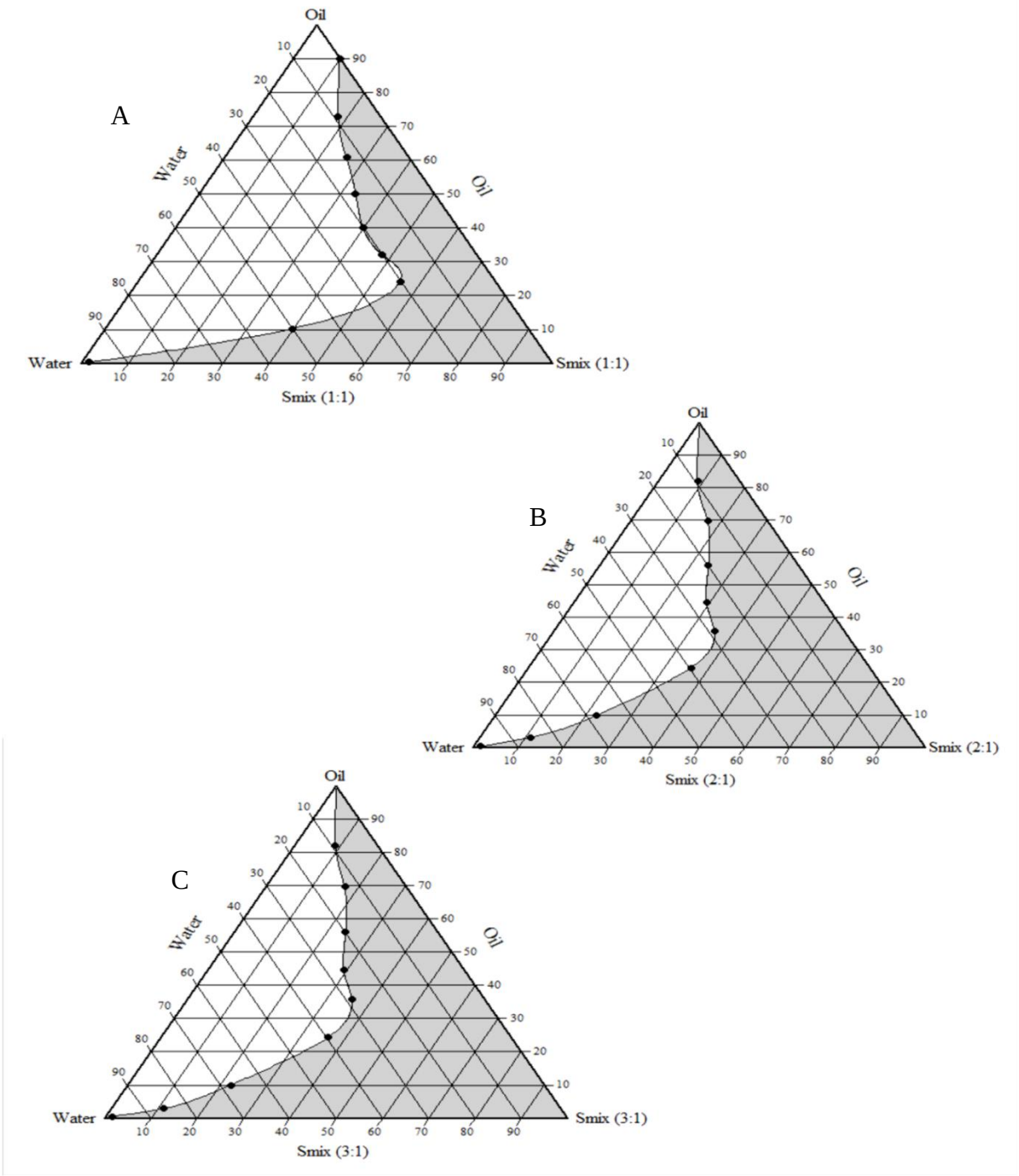

Figure 6.21 Pseudo-ternary diagram for VDN SMEDDS using Tween 20
Oil (Capmul MCM C8) + Smix (Tween 20 + PEG 200) titrated against water
A: For Smix 1:1 Ratio, B: For Smix 2:1 Ratio and C: For Smix 3:1 Ratio

6.7 VDN SMEDDS – Formulation optimization

6.7.1 Batch preparation as per I-optimal design

In this computer generated I-optimal design, the total of the mixture was 100% i.e. the fractions of each component X1 (Oil – Capmul MCM C8), X2 (Surfactant – Cremophor EL) and X3 (Co-surfactant – PEG 200) summed up to 1000 mg in the final formulation. 16 batches were prepared as per I-optimal design generated by design expert 11.0.0 software. The response in terms of size (nm) and % transmittance has been given in table 6.6.

Table 6.7 Three Component I-optimal design for optimization of VDN SMEDDS

Run	Oil (mg) X1	Surfactant (mg) X2	Co-surfactant (mg) X3	Size (nm) Y1	% Transmittance Y2
1	150	454.768	395.232	66.31 ± 2.87	97.25 ± 2.34
2	162.5	500	337.5	41.92 ± 2.17	98.18 ± 2.18
3	200	300	500	145.82 ± 3.48	86.37 ± 2.57
4	150	382.235	467.765	72.32 ± 2.18	96.59 ± 1.93
5	238.063	461.937	300	110.45 ± 3.82	89.37 ± 2.19
6	250	369.288	380.712	286.12 ± 4.31	75.28 ± 2.17
7	201.799	404.427	393.774	96.4 ± 2.73	92.48 ± 1.80
8	201.799	404.427	393.774	98.2 ± 3.72	91.27 ± 1.38
9	201.799	404.427	393.774	95.3 ± 2.18	94.23 ± 2.19
10	198.772	344.327	456.9	124.73 ± 3.92	88.31 ± 1.27
11	250	329.775	420.225	276.26 ± 3.62	77.38 ± 2.46
12	201.1	450.564	348.336	80.43 ± 2.48	95.38 ± 1.37
13	150	382.235	467.765	73.18 ± 1.38	96.16 ± 2.72
14	250	412.341	337.659	256.72 ± 4.29	79.36 ± 3.16
15	200	300	500	148.32 ± 3.18	85.27 ± 3.17
16	162.5	500	337.5	43.12 ± 1.27	97.93 ± 1.80

6.7.2 Formulation optimization

This I-optimal mixture design is characterized by a set of points lying at vertices, center of edges, thirds of edges, triple blends the midpoint of each edge and a replicate center, axial check

blends, interior check blends and overall centroid [33]. By default, optimal designs are augmented with five lack of fit and five replicates along with compulsory model points. The lack of fit runs are picked to maximize the minimum distance to other runs, while not being overly detrimental to the optimality. The replicates are used to estimate pure error, or the variability in the results even though the factor settings didn't change. Taken together they form a test for the lack of fit. A significant result from the lack of fit test is an indicator that a higher-order model may be necessary to approximate the true response surface. Without a lack of fit test, there may be no indication that an inadequate model was fit to the data [34].

Hence, here in total 16 runs design was made which includes 6 model points, 5 lack of fit points and other 5 replicates points. Effect of independent variables on size and % transmittance was studied and its optimization was carried out to generate a control space at 95% confidence interval within design space. Any variation within generated control space makes sure that the batches would never fail to meet the quality criteria. This indicates robustness of design.

6.7.2.1 Effect of independent variables on globule size

The obtained particle size for each batch can be observed from Table 6.6. The globule size varied from 41.92 ± 2.17 (F2) to 286.12 ± 4.31 (F6) which shows the effect of critical variables on globule size. Based on the statistical analysis of ANOVA, models were generated for interpretation of size from I-optimal design as shown in table 6.7.

Table 6.8 Model fit summary for globule size (Y1) of VDN SMEDDS

Source	Sequential p-value	Lack of Fit p-value	Adjusted R^2	PRESS	
Linear	< 0.0001	0.0001	0.7408	32811.38	
Quadratic	0.0001	0.0052	0.9523	14731.21	
Special Cubic	0.0125	0.0202	0.9744	12271.81	
Cubic	0.0656	0.0427	0.9875	1.183E+05	
Special Quartic vs Quadratic	0.0079	0.0562	0.9862	**16884.71**	**Suggested**
Quartic vs Cubic	0.0427		0.9939	*	Aliased
Quartic vs Special Quartic	0.0562		0.9939		Aliased

From the statistical analysis sp. quartic model was chosen to interpret the effect of independent variables on size. The predicted vs. actual values for globule size (Y1) also indicates high R^2 value of 0.99, which is a good correlation (figure 6.22).

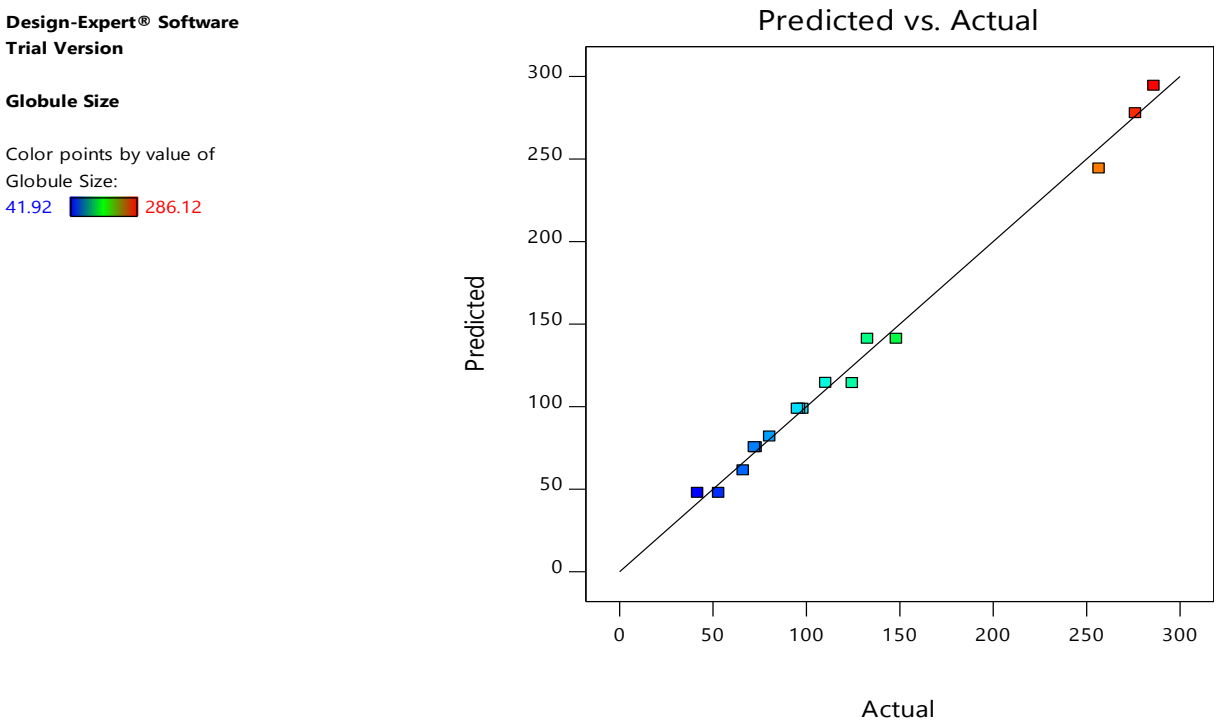

Figure 6.22 Predicted vs Actual plot for Globule size (Y1)

ANOVA analysis of special quartic model (Table 6.8) for globule size indicates that the selected model is significant to interpret the interaction effects on size (p value <0.001). To identify to what extent multicollinearity exists in the model, variance inflation factor (VIF) was calculated for each co-efficient (Table 6.9) [35]. The values for all coefficients were found to be >5, indicating that coefficients were highly correlated. This indicates the complex interrelationship between independent variables. The highest value of VIF for oil also indicated that X1 (oil) had major effect on globule size (Y1).

Table 6.9 Statistical Analysis for Globule Size (Y1)

Source	Sum of squares	df	Mean Square	F-value	p-value	
Model	91782.02	8	11472.75	135.42	< 0.0001	significant
Linear Mixture	71624.28	2	35812.14	422.73	< 0.0001	
X_1X_2	179.44	1	179.44	2.12	0.1889	
X_1X_3	99.73	1	99.73	1.18	0.3139	
X_2X_3	54.95	1	54.95	0.6486	0.4471	
$X_1^2X_2X_3$	685.80	1	685.80	8.10	0.0249	
$X_1X_2^2X_3$	79.76	1	79.76	0.9415	0.3642	
$X_1X_2X_3^2$	191.80	1	191.80	2.26	0.1761	
Residual	593.02	7	84.72	5.41		
Lack of Fit	405.52	2	202.76	5.41	0.0562	not significant
Pure Error	187.50	5	37.50			
Total	92375.03	15				

Table 6.10 Coefficient estimate for Globule size predictors

Component	Coefficient Estimate	Variance Inflation Factor (VIF)
X_1-Oil	859.13	2063.42
X_2-Surfactant	75.75	26.06
X_3-Co-surfactant	117.39	85.66
X_1X_2	-1040.02	849.62
X_1X_3	-779.28	872.56
X_2X_3	-128.23	88.97
$X_1^2X_2X_3$	12232.20	127.36
$X_1X_2^2X_3$	-2462.09	81.46
$X_1X_2X_3^2$	-2725.51	35.82

The inter-relationship of variables and responses was exemplified by 2D contour plot (figure 6.23). It shows that globule size increased as the proportion of oil was increased. On the other hand, by increasing surfactant and co-surfactant, globule size was found to be decreased.

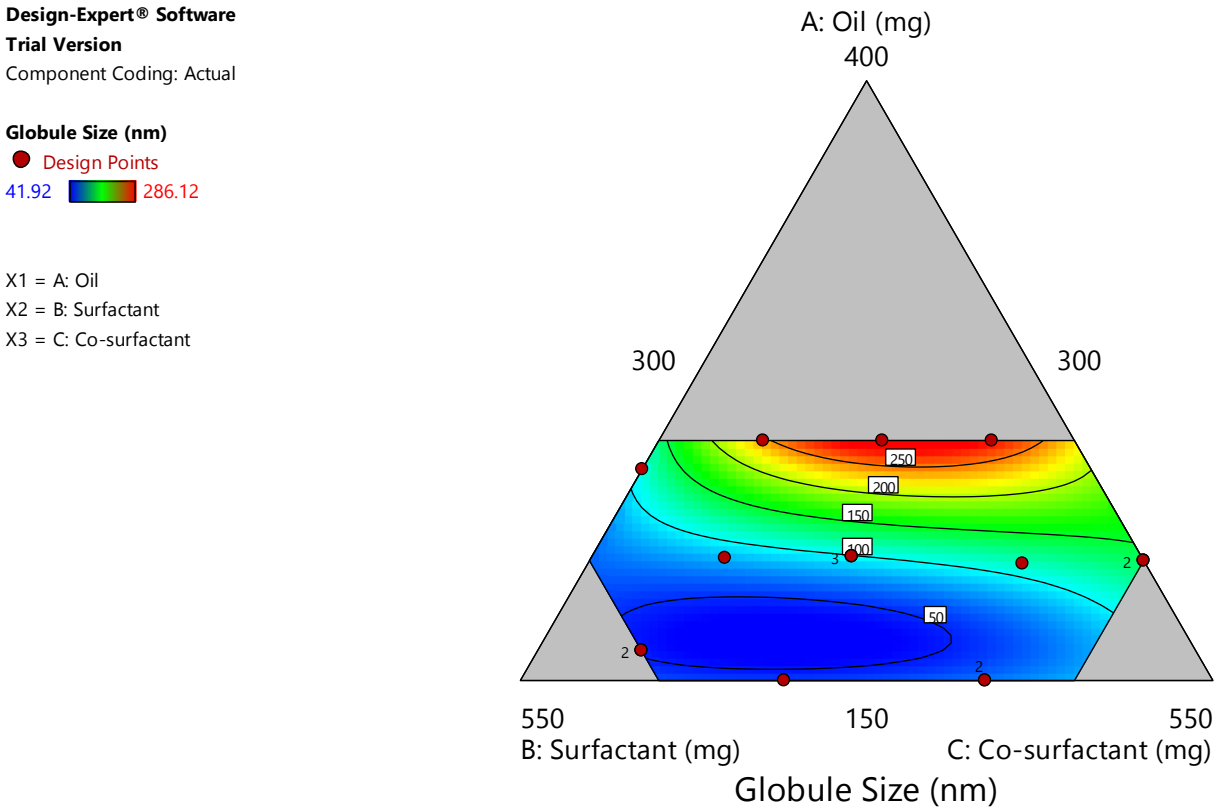

Figure 6.23 Effect of independent factors on globule size

6.7.2.2 Effect of independent variables on % transmittance

The obtained %transmittance for each batch can be observed from Table 6.6. The %transmittance varied from 75.28 ± 2.17 % (F6) to 98.12 ± 2.18 % (F2) which indicated a complex inter-relationship of the critical variables. Based on the statistical analysis of ANOVA, models were generated for interpretation of size from I-optimal design as shown in table 6.10.

Table 6.11 Model fit summary for % transmittance (Y2)

Source	**Sequential p-value**	**Lack of Fit p-value**	**Adjusted R^2**	**PRESS**	
Linear	< 0.0001	0.0063	0.8509	0.8107	
Quadratic	0.0034	0.0570	0.9478	0.8639	
Special Cubic	0.0736	0.0937	0.9601	0.8638	
Cubic	0.0950	0.1907	0.9778	-0.2116	
Special Quartic vs Quadratic	**0.0306**	**0.2566**	**0.9775**	**0.8217**	**Suggested**
Quartic vs Cubic	0.1907		0.9817		Aliased
Quartic vs Special Quartic	0.2566		0.9817		Aliased

Accordingly, from the statistical analysis special quartic model was chosen to interpret the effect of independent variables on %transmittance. Additionally, actual v/s predicted values for %transmittance (Y2), also indicates, high R^2 value of 0.9775 for which is a good correlation (figure 6.24).

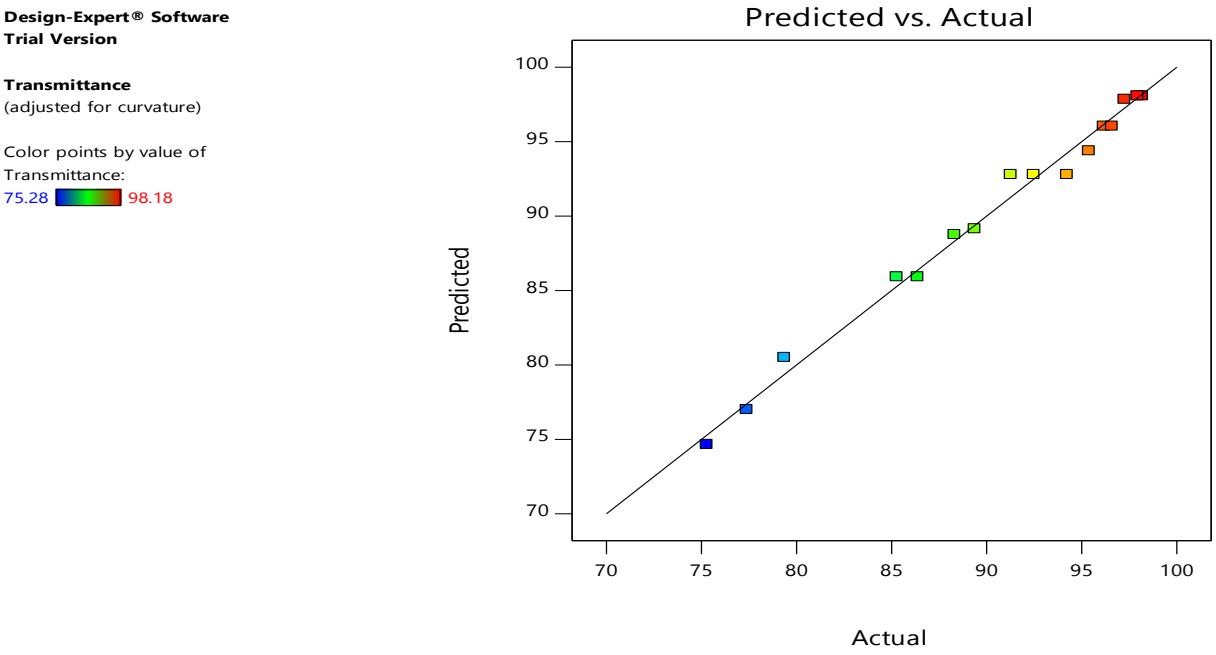

Figure 6.24 Predicted vs Actual plot for % transmittance (Y2)

ANOVA statistical analysis of special quartic model (Table 6.11) for % transmittance indicates that the selected model is significant to interpret the interaction effects on % transmittance (p value <0.001). To identify to what extent multicollinearity exists in the model, variance inflation factor (VIF) was calculated for each co-efficient (Table 6.12) [35]. The values for all coefficients were found to be >5, indicated that coefficients were highly correlated. This indicates the complex interrelationship between independent variables. The highest value of VIF for oil also indicated that X1 (oil) had major effect on %transmittance (Y2).

Table 6.12 Statistical Analysis for % transmittance (Y2)

Source	Sum of squares	df	Mean Square	F-value	p-value	
Model	837.36	8	104.67	82.44	< 0.0001	significant
Linear Mixture	736.93	2	368.46	290.20	< 0.0001	
X_1X_2	0.3145	1	0.3145	0.2477	0.6340	
X_1X_3	0.3287	1	0.3287	0.2589	0.6265	
X_2X_3	1.62	1	1.62	1.28	0.2957	
$X_1^2X_2X_3$	14.13	1	14.13	11.13	0.0125	
$X_1X_2^2X_3$	6.22	1	6.22	4.90	0.0624	
$X_1X_2X_3^2$	2.44	1	2.44	1.92	0.2084	
Residual	8.89	7	1.27			
Lack of Fit	3.73	2	1.86	1.81	0.2566	not significant
Pure Error	5.16	5	1.03			
Total	846.25	15				

Table 6.13 Coefficient estimate for % transmittance predictors

Component	Coefficient Estimate	VIF
X_1-Oil	107.36	2063.42
X_2-Surfactant	94.58	26.06
X_3-Co-surfactant	89.52	85.66
X_1X_2	-43.54	849.62
X_1X_3	-44.74	872.56
X_2X_3	22.02	88.97
$X_1^2X_2X_3$	-1755.62	127.36
$X_1X_2^2X_3$	687.76	81.46
$X_1X_2X_3^2$	307.26	35.82

The inter-relationship of variables and responses was exemplified by 2D contour plot (figure 6.25). It shows that %transmittance increased as the proportion of oil (X1) was decreased. On the other hand by increasing surfactant and co-surfactant, %transmittance was found to be decreased which is owing to formation of transparent and clear emulsion formation upon dilution.

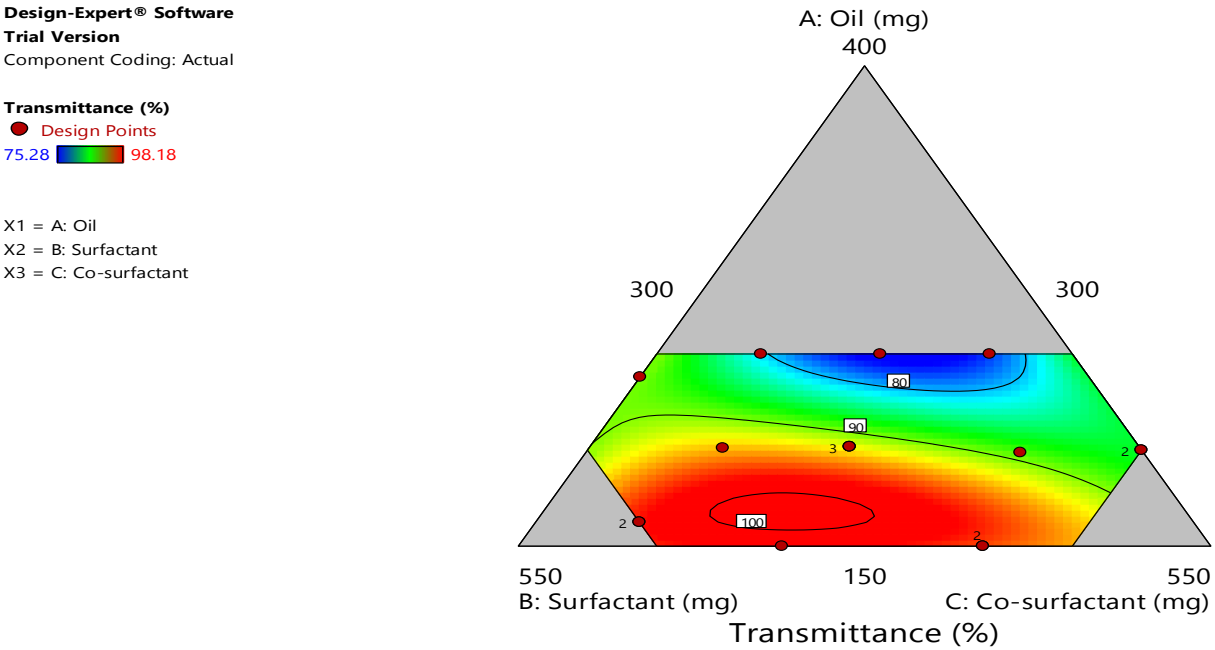

Figure 6.25 Effect of independent variables on %transmittance of VDN SMEDDS

6.7.2.3 Numerical optimization using desirability function

To carry out optimization using mathematical function - desirability criteria was used and desirability plot was generated [36]. Upper or lower desired values of response were selected, based on which software generated values of variables which would help to achieve the desired response. The ramp graph indicates the predicted values of Y1 and Y2 for the optimized amount of independent variables, whereas the bar graph indicates individual desirability for Globule size (Y1) and %Transmittance (Y2) (Figure 6.26). The composite desirability for the predicted response was found to be 0.817.

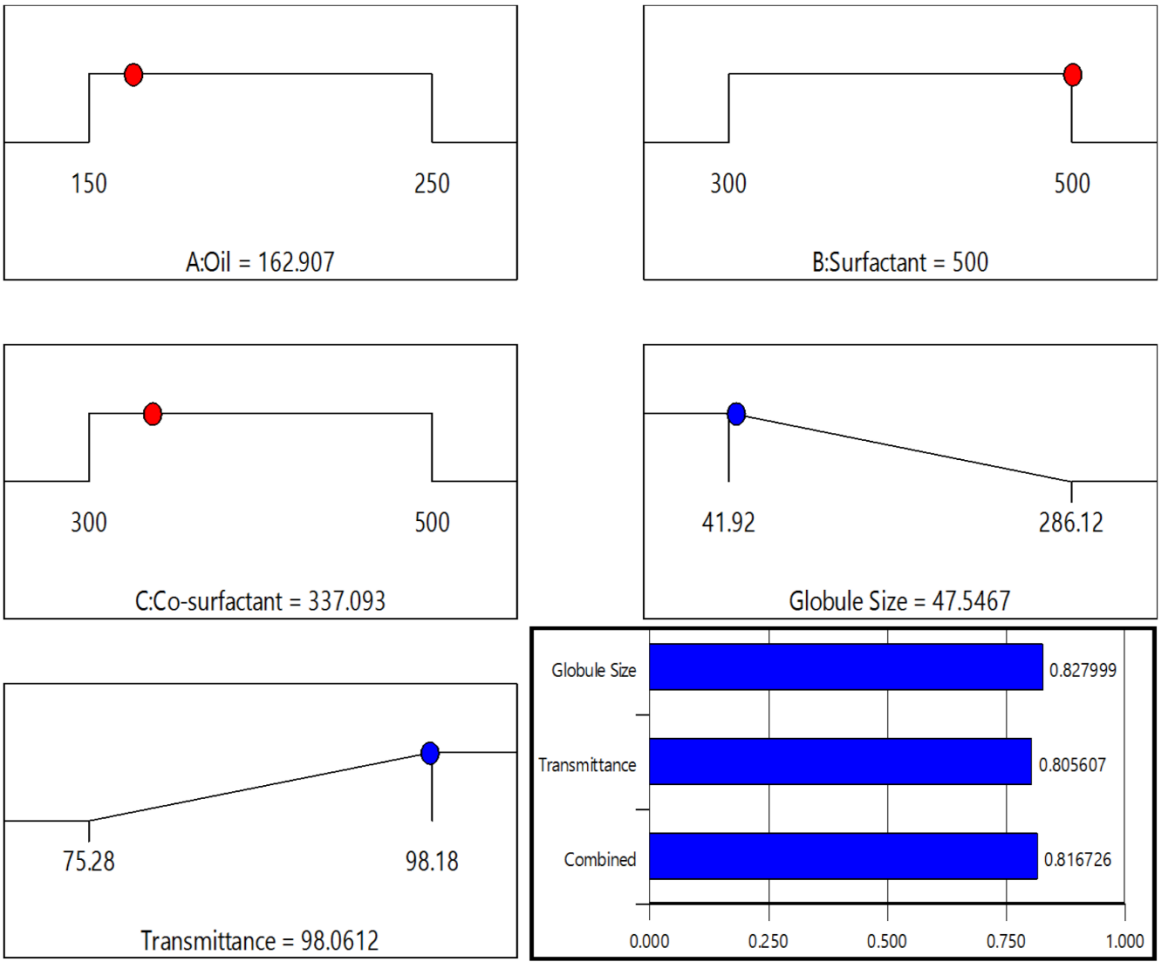

Figure 6.26 Desirability plot for VDN SMEDDS

To assess the suitability of the desirability, VDN SMEDDS was prepared as per suggested batch and obtained values of responses were compared with the predicted responses. Error was found to be less than 5%, indicated suitability of the design for prediction.

Table 6.14 Predicted and obtained responses for VDN SMEDDS prepared as per numerical optimization

Response	Oil X1	Surfactant X2	Cosurfactant X3	Size (nm) Y1	% Transmittance Y2	Desirability
Predicted	162.90	500	337.09	47.54	98.06	0.817
Observed	162.90	500	337.09	49.98±2.03	96.98±1.34	-
% Error	-	-	-	4.88	1.11	-

6.7.2.3 Graphical optimization to generate control space

Using numerical optimization by mathematical function of desirability, one optimized formulation was found. Also, few other suggestions were given based on desirability criteria by generated design. However, there is possibility that a slight change in the composition due to practical error might lead to failure of batch. Hence, using graphical optimization we found a certain area inside the design space termed as control space, which is a robust area where even a change of 5% outside the control space region would not affect the desired response [37]. This makes the design robust by narrowing the design space after applying one sided (inside the design space) 95% tolerance interval to the responses.

Figure 6.27 indicates the overlay plot showing knowledge space (yellow). By fixing upper and lower constraints for Y1 and Y2, we obtained design space (yellow) (Figure 6.28). For Y1, the constraints were 41.92 nm to 200 nm and for Y2 it was 80 to 98.18%. While working on the outer extremities of design space, there is 50% chance that a batch may fail due to error. Therefore, one sided tolerance interval at alpha level of 0.05 was applied to generate control space (yellow) (Figure 6.29). Working inside the control space or ± 5% change in the composition provided by control space won't affect the desired response.

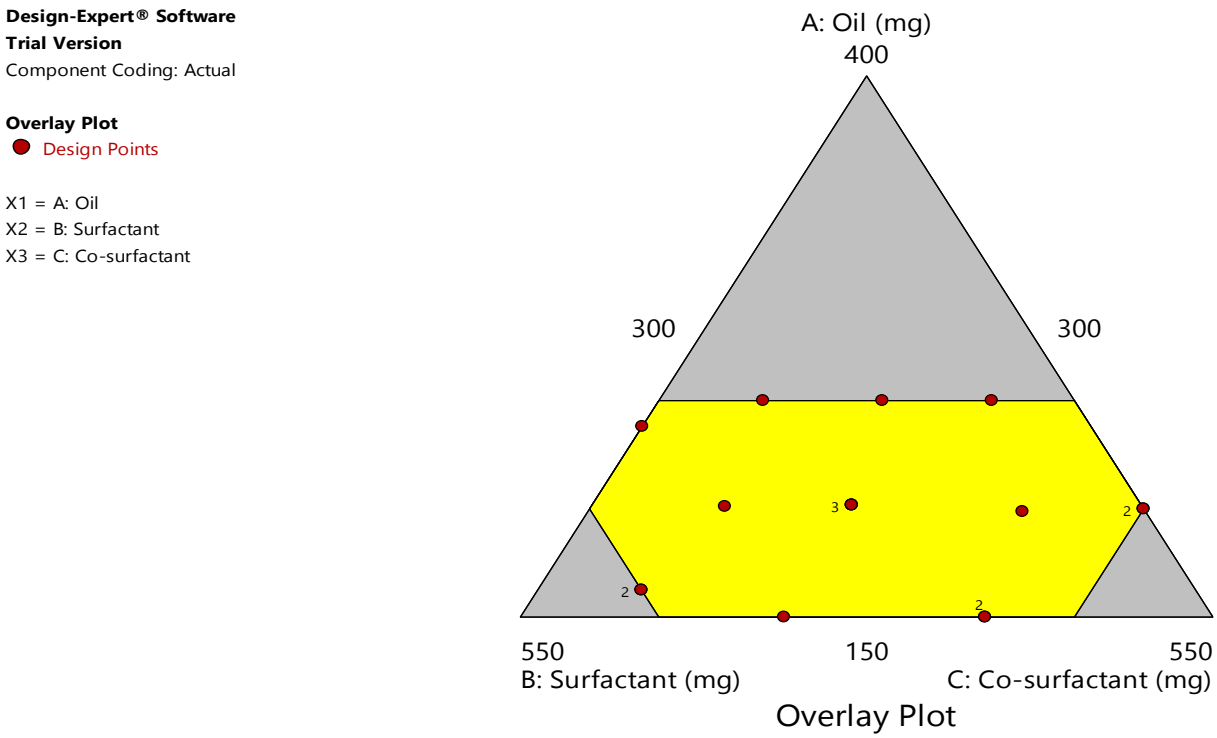

Figure 6.27 Overlay plot showing knowledge space for VDN SMEDDS

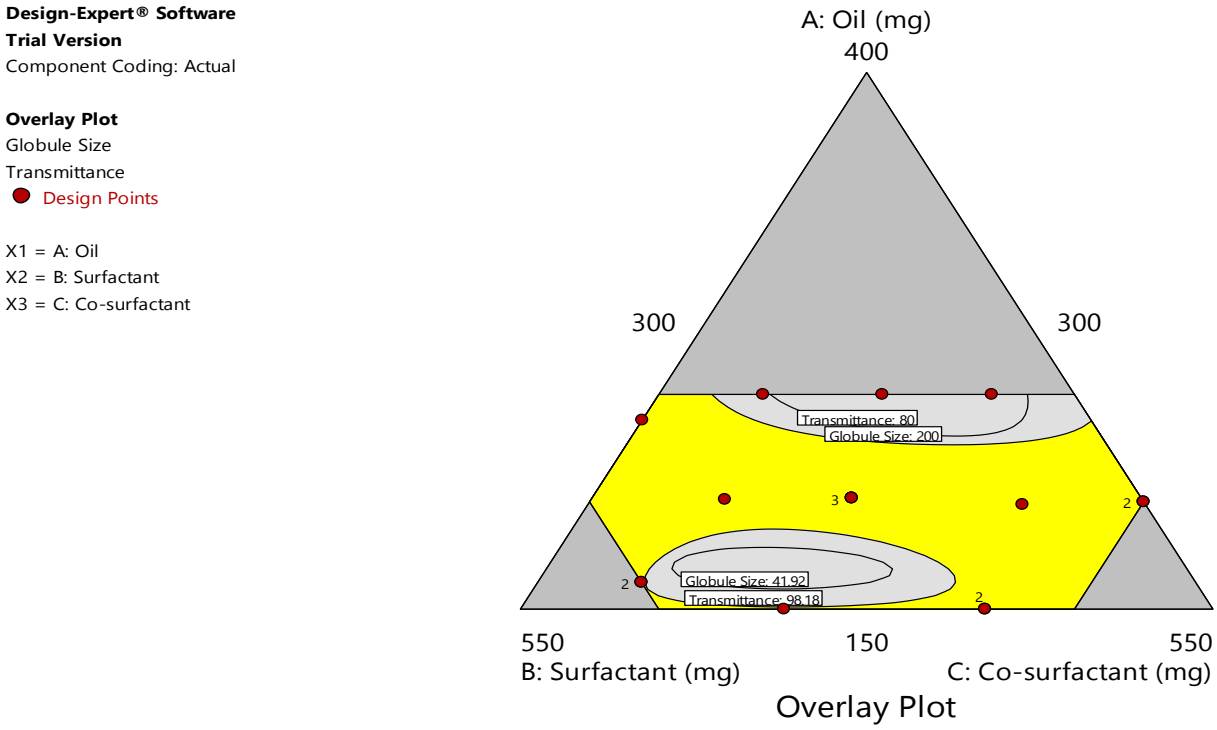

Figure 6.28 Design space for VDN SMEDDS

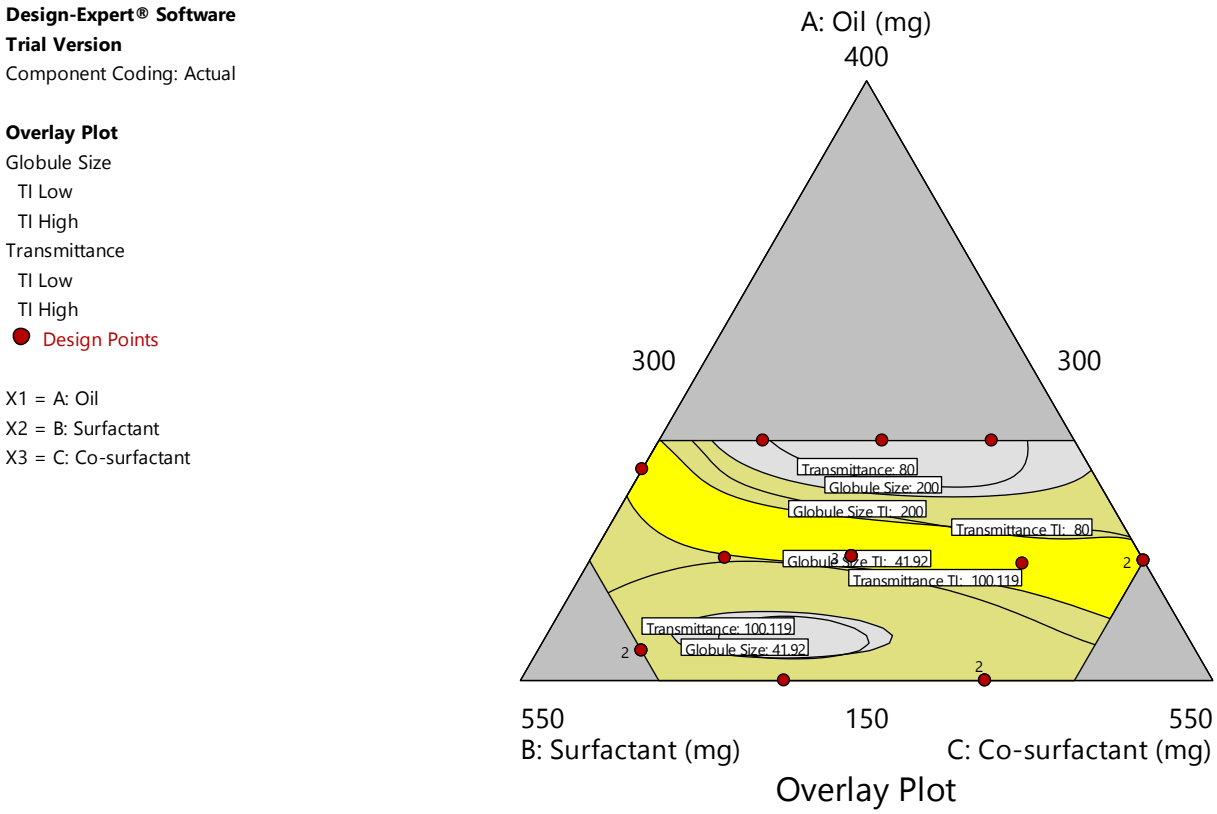

Figure 6.29 Control space for VDN SMEDDS

6.8 VDN SMEDDS preparation using Tween 20 as surfactant

VDN SMEDDS was prepared with Tween 20 (T-20) as surfactant using the same optimized composition as obtained by I-optimal design for Cremophor EL (C-EL) as surfactant. Later on, comparison was made between the two formulations containing two different surfactants. The effect of VDN SMEDDS containing either C-EL or T-20 was studied on *in vitro* and *in vivo* behavior which helped to understand the major effects of surfactants on their performance.

6.9 VDN SMEDDS – Characterization

6.9.1 Formulation Development – Considering the Surfactant effect

Self-assembly of amphiphilic molecules aka surfactant is solely dependent on favorable hydrophilic and hydrophobic interaction in aggregated phase. The two opposing forces i.e. hydrophilic and hydrophobic force decreases interfacial tension between two immiscible phases. The higher concentration of surfactant will form micelles inside the bulk phase by

solubilizing the dispersed phase. Whenever there is formation of normal-phase (oil in water) micelles, it will form oil in water (o/w) microemulsion. This o/w microemulsion is also termed as swollen micelles as the insoluble oil phase is solubilized in water by micelles formation. Considering the adverse effect of toxicity by ionic surfactants, non-ionic surfactants are preferred to a greater extent for drug delivery purpose by microemulsion [38]. These surfactants are often studied for SMEDDS formulation owing to high degree of compatibility with other components, physicochemical stability and being less affected by change in pH and ionic strength.

For VDN SMEDDS formation, we selected two types of non-ionic surfactants i.e C-EL and T-20. Alkyl esters, polyoxyethylene sorbitan fatty acid esters (Tween), are regarded as non-toxic and non-irritant [39]. This could be attributed to the possible enzymatic degradation of ester bonds. T-20 is formed by the ethoxylation of sorbitan before addition of lauric acid. Cremophor, an ethoxylated derivative of castor oil, has better emulsifying capacity in comparison to Tween. To examine the influence of surfactant type on the emulsifying capability (measured as %T), a series of emulsions with oil (Capmul MCM C8, 300 mg) were prepared using different surfactants under similar condition. The weight ratio of oil-to-surfactant and the oil content were defined on the basis of previous investigations for spontaneously emulsifying systems [3]. Both T-20 and C-EL showed highest and comparable %T. The %T of C-EL was 98.78±1.46%, whereas for T-20 it was 97.48±2.11% (see section 6.6.2 – Screening of surfactant). Hence, both surfactants were used for further studies to evaluate their effect on the physicochemical properties and performance of the SMEDDS.

After selection of surfactants, various drug loaded batches of VDN-SMEDDS were prepared. The drug (40 mg) was dissolved in Capmul MCM C8 under continuous stirring. Smix of C-EL or T-20 with PEG 200 was added to the drug-oil mixture and stirred for 10 min using a magnetic stirrer (Remi, India). Clear, transparent SMEDDS formulations thus prepared were further characterized for size and %T.

6.9.2 Globule Size and Surface Charge

Scattering techniques can provide information about the structure as well as size of nano-materials. Amongst the commonly used scattering techniques are DLS, SANS, small-angle X-

ray scattering (SAXS) and static light scattering (SLS) [40]. SLS, SAXS and SANS can be used to find interactions of the particles, structure and size. DLS is based on diffusion of particles in solution, which is related to its hydrodynamic size.

The type of samples that can be studied by scattering techniques, the sample environment that can be applied, the actual length scale probed and the information that can be obtained, all depend on the nature of the radiation employed. For example, SANS with high penetration depth of monochromatic beam of neutrons can easily be applied to opaque samples which cannot be studied by DLS. SANS measures the actual size of the particle (D_{core} – Core diameter), whereas DLS measures the hydrodynamic size of the particle (D_h – Hydrodynamic diameter) (Figure 6.30). As the LASER diffracts from the hydration layer around the particles, the hydrodynamic diameter is always larger than the actual. DLS results are biased towards larger length scale present in the system, whereas SANS provides more statistical results. Thus, to a large extent these techniques are complementary to each other, whilst sharing many similarities also [18].

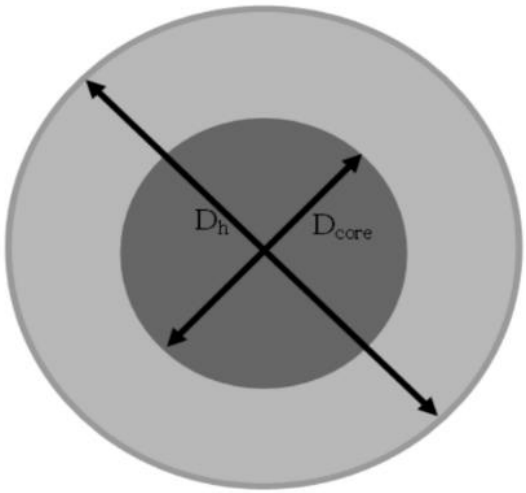

Figure 6.30 O/W microemulsion droplet defining size parameters by DLS (D_h) and SANS (D_{core})

The globule size (diameter) of C-EL VDN SMEDDS was 49.98±2.03 nm (PDI = 0.21) and for T-20 VDN SMEDDS it was 214.50±6.82 nm (PDI = 0.32) when measured by DLS technique.

Whereas by SANS, it was 10.2 and 7.2 nm respectively for C-EL and T-20 based VDN SMEDDS, which were significantly different when compared by t-test.

From the figure 6.31 for scattered intensity by SANS, it was obvious that the size of C-EL based SMEDDS was more than T-20 based system as evident from the sigmoid curve's y-axis. Applying the model fitting for these curves, it was found that VDN SMEDDS system was followed polydisperse core-shell hard sphere model. The increase in oscillations at higher Q values indicates polydispersity [19]. The model fitting was carried out using open access SASfit software (Version: 0.94.8, developed by Joachim Kohlbrecher for Paul Scherrer Institute, Laboratory for Neutron Scattering and Imaging, Switzerland).

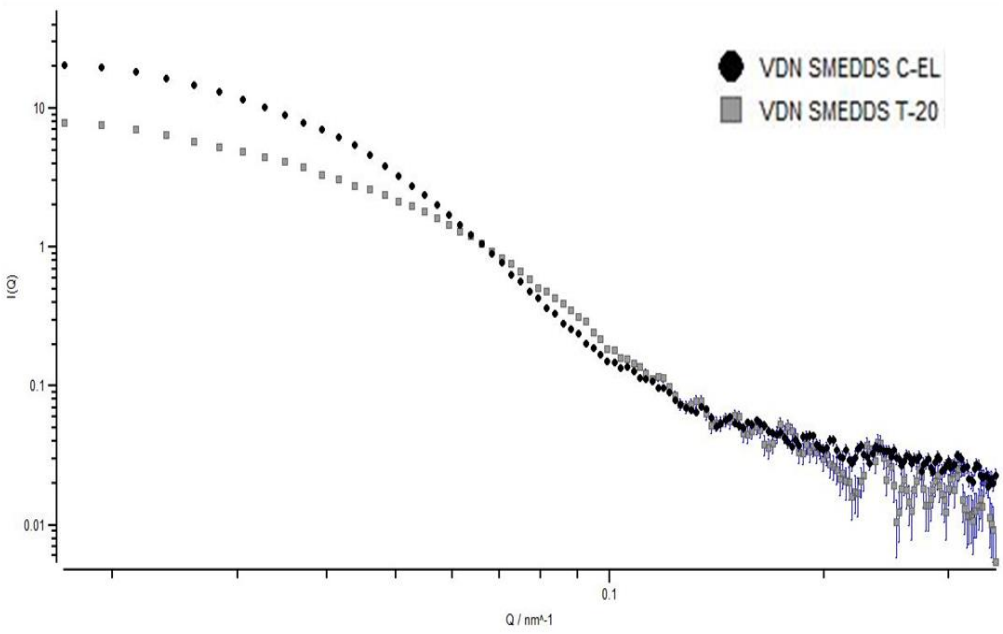

Figure 6.31 Scattered intensity as observed by SANS for VDN SMEDDS

DLS yields D_h, which is supposed to be the oil core with stronger-bounded surfactant film and perhaps may contain some solvent molecules too around it, whereas SANS yield actual core size. As a consequence, the size as measured by DLS was higher than SANS for any of the reconstituted VDN SMEDDS system.

However, there was larger difference between the DLS and SANS results for T-20 based SMEDDS than C-EL. This may be attributed to the higher film thickness of absorbed water for T-20 system than C-EL. This in turn may be related with the HLB value which is 16.7 for T-20 and 12~14 for C-EL [41,42]. The molecular weight of hydrophilic portion for T-20 is 1044 g/mol, which may provide more attraction for water molecules than the C-EL as it has only 759 g/mol for hydrophilic part of the molecule.

The zeta potential of reconstituted SMEDDS was -9.34±3.5 mV and -11.34±2.1 for C-EL and T-20 based SMEDDS system respectively. The negative charge may be because of the fatty acid of the oil (Capmul MCM C8) in the formulation.

6.9.3 Spectroscopic characterization for optical clarity

The %T was found to be 98.51±3.12% and 97.72±2.72% for reconstituted C-EL VDN and T-20 VDN SMEDDS respectively indicating nearly equivalent emulsification ability of both surfactants.

6.9.4 Morphology

The morphology of SMEDDS was assessed by cryo-TEM after dilution with water [43]. The images in figure 6.32 for both the SMEDDS shows resemblance between two systems. The cryo-TEM micrographs show presence of discrete droplets of oil in water microemulsion of few nanometers mean diameter size.

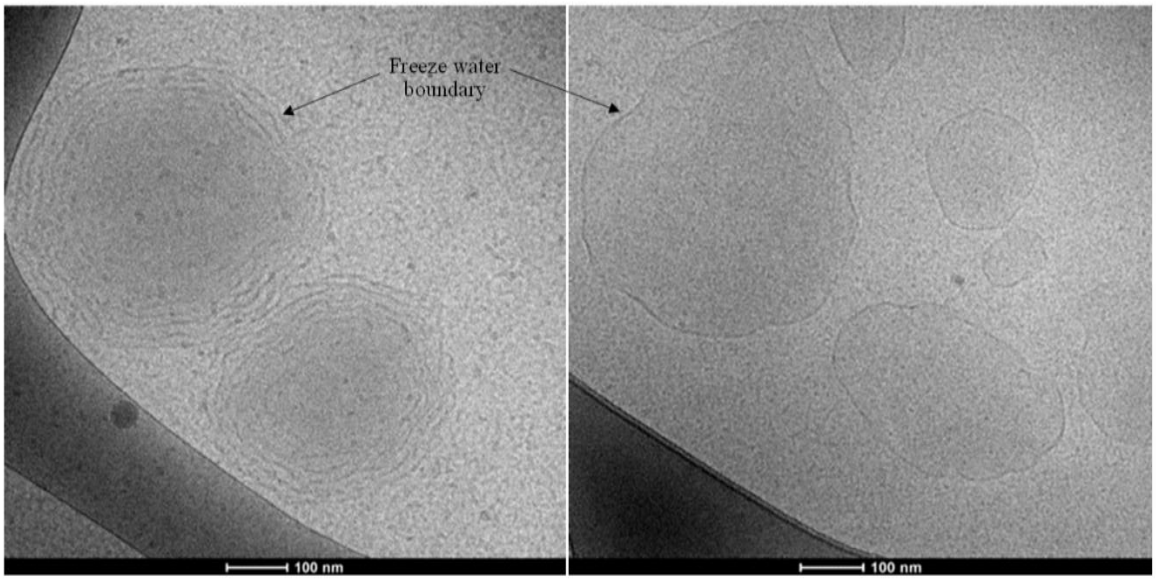

Figure 6.32 Cryo-TEM of VDN SMEDDS

Thus, the size of VDN SMEDDS obtained by SANS and Cryo-TEM was found to be similar. Hence, merely relying on intensity weighed mean diameter obtained by DLS may be a bit misleading in case when presence of surfactant leads to larger hydrodynamic diameter than the actual core size.

6.9.5 Thermodynamic stability

The objective of thermodynamic stability study was to evaluate the phase separation and effect of temperature variation on diluted SMEDDS formulations so as to avoid formation of metastable formulations [22]. The VDN SMEDDS did not show any signs of phase separation, cracking or creaming when subjected to centrifugation, heating – cooling cycle and freeze thaw cycle stress tests indicating thermodynamic stability of the developed system.

6.9.6 Rheology study

The viscosity was found to be 145.2±5.16 and 124.7±3.92 mPa.s for C-EL and T-20 based SMEDDS respectively. These values fitted into the ideal range of 100 to 1000 mPa.s for capsule

filling. Viscosity depends on the component mixture. As the components used herein are same other than the surfactant, the difference in viscosity of the two systems depends only on surfactant. The high viscosity of C-EL is due to presence of ricinoleic acid, a mono-unsaturated having hydroxyl group at 12th carbon. Upon ethoxylation, the molecular weight of C-EL further increases leading to increased viscosity. Whereas T-20, polyethylene glycol sorbitan monolaurate, has less number of carbons and hence lower viscosity as compared to C-EL based VDN system.

Rheogram for both the systems yielded a nearly straight line indicating Newtonian system as shown in figure 6.33 [24]. This indicates that even if there is any variation in shear stress there will be no change in viscosity, which is a required property during soft gelatin capsule machine filling operation.

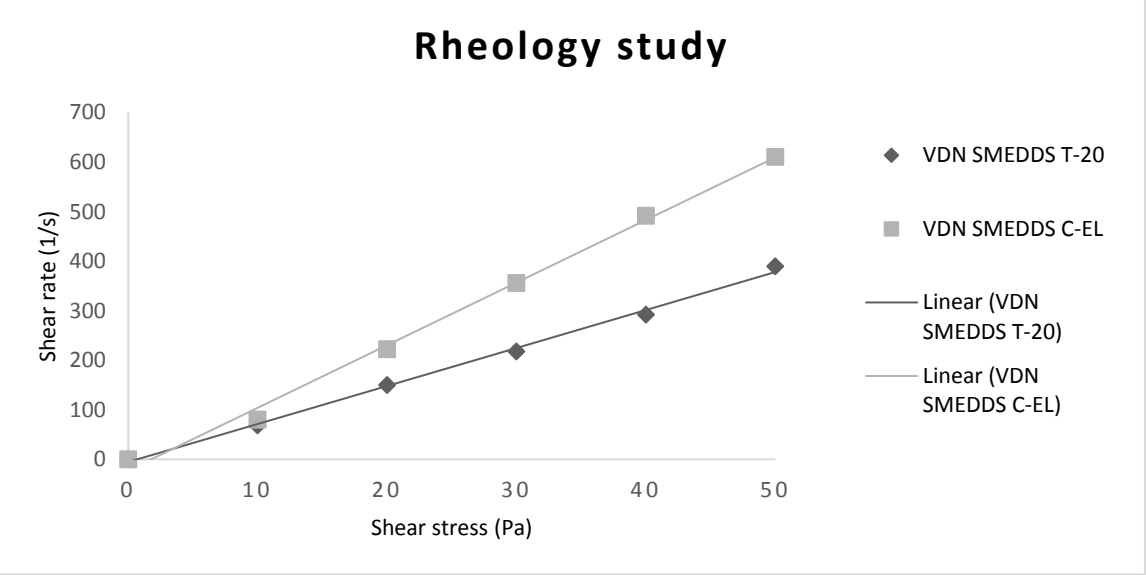

Figure 6.33 Rheology Study of VDN SMEDDS

6.9.7 Cloud Point Measurement

Tc was 65°C for polysorbate based VDN SMEDDS and 85°C for castor oil derivative based system. As the Tc was substantially higher than 37°C, it indicated that the micro-emulsion will

remain stable at physiological temperature [25]. The variance amid the two systems is due to polyoxyethylene content of the surfactant, which is higher for C-EL as compared to T-20. Further, the branching in the hydrophobic part of the surfactants may affect Tc. In C-EL, there is a network of branched alkyl chains whereas in T-20, the hydrophobic tail is a 12 C straight chain. Favorably, shorter the chain length, higher the cloud point. As a result, the C-EL system showed higher Tc than the T-20 system.

6.9.8 Dispersibility Study

As per the requirement for a promising SMEDDS, its dispersibility should be grade A or grade B (Table 5.1). C-EL and T-20 containing VDN SMEDDS passed the dispersibility test. There was no observed precipitation upon dilution of SMEDDS. This might be due to the solubilization capacity of the surfactants were enough for the microemulsion micelles formation [38].

6.9.9 *In vitro* drug release

The drug release is an important quality control tool for the dosage forms. The dissolution profile of VDN from these formulations is presented in Figure 6.34.

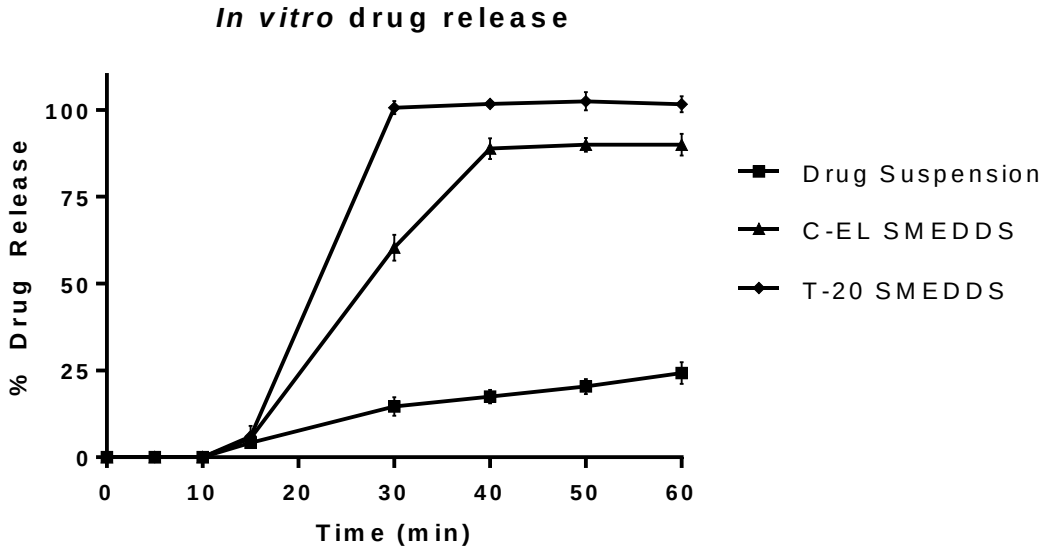

Figure 6.34 In vitro drug release of VDN SMEDDS

T-20 VDN SMEDDS dispersed instantaneously after dissolution of the capsule shell indicating the high self-microemulsion efficiency of the developed formulations. T-20 VDN SMEDDS showed more rapid dissolution of the drug (>75% drug released within 30 min) as compared to the C-EL VDN SMEDDS and drug suspension. The longer lag time for C-EL SMEDDS may be attributed to its higher viscosity.

Compared to drug suspension, VDN SMEDDS of C-EL and T-20 drastically enhanced solubilization of drug. The pure drug release was only 25% at the end of 60 min whereas it was more than 75% from VDN C-EL SMEDDS and T-20 SMEDDS. This clearly demonstrated the superior performance of the developed SMEDDS as compared to the drug. The SMEDDS, as expected, quickly present VDN in solubilized form in the dissolution media leading to enhanced dissolution rate [26].

6.9.10 *Ex vivo* drug release

From *ex vivo* diffusion study of the drug suspension and VDN SMEDDS, it was observed that drug diffusion across the intestinal barrier from the SMEDDS was faster than drug suspension. Reasonably, it might be due to solubilization of the drug in the SMEDDS formulation. Within 5 h, 53.58±3.91% and 58.81±5.21% drug diffused from VDN C-EL SMEDDS and VDN T-20 SMEDDS respectively. On the other hand, only 21.94±4.82% drug diffusion was observed from drug suspension (Figure 6.35). This may be due to the rate limiting step of dissolution of drug itself.

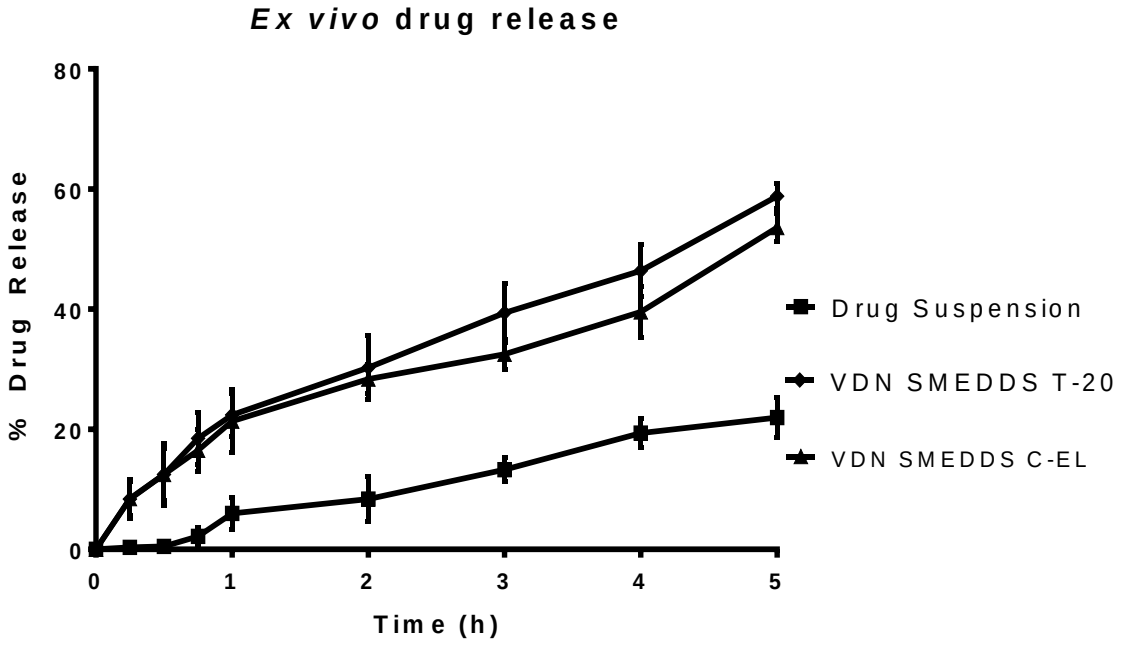

Figure 6.35 Ex vivo drug release of VDN SMEDDS

These results suggest that the physicochemical characteristics of the SMEDDS improved diffusion through the mucosa. The SMEDDS permeation might be associated with a non-specific diffusion process driven by a concentration gradient. It is also important to bear in mind that increased drug solubility might have increased the permeation rate.

The capacity to enhance the permeation of the drug of these formulations is purely based on the nature of the surfactant and specifically on the chemical structure of the surfactant used [44]. While comparing the formulations, the one containing the polysorbates T-20 surfactant enhanced permeation of the drug more than C-EL. It can be owing to the ability of the emulsifying dispersion to interact with the intestinal surface. Surfactants with medium chain were able to interact well with the intestinal cells layer and increase the transport of the drug as in the case of T-20. On the other hand, C-EL showed poor permeation ability for the drug because of its bulky nature which retarded the actual interaction with the cell surface [25]. Thus, from the above results it can be concluded that judicious selection of the SMEDDS excipients are needed for better *in vitro* and *ex vivo* performance of the formulation.

Enhancement ratio (Er) was found to be 1.94 for VDN SMEDDS (C-EL) and 2.25 for VDN SMEDDS (T-20), clearly indicated enhancement in permeation by incorporation of VDN in SMEDDS, which is expected to enhance its absorption and bioavailability. VDN is a BCS II drug, having low solubility and high permeability. Thus, formulation as SMEDDS could significantly enhance its permeability owing to increase in solubility of drug.

6.9.11 Stability – VDN SMEDDS

As per the ICH guideline Q1A (R2) and Q1C, stability studies should be performed on a drug product intended for storage at room temperature for long term and accelerated conditions. Hence, samples of VDN SMEDDS were stored at 25±2°C - 60±5%RH and 40±2°C - 75±5%RH conditions. After the predefined time intervals of 1, 2, 3 and 6 months, SMEDDS samples were analyzed for physico-chemical stability. The results of the evaluations carried out are shown in table 6.15. No significant change in globule size and drug content was observed at the end of 6 months stability study.

Table 6.15 Stability study results of VDN SMEDDS

SMEDDS	VDN SMEDDS (C-EL)			VDN SMEDDS (T-20)		
Time (months)	Long term study (25±2°C - 60±5%RH)					
	Physical description	Globule size (nm)	Drug content (%)	Physical description	Globule size (nm)	Drug content (%)
Initial	Clear liquid	49.98±2.0	98.14±2.6	Yellow liquid	214.50±6.8	97.72±3.1
1	Clear liquid	53.29±2.4	97.36±2.6	Yellow liquid	220.19±4.3	95.28±2.7
2	Clear liquid	48.97±2.4	95.27±3.2	Yellow liquid	217.38±5.3	98.36±3.4
3	Clear liquid	50.53±4.1	97.26±2.5	Yellow liquid	223.42±4.7	96.23±3.1
6	Clear liquid	51.29±2.4	96.36±3.1	Yellow liquid	219.41±5.3	97.12±4.2

	Accelerated study (40±2°C - 75±5%RH)					
1	Clear liquid	52.34±3.2	97.48±2.4	Yellow liquid	219.27±4.5	98.67±1.4
2	Clear liquid	48.83±1.5	95.68±3.2	Yellow liquid	208.28±5.3	98.27±2.2
3	Clear liquid	47.98±2.4	97.37±2.5	Yellow liquid	217.38±3.6	95.67±3.2
6	Clear liquid	48.39±4.2	95.43±3.4	Yellow liquid	215.32±4.5	95.36±2.6

6.10 NIOSOMES – Formulation development

The present investigation describes the preparation and evaluation of ILO niosomes and VDN niosomes along with identification of various critical parameters which affect the particle size and %EE. After identification and selection of critical factors, preliminary investigation was done for critical factors in order to obtain a suitable working range of each factor which was further utilized for optimization of each factor using combined D-optimal design.

6.11 Preliminary Investigation for ILO Niosomes development

6.11.1 Selection of method and surfactant

Retrospective literature along with prior research provided the list of factors which could affect the size and %EE of niosomes. From multiple factors affecting the quality attributes of niosomes, important factors which could have maximum and significant effect on the desired quality attributes of niosomes were selected for preliminary investigation [45].

Table 6.16 Method selection for ILO niosomes preparation

	%EE	Size (nm)
Method of Preparation		
Ethanol Injection	17.30 ± 4.94	169.9 ± 5.26
Reverse Phase Evaporation	4.48 ± 1.27	467.7 ± 7.24
Thin Film Hydration	70.02 ± 5.61	114.4 ± 6.36

For the development of niosomes, selection of the best suited techniques amongst the available techniques is an important criterion. Alongside, selection of surfactant also plays a major role for drug entrapment [46]. Hence, preliminary trials were taken for selection of suitable method to formulate niosomes. Amongst the various methods we tried ethanol injection, thin film hydration and reverse phase evaporation. As the highest entrapment was obtained using thin film hydration technique, it was used for niosomes preparation. The next major factor affecting entrapment is surfactant type. Amongst the Tween and Span series of surfactants, Span 60 showed highest entrapment (70.02 ± 5.61%). Whereas for Span 20 (60.54 ± 2.84%), Span 40

(60.85 ± 3.18%), Span 80 (58.68 ± 4.39%), Tween 20 (57.46 ± 5.36%) and Tween 80 (18.50 ± 3.72%) %EE was very less. Hence, Span 60 was used as surfactant for niosomes preparation.

Major factor considered here was %EE, because it is directly related to the quantity of excipients needed to entrap the drug in the hydrophobic bilayer or hydrophilic cavity. If %EE is less, then we need to add more excipients (i.e. increase drug: lipid ratio) to increase the %EE. This is not practical because it unnecessarily increases the cost of the formulation. Hence, first selection criterion was %EE. After selection of the surfactant on the basis of %EE for niosomes development, the next step was size reduction by optimizing sonication cycles.

Comparing the Span series surfactants, highest entrapment was found in Span 60. The entrapment efficiency is found to be affected by phase transition temperature (T_C) of the surfactant molecule. As Span 60 has highest T_C, this might be the reason behind the highest entrapment efficiency [47]. Comparing the acyl chain length, Span 60 and Span 80 has longest chain of 18 C [48]. However, due to unsaturation in Span 80 owing to oleyl chain, % EE was less in Span 80 niosomes than Span 60 niosomes.

Compared to Span, Tween series of surfactants showed less entrapment. This might be related to HLB values of surfactants as HLB value of the surfactant plays a key role in drug entrapment. A surfactant with higher HLB value in the range of 14–17 is not suitable to produce smaller niosomes whereas the one with an HLB value of ~8 or less gives niosomes with higher entrapment efficiency and smaller size [46]. However, with further decrease in HLB value, entrapment efficiency decreases and size increases. This might be due to the fact that surface free energy decreases with an increase in hydrophobicity of surfactant. Less entrapment of ILO in Tween 80 than Tween 20 might be related to unsaturation in Tween 80 even though the C chain length is longer in Tween 80 than Tween 20.

6.11.2 Risk Analysis and mitigation

After selection of Thin Film Hydration (TFH) method and Span 60 as surfactant, risk analysis was studied for preparation of ILO niosomes using TFH method.

Risk analysis is selection of critical parameters, a small change in which can lead to deterioration in product quality [49]. For identification of formulation and process variables

which have the potential to affect the quality of niosomes, FishBone diagram was created (Figure 6.35) on the basis of literature survey to find the possible factors that might affect niosomes formulation development [49]. Further, selection of high risk factors was carried out by Failure Mode Effective Analysis (FMEA) approach - assigning low, medium and high values to each factor studied [50]. This relative risk ranking system was used throughout for the formulation development (Table 6.15). The quality target for niosomes was smaller size with higher entrapment, as these parameters are related to clinical effectiveness of the formulated niosomes. The factors showing low or medium impact on product were optimized during initial trials by One Variable At a Time (OVAT) approach, whereas the high-risk factors were further taken into consideration to be optimized by factorial design – Combined D-optimal mixture design.

Here, only process and formulation variables were taken into consideration for risk analysis whereas drug substance attributes were considered constant as drug used was of the same lot number for entire work.

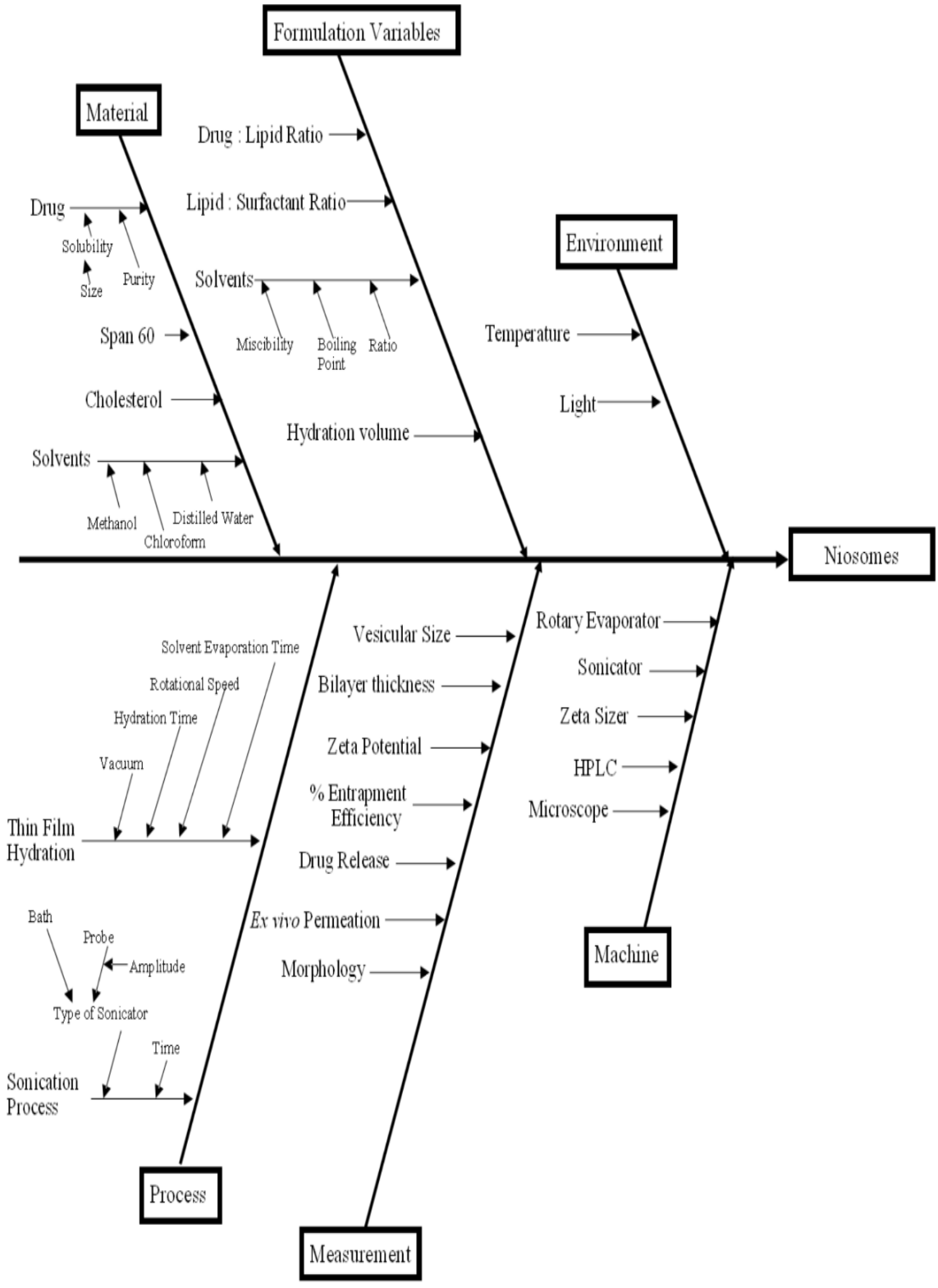

Figure 6.36 Fishbone diagram for selection of factors for niosomes development

Table 6.17 Risk Analysis by FMEA to identify criticality to potential failure causes for niosomes

Drug Product Quality Attributes	**Process Variables**				**Formulation Variables**				**Drug Substance attributes**		
	Solvent evaporation time	Rotation speed	Hydration time	Sonication time amplitude	Drug: Lipid ratio	Lipid: Surfactant ratio	Organic solvents mixture ratio	Hydration volume	Particle Size	Solubility	Degradation products
Size	L	M	M	M	H	H	L	M	-NA-		
Entrapment efficiency	M	L	M	M	H	H	L	M			

6.12 Optimization using OVAT approach

6.12.1 Effect of evaporation time

The presence of residual solvent may lead to physical destabilization of niosomes due to interference in hydrophobic interactions between Span 60's methylene groups which holds the structure together [51]. The lamellar stacking of the surfactant and incorporation of drug inside may be impeded due to presence of the organic solvent. As mixture of organic solvents was used, the polarity of the solvent system gradually changes during solvent evaporation owing to difference in volatility of the component mix. This may lead to different quality of thin film when process parameters are varied [52]. To optimize the process parameter i.e. solvent evaporation time, the ratio of chloroform: methanol mixture was fixed to 2:1 as this combination provided required solubilization capacity for cholesterol and surfactant used herein. The solvent evaporation time was varied from 15 to 60 min (table 6.16).

Table 6.18 Effect of solvent evaporation time on thin film formation

Solvent Evaporation Time	Film appearance	Residual solvent by GC
15 min	Gel like, sticky	-NA-
30 min	Thin, dry film	Pass
45 min	Thin, dry film	Pass
60 min	Dry, brittle film	-NA-

At the end of 15 min, there was gel like appearance of the film which clearly indicated that still more time was needed to evaporate the organic solvent mix. At the end of 30 and 45 min, thin film formation occurred. At the end of 60 min, brittle film was formed which was difficult to remove easily from RBF after hydration step.

To check whether there was residual solvent remaining or not at the end of 30 min and 45 min, GC analysis was carried out. For both the trials, the batches passed in residual solvent analysis. At the end of 30 min and 45 min, residual solvent was below maximum allowed limit [53].

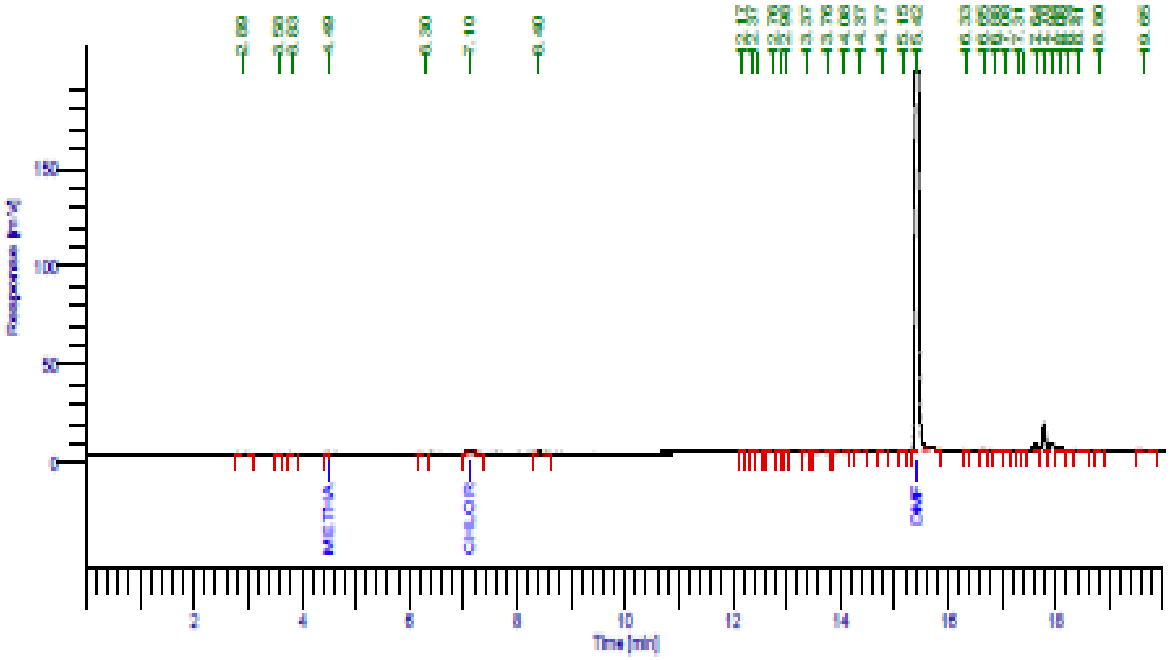

Figure 6.37 GC chromatograph at the end of 30 min of solvent evaporation time

At the end of 30 min of solvent evaporation time, methanol concentration was found to be 0.90 ppm whereas chloroform was 11.11 ppm for niosomes formulation development (Figure 6.37). As the concentration of both the organic solvents was under residual solvent limit approved by FDA guidelines, 30 min of solvent evaporation time was used. As 30 min was found to be sufficient for solvent evaporation, it was taken as the optimized time for solvent evaporation as proper drying and thin film formation occurred.

6.12.2 Effect of rotation speed

A) Optimization of rotation speed for thin film formation

Depending on the rotation speed for RBF, there will be change in effective surface area for evaporation during film formation [54]. The speed at which the round bottom flask rotates affects the uniformity and thickness of the film which after hydration leads to large variation in particle size and polydispersity index. To control the particle size, the rotation speed needs to be optimized [55]. The rotation speed was varied between 50 to 150 rpm (Table 6.17). At low speeds of 50 and 75 rpm, the film was thick and exhibited gel like structure due to inefficient

solvent evaporation, whereas at higher speed of 150 rpm, non-uniform distribution of film was observed. Variable thickness of film was produced with thicker film in the center and thinner film at the periphery. Adequate speed of rotation was found to be 125 rpm as it formed thin, uniform and dry film.

B) Optimization of rotation speed during hydration

Rotation speed during hydration along with hydration time affects the quality of film, further affecting size and the entrapment efficiency of niosomes. At low rotation speed, incomplete hydration of the thin film was observed while higher speed of 100 rpm caused improper removal of film (Table 6.17). 75 rpm speed, which showed complete hydration of film was selected.

Table 6.19 Optimization of rotation speed

Rotation Speed for film formation (rpm)		Rotation Speed for hydration (rpm)	
50	Thick, Gel like	25	Incomplete hydration
75	Thick, Gel like	50	
100	Thin, Uniform, Sticky	75	Complete hydration
125	Thin, Uniform, Dry	100	Improper removal of film
150	Non-uniform distribution	-	-

6.12.3 Effect of hydration time

Optimization of hydration time was based upon highest entrapment efficiency. After hydration, MLVs formation takes place during which the drug gets incorporated inside the vesicles. Sufficient hydration time with intermittent shaking of RBF is necessary for complete hydration of the film, as it leads to formation of proper vesicular structure. Lesser hydration time leads to incomplete film removal from the RBF which may affect quality of niosomes and decrease the drug entrapment.

30 min hydration time led to improper hydration leaving behind gel in RBF whereas 45 min time showed complete hydration with entrapment efficiency of 70.02 ± 5.61% of ILO. 30 min hydration time might be less time for formation of vesicles. Beyond 45 min times, 60 to 90 min time of hydration was also tried but no significant increase in EE was observed.

Table 6.20 Effect of hydration time

Hydration Time	Film removal	%EE
30 min	Incomplete film removal	-
45 min	Complete hydration	70.02 ± 5.61
60 min		72.62 ± 4.61
90 min		74.42 ± 6.61

6.12.4 Effect of hydration volume

For hydration, distilled water and pH 6.8 buffer were tried but as no significant difference was observed in %EE while comparing the two media, distilled water was used for further experiments. Change in the hydration media volume from 3 to 9 mL showed significant effect on entrapment. With increase in hydration volume, increase in %EE may be due to increased interaction between hydrophobic drug ILO and the lipid layer. 3 mL of distilled water might be insufficient for removal of thin film which may have led to decrease in %EE. As volume was increased from 3 to 6 mL, there was increase in %EE. However, there was no significant increase in %EE when 9 mL media volume was used. Hence, 6 mL distilled water was considered as optimized.

Table 6.21 Effect of hydration volume

Hydration Volume (mL)	Film removal	%EE
3	Incomplete film removal	42.75 ± 4.28
6	Complete hydration	70.02 ± 5.61
9		73.76 ± 6.36

6.12.5 Effect of sonication

Sonication is required to convert the micro sized vesicular suspension to nano size as it affects permeation through intestine and release of drug. As compared to bath sonication, probe sonication gives smaller vesicular size as it provides higher energy [56]. So, the prepared Multi Lamellar Vesicles (MLV) suspension was subjected to probe sonication cycles. Based on the vesicular size and entrapment, sonication cycle was optimized. The optimized sonication cycle was found to be 2 as compared to 1 and 3, as it provided EE of 70.02 ± 5.61% of ILO with average vesicular size of 114.4 ± 6.36 nm niosomes. Increase in sonication cycle showed great impact on size, reducing it to less than 100 nm but at the cost of decrease in %EE. After every sonication cycle, 1 min of annealing time was given to allow the reformation of MLVs to SUVs. During this, the vesicular layer forms which incorporates drug inside the layer. When higher sonication cycles were tried, the smaller sized vesicles formed but as MLVs (>1 bilayer) convert to SUVs (1 bilayer), the number of bilayers decreases which decreased entrapment [57].

Table 6.22 Effect of Sonication cycles

Sonication Cycle	Size (nm)	%EE
1	215.21± 6.28	73.16 ± 3.36
2	114.40 ± 6.36	70.02 ± 5.61
3	92.28 ± 8.36	64.26 ± 3.29

Table 6.21 enlists the optimized range of variables after preliminary studies. Keeping these variables as constant, the high-risk parameters were optimized by design of experiment strategy.

Table 6.23 Optimized values of process parameters for Niosomes preparation

Parameter	Optimized value
Solvent evaporation time	30 min
Rotation speed for thin film formation	125 rpm
Rotation speed for hydration	75 rpm
Hydration time	45 min
Hydration volume	6 mL
Sonication cycle	2 cycles

6.13 Design of Experiment – Combined D-optimal mixture design for optimization of ILO niosomes

Combined D-optimal mixture design is a custom type of optimal mixture design in which mixture component can be combined with numeric component. Here, we took Span 60 and cholesterol as mixture component and Drug (ILO) as numeric component.

As Span 60 and cholesterol are mixture components, whose total should be 10, the range covered by design was 7:3 to 9:1 (Span 60: cholesterol). Whereas drug being numeric component, it was between 1 to 2. Accordingly, Drug: Lipid ratio between 2:10 (i.e. 1:5) to 1:10 was studied.

6.13.1 Design matrix

Table 6.24 design matrix for ILO Niosomes

Run	Span 60 (A)	Cholesterol (B)	Drug (C)	%EE (R1)	Size (R2)
F1	8.5	1.5	1.25	86.83 ± 3.26	107.3 ± 2.28
F2	7	3	2	27.54 ± 4.24	257.5 ± 4.28
F3	8	2	2	78.23 ± 2.73	116.9 ± 5.27
F4	7	3	2	30.45 ± 4.62	262.1 ± 5.28
F5	8	2	1.5	88.72 ± 3.28	115.6 ± 2.26
F6	9	1	1	75.38 ± 4.28	250.4 ± 4.26
F7	7	3	1.25	80.46 ± 4.26	120.2 ± 4.62
F8	8.5	1.5	1.75	77.36 ± 3.96	117.1 ± 2.28
F9	7.5	2.5	1.75	74.53 ± 2.48	111.2 ± 1.39
F10	9	1	1.5	86.12 ± 3.18	107.9 ± 3.25
F11	7	3	1	85.23 ± 4.52	130.2 ± 3.19
F12	9	1	1	72.31 ± 4.28	254.1 ± 3.78
F13	8	2	1	89.67 ± 3.28	120.8 ± 3.29
F14	7	3	1.5	73.50 ± 4.28	112.3 ± 3.28
F15	7.5	2.5	1.25	90.61 ± 5.27	123.3 ± 2.49
F16	9	1	2	54.78 ± 5.57	123.5 ± 4.24
F17	7	3	1	88.66 ± 4.28	135.6 ± 3.19
F18	8	2	2	75.49 ± 3.86	112.5 ± 5.27
F19	9	1	2	50.15 ± 3.28	112.1 ± 4.28

As shown in table 6.22, 19 niosomes formulations were prepared as per combined D-optimal design matrix. All the formulations were evaluated for %EE and size.

6.13.2 Effect of independent variables on %EE

The obtained %EE for each formulation is observed in Table 6.22. The %EE varied from 27.54 ± 4.62 (F2) to 90.61 ± 5.27% (F15) indicated multicollinearity of the studied factors. From the statistical analysis (figure 6.38), we can observe that R^2 value for actual v/s predicted values for %EE was 0.9761 which is a good correlation.

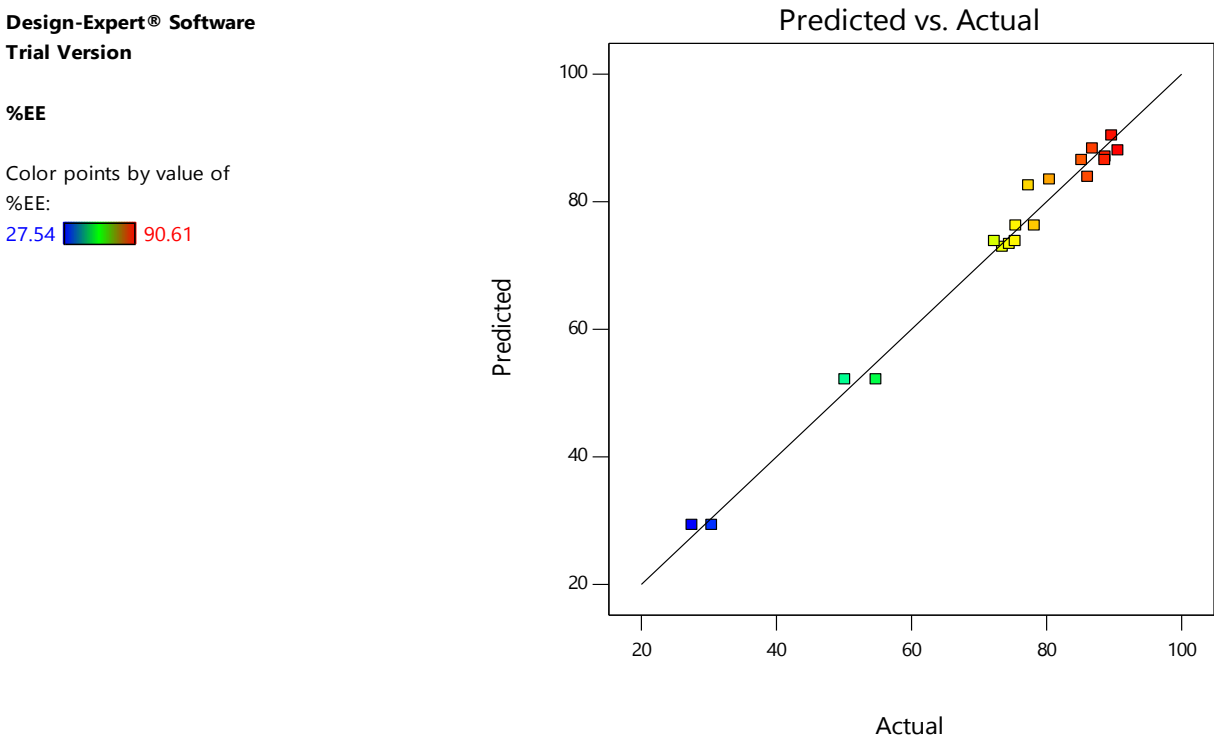

Figure 6.38 Predicted vs Actual plot for %EE

Overall effect analysis in terms of coefficients of coded factors indicated multicollinearity (table 6.23).

Table 6.25 Coefficients in terms of coded factors for %EE predictors

Component	Coefficient estimate	VIF
A-Span 60	83.89	6.33
B-Cholesterol	72.92	4.97
AB	34.64	6.33
AC	-10.84	1.24
BC	-28.61	1.25
ABC	50.68	1.59
AC^2	-20.92	5.52
BC^2	-15.00	4.48
ABC^2	56.77	5.08

The results of ANOVA prove that the model was significant to study the effect of selected variables on %EE (Table 6.24).

Table 6.26 Statistical analysis for %EE

Source	Sum of Squares	df	Mean Square	F-value	p-value	
Model	6355.75	8	794.47	92.73	< 0.0001	significant
Linear Mixture	53.89	1	53.89	6.29	0.0310	
AB	73.99	1	73.99	8.64	0.0148	
AC	478.89	1	478.89	55.89	< 0.0001	
BC	3470.76	1	3470.76	405.10	< 0.0001	
ABC	360.65	1	360.65	42.09	< 0.0001	
AC^2	382.77	1	382.77	44.68	< 0.0001	
BC^2	245.57	1	245.57	28.66	0.0003	
ABC^2	124.60	1	124.60	14.54	0.0034	
Residual	85.68	10	8.57			
Lack of Fit	56.38	5	11.28	1.92		Not significant
Pure Error	29.30	5	5.86			
Cor Total	6441.43	18				

The obtained results from reduced model of estimate analysis of critical variables on %EE for niosomes shows that the factors have both positive and negative effect on response (equation 6.3).

Final equation of effect analysis was:

$$\%EE = 83.89A + 72.92B + 34.64AB - 10.84AC - 28.61BC + 50.68ABC - 20.92AC^2 - 15.00BC^2 + 56.77ABC^2 \quad \text{….. Equation 6.3}$$

The complex interdependent effect of factors on R1 can be observed from the contour plot (Figure 6.39). We can observe that increase in cholesterol increased %EE but up to a certain range of drug amount (1.5), after that there is steep decrease in %EE. Whereas at 8:2 Span 60: cholesterol ratio, highest entrapment is found even at drug amount up to 1.8.

At 7:3:2 (F4) level, %EE was low (~30%), which indicated requirement of more surfactant to encapsulate the drug, whereas, at 8:2:2 (F18) level, more encapsulation of drug was confirmed (~80%). However, still increasing the ratio to 9:1:2 (F19) indicated decrease in %EE (54%). This indicates that at constant drug amount, by increasing surfactant from 7:3 to 8:2, there might be encapsulation of drug inside the hydrophobic pockets formed by acyl chain of Span 60. Whereas, still increase in surfactant concentration showed negative effect on %EE. This might be due to leakiness of the bilayer, as less quantity of cholesterol is not adequate enough to provide stiffness [58].

Here, the amount of drug varies from 1 to 2. Hence, the ratio of drug(A): lipid(B+C) is 1:10 to 2:10 (i.e. 1:5). Hence, from 1:5 to 1:10 ratio, there is increase in %EE. This is due to increased availability of lipid for solubilization and entrapment of drug molecules inside the bilayer formed by surfactant and cholesterol.

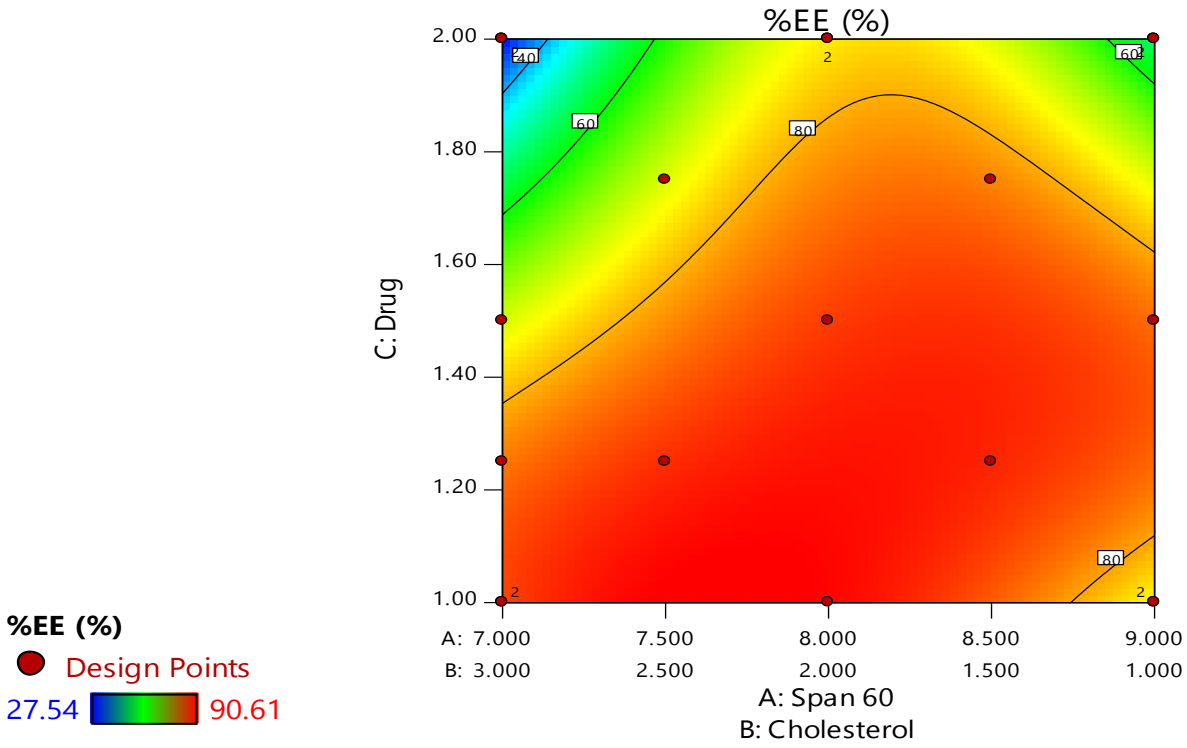

Figure 6.39 Contour plot showing effect of independent variables on %EE

6.13.3 Effect of independent variables on Size

The obtained size for each formulation is observed in Table 6.22. The size varied from 107.3 ± 2.28 (F1) to 262.1 ± 5.28 nm (F4) indicated multicollinearity of the studied factors. From the statistical analysis (figure 6.37), we can observe that R^2 value for actual v/s predicted values for size was 0.9959 which is a good correlation.

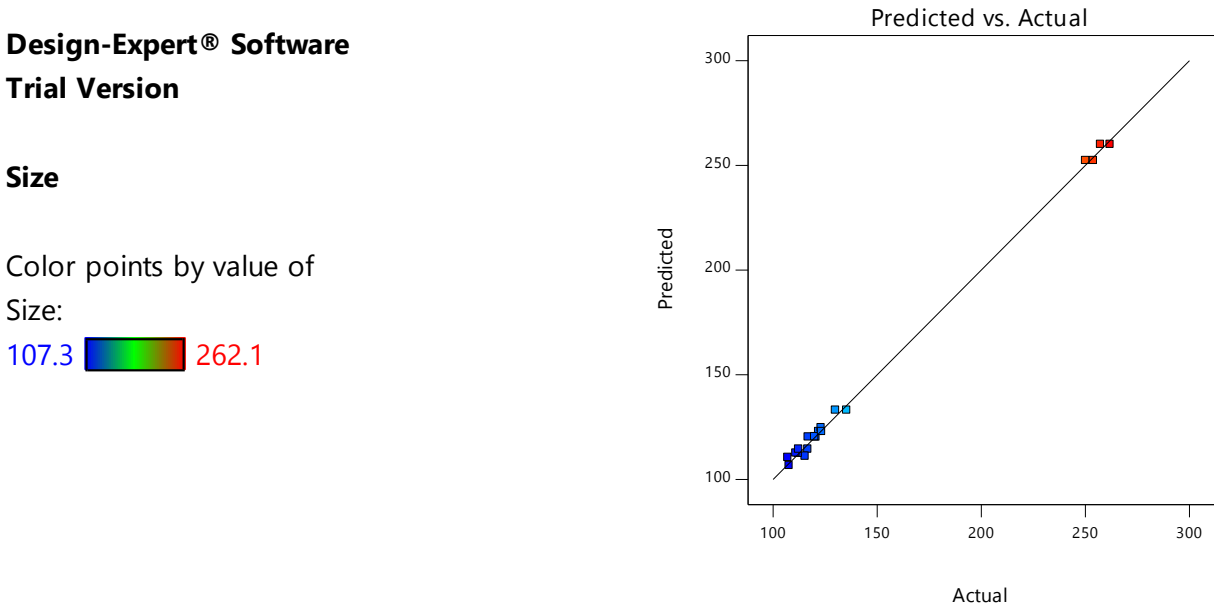

Figure 6.40 Predicted vs Actual plot for size

Overall effect analysis in terms of coefficients of coded factors indicated multicollinearity (table 6.25).

Table 6.27 Coefficients in terms of coded factors for size predictors

Component	Coefficient estimate	VIF
A-Span 60	106.44	6.35
B-Cholesterol	112.18	7.23
AB	6.26	7.08
AC	114.70	198.31
BC	13.57	56.99
ABC	-346.14	124.28
AC^2	80.96	5.53
BC^2	84.16	5.60
ABC^2	-305.11	5.41
AC^3	-179.42	188.82
BC^3	49.88	53.32
ABC^3	337.28	108.47

The results of ANOVA prove that the model was significant to study the effect of selected variables on size (Table 6.26).

Table 6.28 Statistical analysis for Size

Source	Sum of Squares	df	Mean Square	F-value	p-value	
Model	60645.99	11	5513.27	434.17	< 0.0001	significant
Linear Mixture	25.78	1	25.78	2.03	0.1972	
AB	2.16	1	2.16	0.1702	0.6923	
AC	335.84	1	335.84	26.45	0.0013	
BC	17.17	1	17.17	1.35	0.2830	
ABC	214.66	1	214.66	16.90	0.0045	
AC^2	5719.46	1	5719.46	450.41	< 0.0001	
BC^2	6180.53	1	6180.53	486.72	< 0.0001	
ABC^2	3375.06	1	3375.06	265.79	< 0.0001	
AC^3	813.18	1	813.18	64.04	< 0.0001	
BC^3	223.25	1	223.25	17.58	0.0041	
ABC^3	198.95	1	198.95	15.67	0.0055	
Residual	88.89	7	12.70			
Lack of Fit	46.22	2	23.11	2.71	0.1596	Not significant
Pure Error	42.67	5	8.53			
Cor Total	60734.88	18				

The obtained results from reduced model of estimate analysis of critical variables on size for niosomes shows that the factors have both positive and negative effect on response (equation 6.4)

Final equation of effect analysis was:

$$Size = 106.44A + 112.18B + 6.26AB + 114.70AC + 13.57BC - 346.14ABC + 80.96AC^2 + 84.16BC^2 - 305.11ABC^2 - 179.42AC^3 + 49.88BC^3 + 337.28ABC^3 \ldots..\text{Equation 6.4}$$

The complex interdependent effect of factors on R2 can be observed from the contour plot (Figure 6.41). We can observe that there is a complex effect of variables on the size. As observed, at extremities, size is more whereas at the intermediate level, size is in desirable range (<200 nm). Highest size is observed when drug: lipid ratio is less (2:10 or 1:5). This is due to insufficient quantity of lipid to encapsulate the drug.

Cholesterol doesn't form a bilayer itself but it gets dissolved in the Span 60's bilayer. After a point, at higher concentration of cholesterol, irrespective of amount of Span 60, more cholesterol molecules will be distributed in the surfactant bilayer, leading to swelling of the bilayer. This might have increased in the niosomes mean diameter [59]. Cholesterol had a positive impact on size of niosomes. At 7:**3**:2 (F4), highest size was observed. Decrease in cholesterol from 7:**3**:2 (F4) to 8:**2**:2 (F3) indicated decrease in size in a steep fashion. At higher amount of cholesterol (7:3:2 – F4), cholesterol molecules get incorporated into Span 60's bilayers. The small hydrophilic head group (3ß-hydroxyl) of cholesterol is located in the vicinity of C=O of ester of Span 60, and the hydrophobic steroid ring orients itself parallel to the alkyl group of fatty acid (stearic acid) of Span 60. Thus, the movement of the acyl chains of the Span 60's bilayer gets restricted leading to failure of tight packing arrangement of other Span 60 molecules. This explains the direct increase of niosomes size observed at 7:3 Span 60: Cholesterol ratio. Then as the ratio was changed to 8:2, mean diameter of the niosomes decreased due to increased amount of Span 60 which resulted in tight packing of niosomes. But at 9:**1**:2 (F19), as Span 60 increased, it tended to align itself on the outer surface of niosomes, ultimately leading to increase in mean diameter of niosomes [60,61].

Considering the effect of drug, the trend was found to be increased with changing ratio from 1:5 to 1:10 (drug: lipid). This can be attributed to increased lipid content per drug molecule.

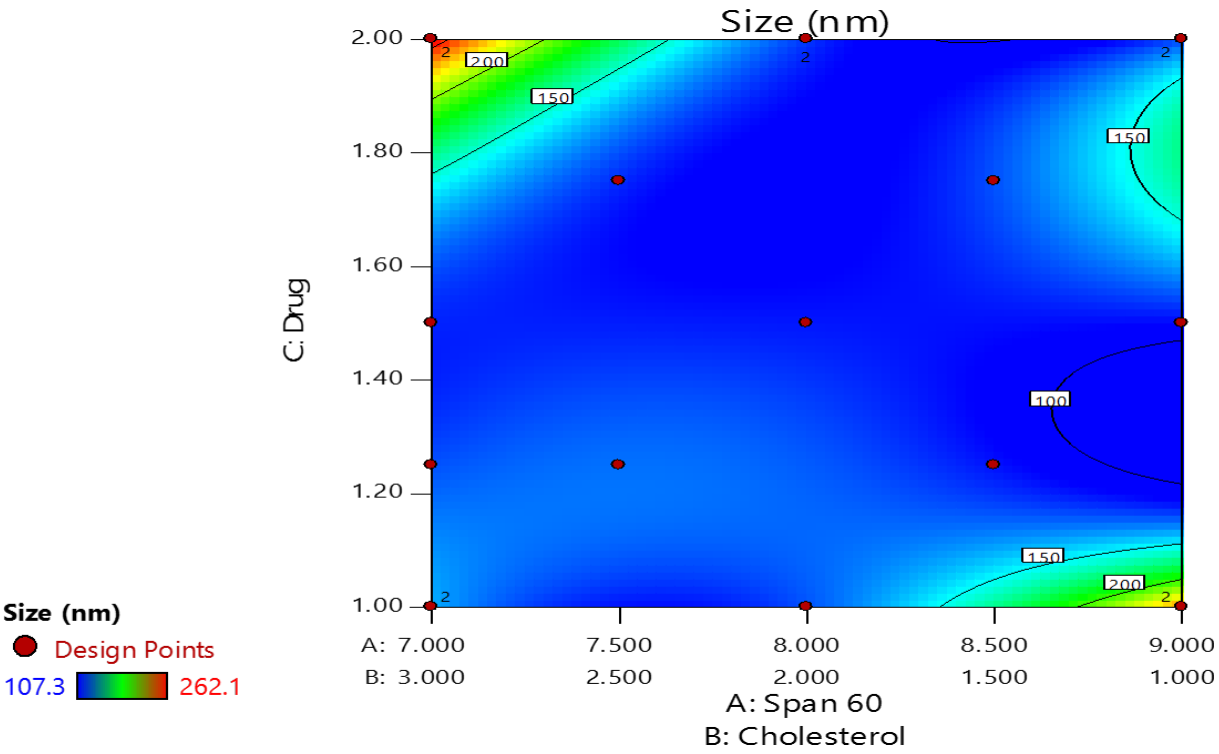

Figure 6.41 Contour plot showing effect of independent variables on Size

6.13.4 Numerical optimization using desirability function

To carry out optimization using mathematical function – desirability criteria was used and desirability plot was generated. For this, upper or lower desired values of response were selected, based on which software generated values of variables which would help to achieve the desired response. The ramp graph indicates the predicted values of R1 and R2 for the optimized concentration of independent variables, whereas, the bar graph indicates individual desirability for R1 and R2 (Figure 6.41). The composite desirability for the predicted response was found to be 0.997.

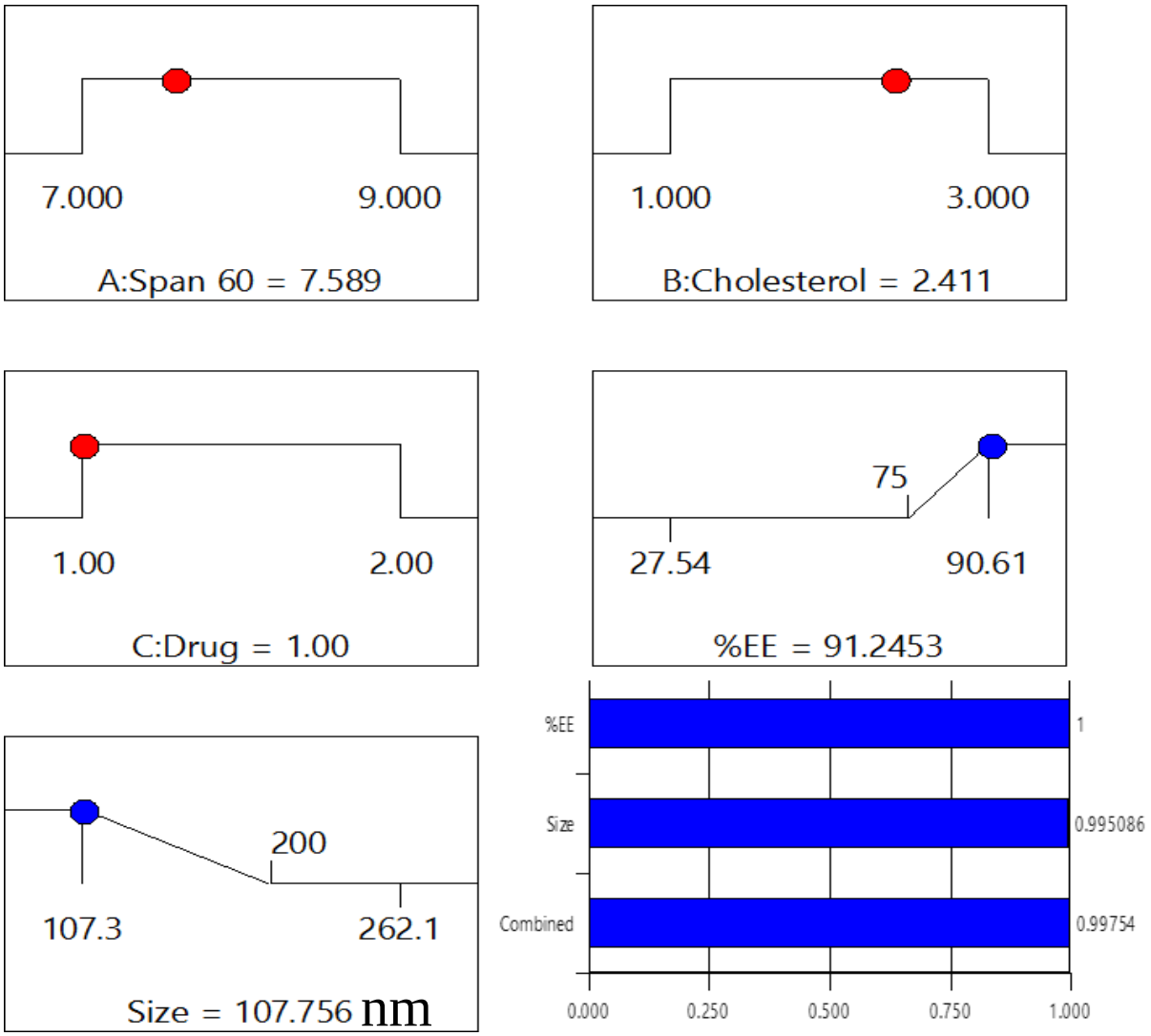

Figure 6.42 Desirability plot for ILO Niosomes

To assess the suitability of the desirability, ILO Niosomes formulation was prepared as per suggested batch and obtained values of responses were found to be comparable with the predicted responses. Moreover, error was found to be less than 5%, indicated suitability of the design for prediction (table 6.23).

Table 6.29 Predicted and obtained responses for ILO Niosomes prepared as per numerical optimization

Response	Span 60 (A)	Cholesterol (B)	Drug (C)	%EE (R1)	Size (nm) (R2)	Desirability
Predicted	7.589	2.411	1.000	91.24	107.75	0.997
Observed	7.589	2.411	1.000	87.57±5.26	112.1±7.26	-
% Error	-	-	-	4.02	4.03	-

Thus, the final optimized formulation consisted of Drug: Lipid in 1:10 ratio and Span 60:Cholesterol in 7.811:2.189 ratio as per numerical optimization of combined D-optimal design.

6.13.5 Graphical optimization to generate control space

As it is observed that there might be possibility that a slight change in the composition due to practical error might lead to failure of batch, we found control space, using graphical optimization technique. This approach makes the design robust by narrowing the design space by applying one sided (inside the design space) 95% tolerance interval to the responses. Figure 6.42 indicates the control space obtained after applying one sided tolerance interval at alpha level of 0.05. For R1, the lower constraint was 75% EE and for R2, the upper constraint was fixed to 200 nm size. Working inside the control space or ± 5% change in the composition provided by control space won't affect the desired response.

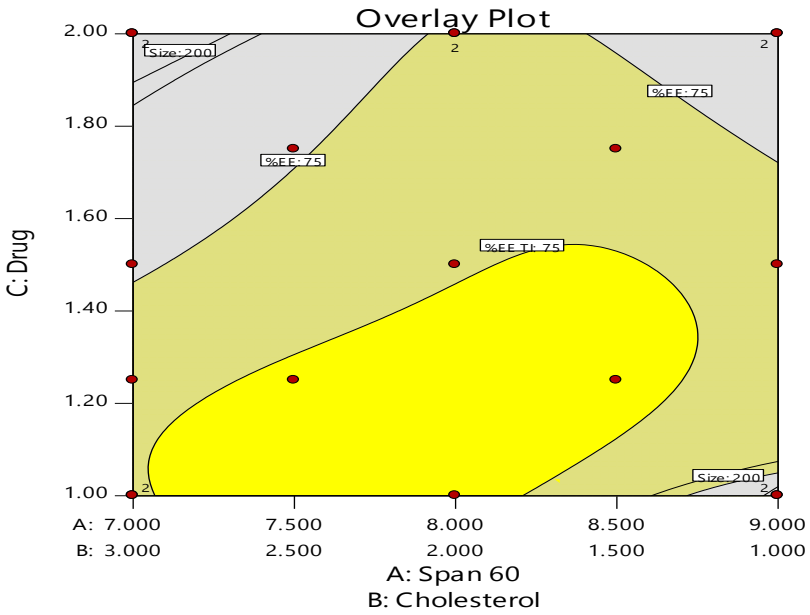

Figure 6.43 Control space for ILO Niosomes

6.14 VDN Niosomes development

Here, for the development of VDN Niosomes, we adopted the in-house optimized niosomal formulation technology developed for ILO Niosomes. The aim was to assess the niosomes developed using a risk-based approach in combination with QbD, for one drug (ILO) can be used for another drug, VDN. For VDN niosomes development, we used optimized process and formulation parameters as of ILO niosomes.

6.15 Design of Experiment – Combined D-optimal mixture design for optimization of VDN niosomes

Combined D-optimal mixture design is a custom type of optimal mixture design in which mixture component can be combined with numeric component. Here, we have taken Span 60 and cholesterol as mixture component and Drug (VDN) as numeric component.

As Span 60 and cholesterol are mixture components, which total should be 10, so the range covered by design will be 7:3 to 9:1 (Span 60:cholesterol). Whereas drug being numeric component, it will be between 1 to 2. Hence, Drug: Lipid ratio we studied was between 2:10 (i.e. 1:5) to 1:10.

6.15.1 Design matrix

Table 6.30 Design matrix for VDN Niosomes

Run	Span 60 (A)	Cholesterol (B)	Drug (C)	%EE (R1)	Size (R2)
F1	8.500	1.500	1.25	79.09 ± 3.28	164.9 ± 4.92
F2	8.500	1.500	1.75	79.31 ± 3.58	168.4 ± 4.38
F3	7.000	3.000	1.00	77.68 ± 5.39	186.9 ± 3.49
F4	7.000	3.000	2.00	70.55 ± 5.39	232.4 ± 5.43
F5	7.000	3.000	2.00	64.90 ± 5.39	228.6 ± 5.43
F6	8.000	2.000	2.00	78.67 ± 4.29	218.3 ± 4.58
F7	9.000	1.000	2.00	75.38 ± 5.29	279.9 ± 4.20
F8	7.500	2.500	1.75	86.57 ± 2.49	231.4 ± 3.58
F9	9.000	1.000	1.00	67.04 ± 4.29	263.9 ± 4.28
F10	7.500	2.500	1.25	86.38 ± 4.39	98.4 ± 6.49
F11	8.000	2.000	1.00	84.74 ± 2.59	184.2 ± 5.48
F12	9.000	1.000	2.00	72.91 ± 5.29	275.4 ± 4.20
F13	7.000	3.000	1.50	92.03 ± 3.29	220.1 ± 3.49
F14	9.000	1.000	1.50	89.46 ± 2.48	180.5 ± 3.28
F15	8.000	2.000	1.50	95.46 ± 3.29	174.2 ± 5.28
F16	7.000	3.000	1.00	75.96 ± 5.39	184.3 ± 3.49
F17	7.000	3.000	1.25	66.25 ± 4.39	117.4 ± 4.39
F18	9.000	1.000	1.00	62.90 ± 4.29	258.9 ± 4.28
F19	8.000	2.000	2.00	74.96 ± 4.29	212.5 ± 4.58

As shown in table 6.28, 19 batches of VDN niosomes were prepared as per combined D-optimal design matrix. All the formulations were evaluated for %EE and size.

6.15.2 Effect of Span 60 and Cholesterol (surfactant: cholesterol ratio)

Effect of various levels of Span 60: Cholesterol was studied from 7:3 to 9:1 ratio as shown in table 6.28. The desired responses selected were entrapment efficiency (R1) and size (R2). At

7:3 (F4) level, %EE was low (~70%), which indicated requirement of more surfactant to encapsulate the drug. %EE increased when ratio was increased to 8:2. This indicates that by increasing surfactant from 7:3 to 8:2, there might be encapsulation of drug inside the hydrophobic pockets formed by acyl chain of Span 60. However, still increasing the ratio to 9:1 indicated decrease in %EE (~75%). This might be due to leakiness of the bilayer, as less quantity of cholesterol is not adequate enough to provide stiffness [60].

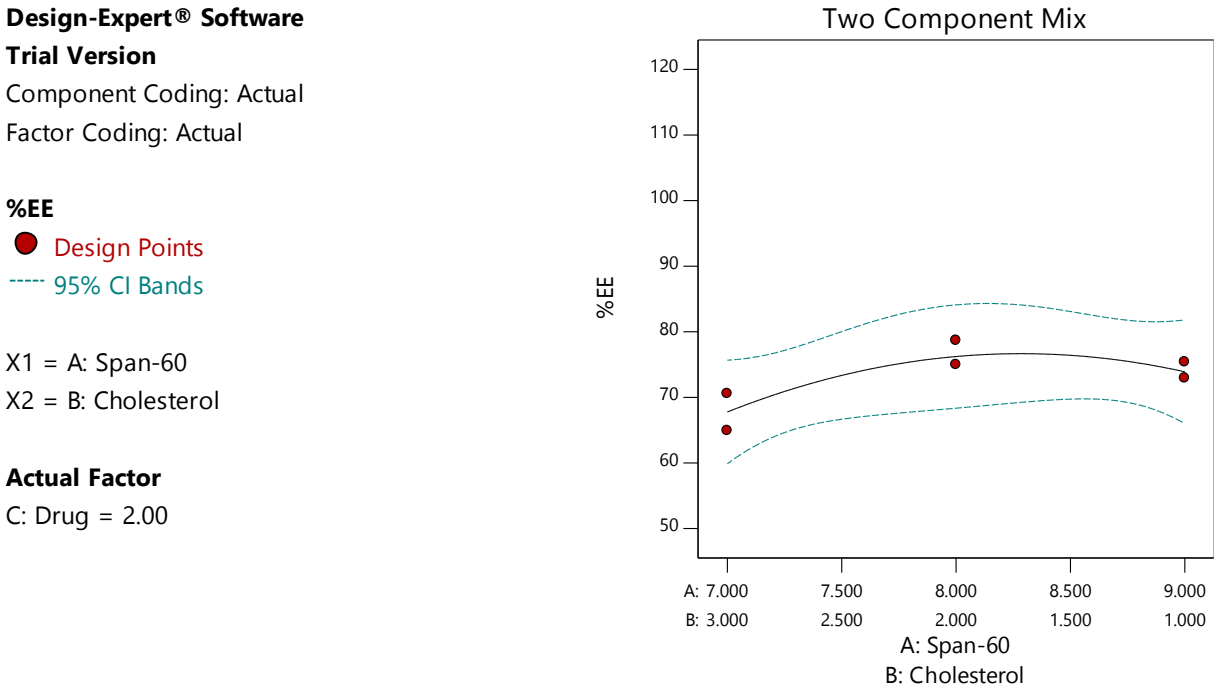

Figure 6.44 Effect of Span 60 and cholesterol on %EE

On size also, similar trend was found as %EE. At 7:3 ratio, highest size was observed while at 8:2 ratio, size decreased. But at 9:1 ratio, there was increase in size. At higher amount of cholesterol (7:3 ratio), cholesterol molecules get incorporated into SPAN 60's bilayers. At 8:2 ratio, mean diameter of the niosomes decreased due to increased amount of Span 60 which resulted in tight packing of niosomes. But after this, at 9:1 ratio, as Span 60 increased, it tends to align itself on outer surface of niosomes, ultimately leading to increase in mean diameter of niosomes.

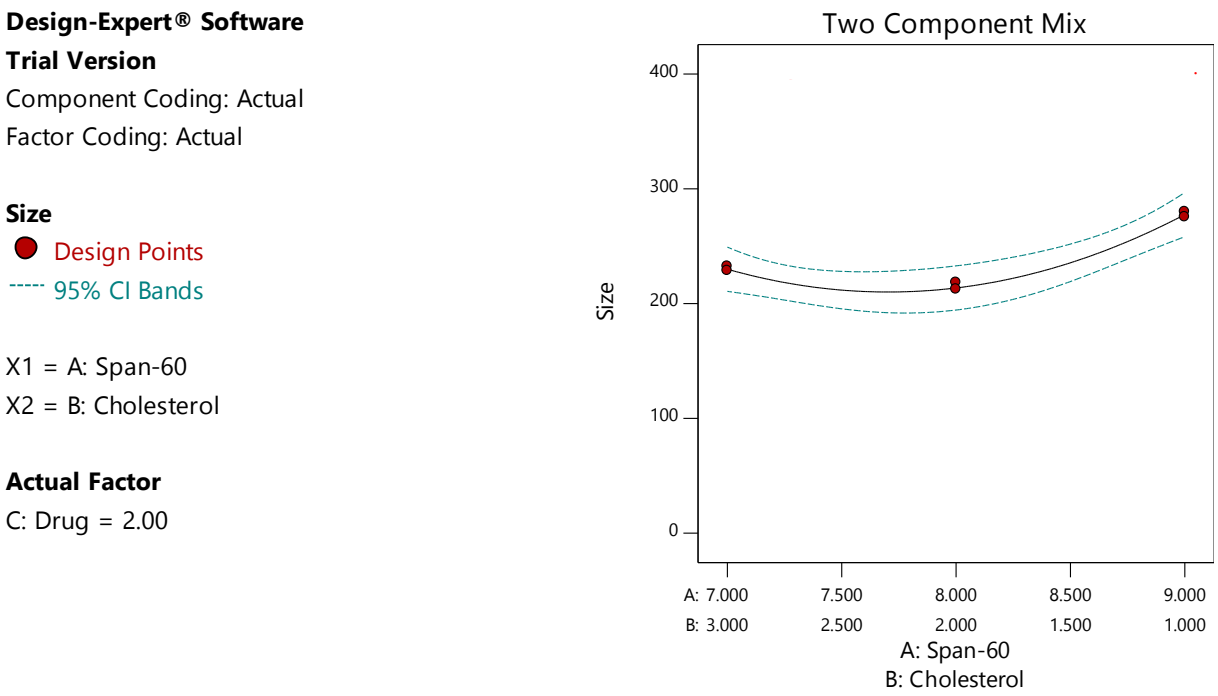

Figure 6.45 Effect of Span 60 and cholesterol on Size

6.15.3 Effect of Drug

More than 80% EE was found up to 1.5 parts of drug. Highest entrapment was found at 1.25 parts of drug when Span 60: cholesterol is 8:2, might be due to increased availability of lipid for solubilization and entrapment of drug molecules inside the bilayer. However, after that, still increasing drug amount did not show any increase in %EE. This might be due to less amount of lipid available for encapsulation.

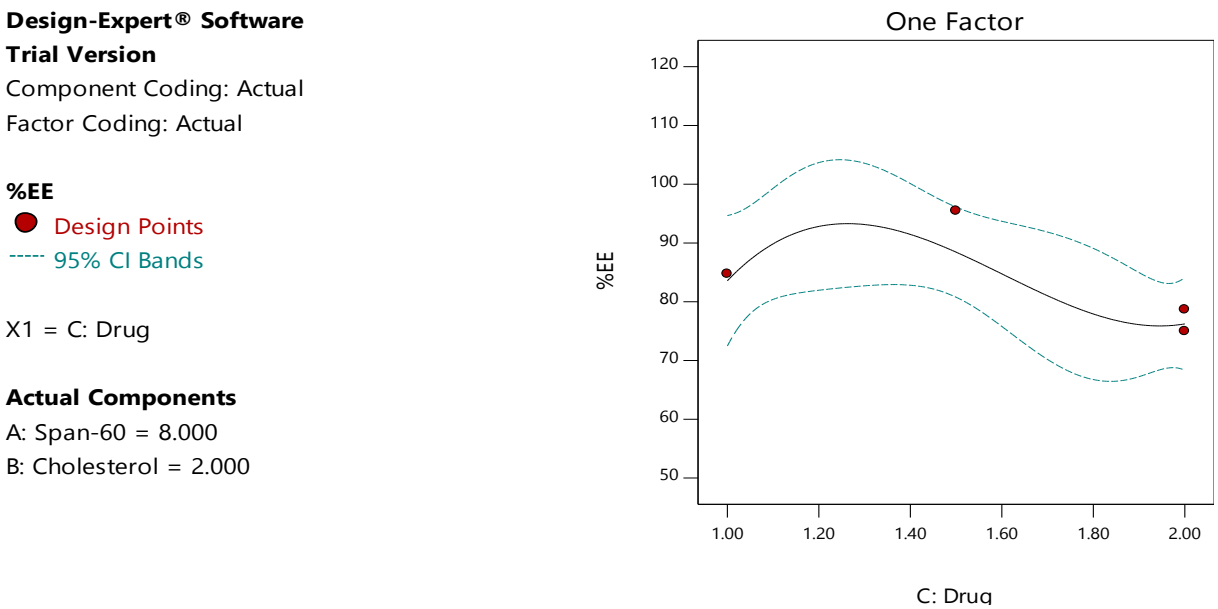

Figure 6.46 Effect of drug on %EE

From 1 to 1.25 parts of drug, there was decrease in size, whereas after that increasing drug amount led to increase in size as shown in figure 6.47.

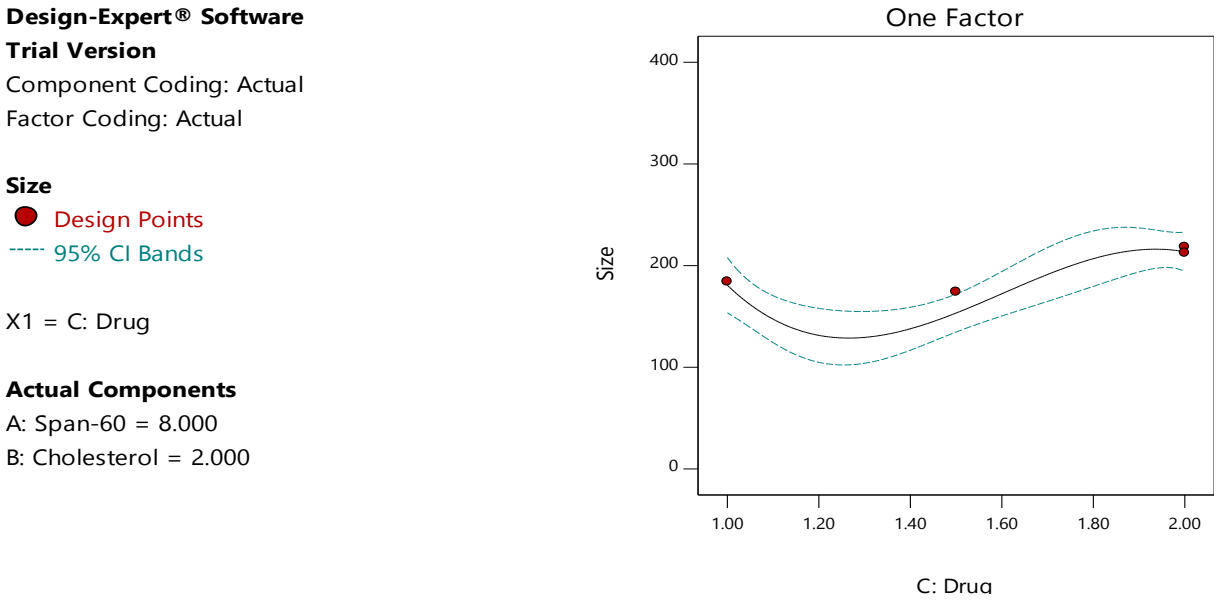

Figure 6.47 Effect of drug on Size

6.15.4 Effect of independent variables on %EE

The obtained %EE for each formulation is observed in Table 6.24. The %EE varied from 62.90 ± 4.29 (F18) to 95.46 ± 3.29 (F15) indicated multicollinearity of the studied factors.

Final coded equation for effect of independent variables on %EE was:

$$\%EE = 86.52A + 92.55B - 5.41AB + 56.56AC + 59.05BC - 303.33ABC - 15.55AC^2 - 18.39BC^2 + 38.34ABC^2 - 52.39AC^3 - 62.62BC^3 + 291.19ABC^3 \quad \text{…. Equation 6.5}$$

Equation 6.5 indicates multi-collinearity amongst the independent variables.

Contour plot (2D) for %EE is shown in figure 6.48 and 3D plot for the same is shown in figure 6.49.

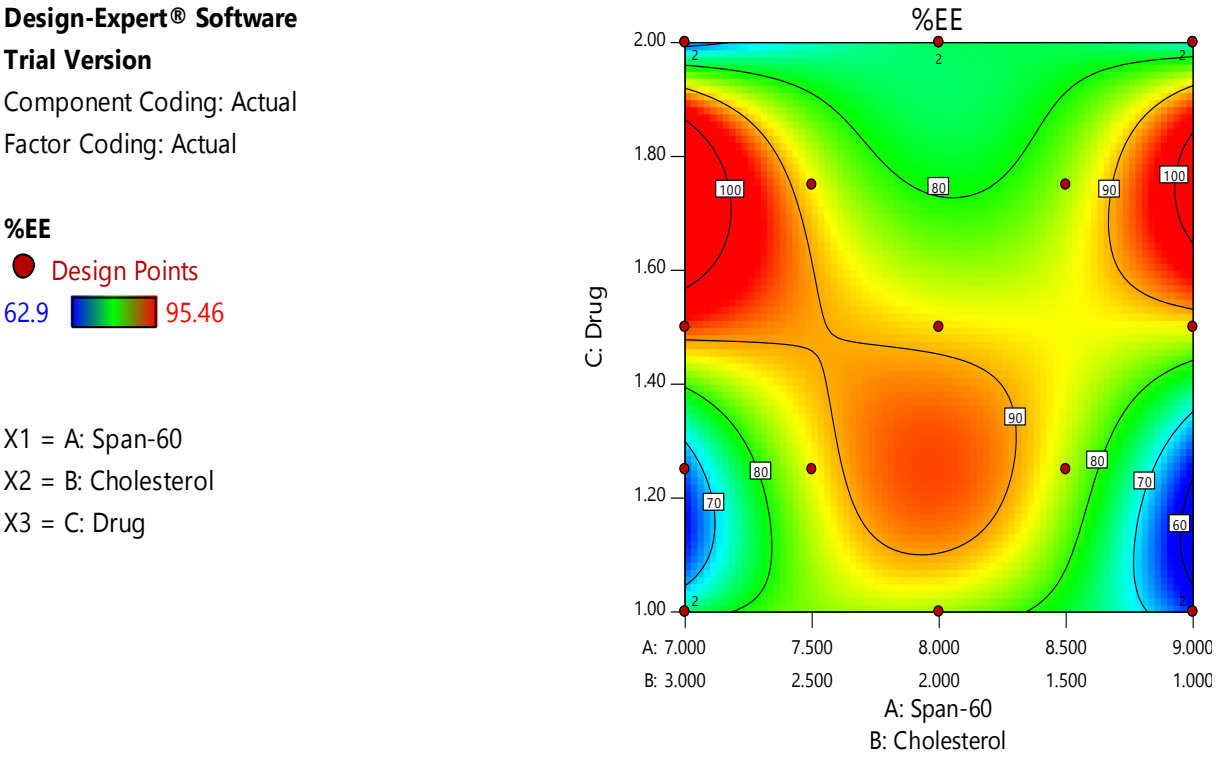

Figure 6.48 2D contour plot showing effect of independent variables on %EE

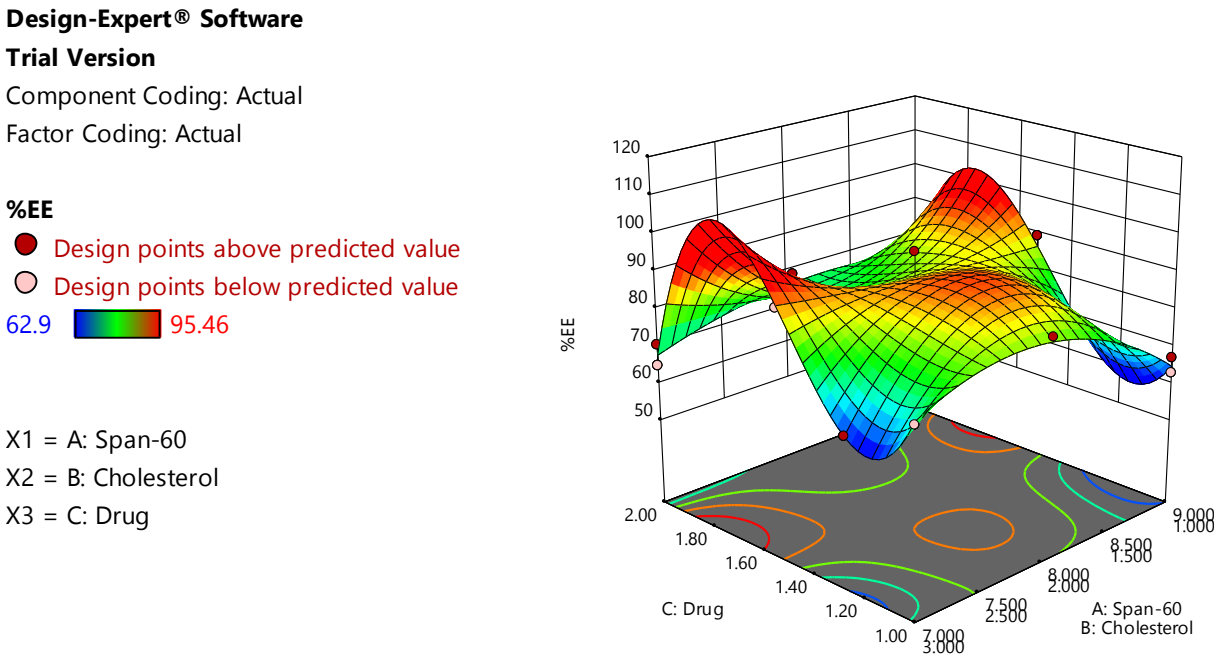

Figure 6.49 3D plot showing complex interaction of independent variables for %EE

6.15.5 Effect of independent variables on Size

The obtained size for each formulation is observed in Table 6.24. The size varied from 98.4 ± 6.49 (F10) to 279.9 ± 4.20 (F7) indicated multicollinearity of the studied factors.

Final coded equation for effect of independent variables on size is:

$$Size = 179.53A + 214.00B - 175.15AB - 93.64AC + 246.77BC + 46.25ABC + 92.29AC^2 - 4.86BC^2 + 7.62ABC^2 + 101.64AC^3 - 224.02BC^3 - 36.01ABC^3 \quad \text{…. Equation 6.6}$$

Equation 6.6 indicates multi-collinearity amongst the independent variables.

Contour plot (2D) for size is shown in figure 6.50 and 3D plot for the same is shown in figure 6.51. From the 2D or 3D plot, we can study the complex interdependence of independent variables on size.

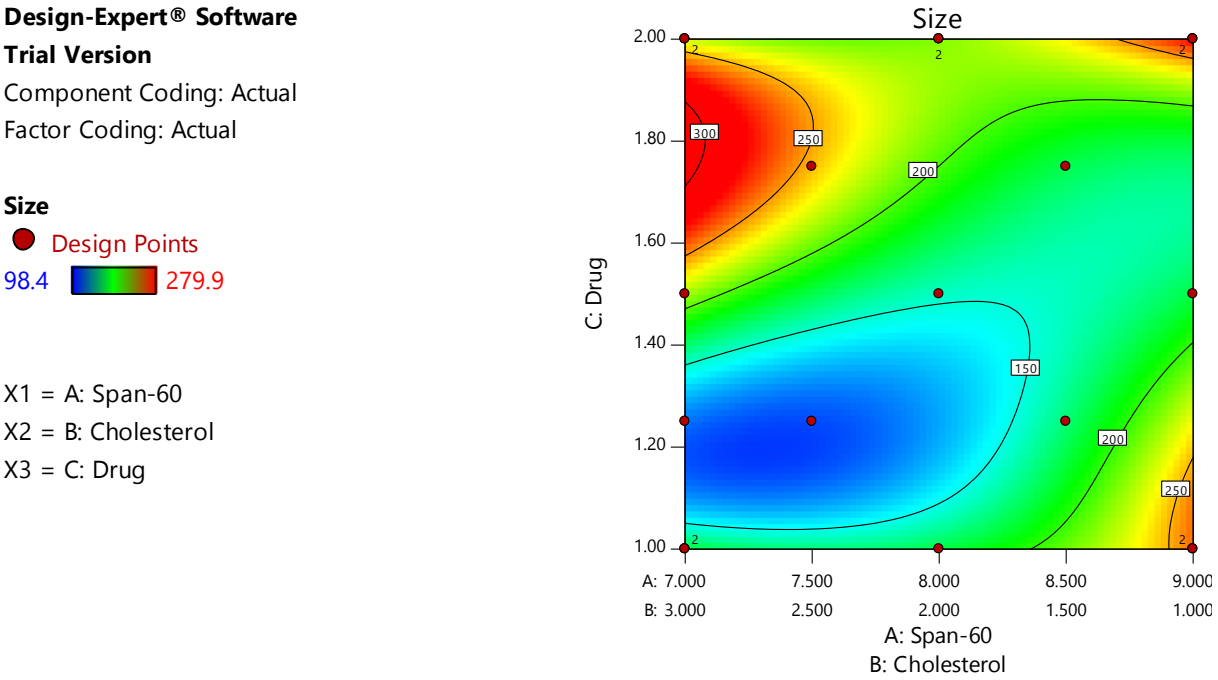

Figure 6.50 2D contour plot showing effect of independent variables on size

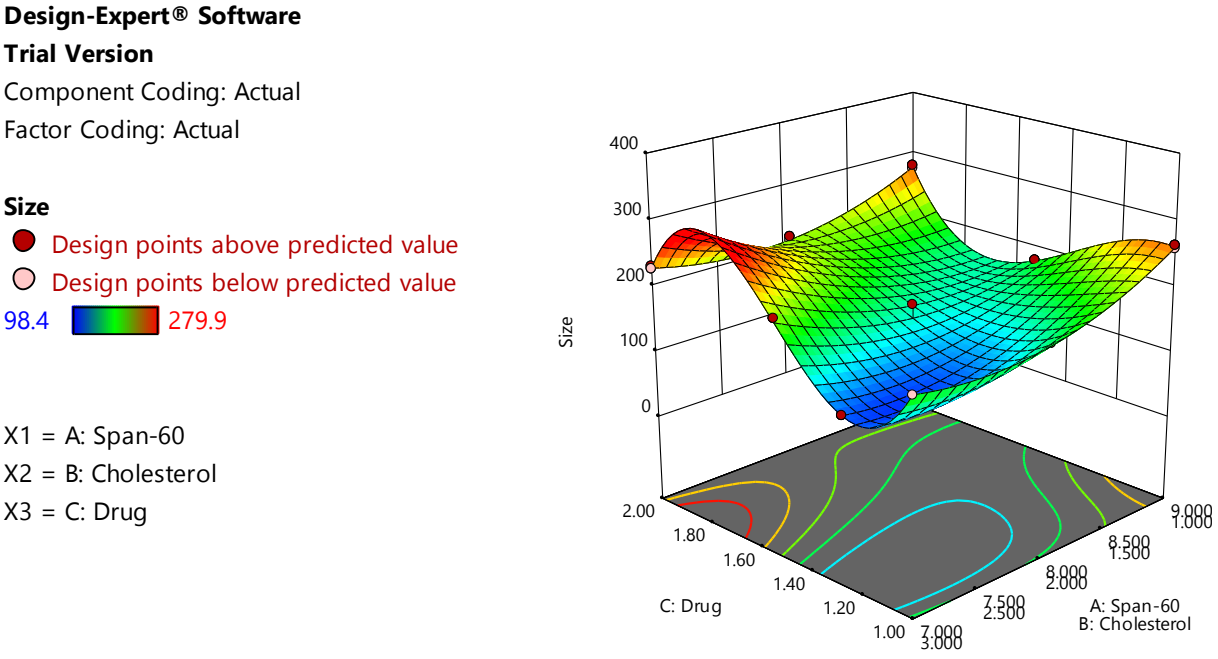

Figure 6.51 3D plot showing complex interaction of independent variables for size

6.15.6 Coefficients Table for independent variables of VDN Niosomes

From the table 6.29, we can observe p-Value for each co-efficient of independent terms that effects %EE and size in VDN niosomes formulation development. p-value less than 0.05 have been highlighted with black bold numerical. This indicates that these factors or their interaction terms have significant effect on the desired response. The equation of the same has already been given. (see equation 6.5 and equation 6.6).

Table 6.31 p-Value of coefficients for independent variables

	A	B	AB	AC	BC	ABC	AC^2	BC^2	ABC^2	AC^3	BC^3	ABC^3
%EE	86.5539	92.5984	-4.51696	55.2943	**58.2593**	**-296.467**	**-17.2386**	**-20.2786**	40.85	-50.7068	**-62.8068**	**281.706**
p-value	0.5971	0.5971	0.8288	0.1039	**0.0071**	**0.0328**	**0.0114**	**0.0051**	0.1440	0.1321	**0.0053**	**0.0415**
Size	**179.618**	**214.031**	**-173.907**	-94.6835	**245.875**	53.4036	**89.8333**	-6.4867	8.6897	102.809	**-223.425**	-48.6782
p-value	**0.0002**	**0.0002**	**0.0095**	0.2314	**0.0003**	0.8503	**0.0002**	0.6159	0.8901	0.1999	**0.0007**	0.8650

6.15.7 Numerical optimization using desirability function

To carry out optimization using mathematical function – desirability criteria was used. For this, desirability plot was generated (figure 6.51). According to color coding, we can find that there are two regions having highest desirability of ~0.8. For this, Drug amount and Span 60: Cholesterol ratio can be read from the desirability plot.

To assess the suitability of the desirability, VDN Niosomes formulation was prepared as per suggested batch and obtained values of responses were found to be comparable with the predicted responses. Moreover, error was found to be less than 5% which indicated suitability of the design for prediction (table 6.30).

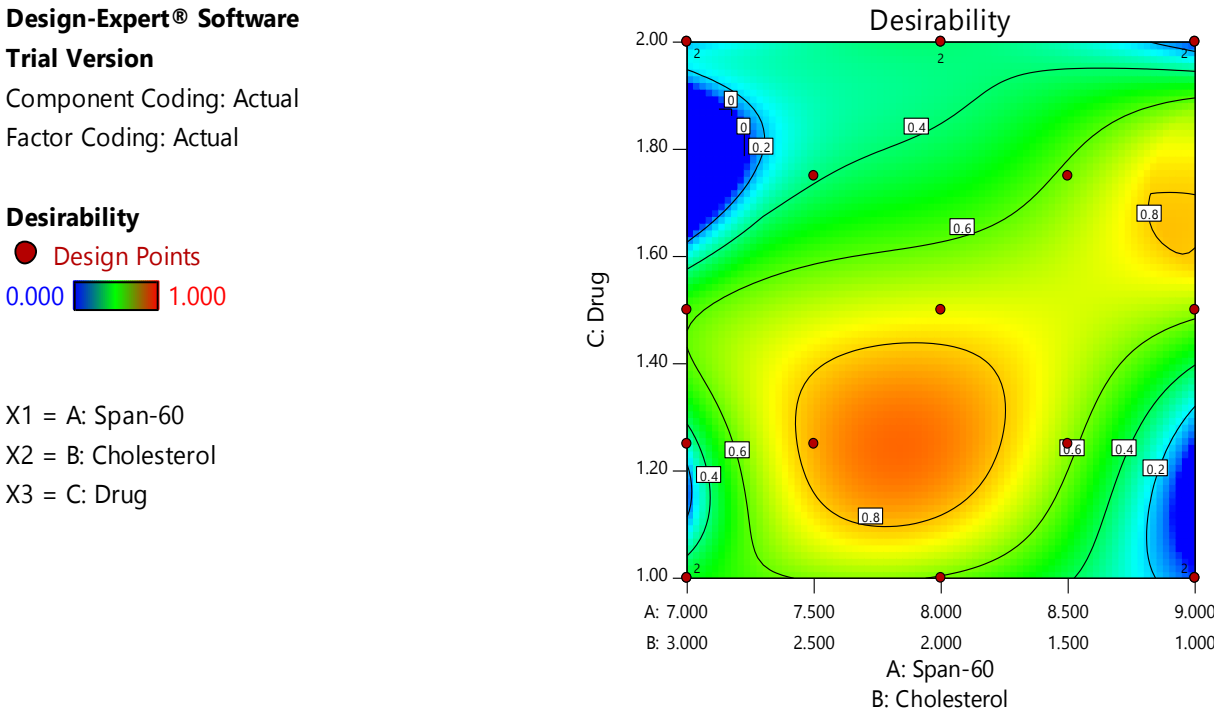

Figure 6.52 Desirability plot for VDN Niosomes

Table 6.32 Predicted and obtained responses for VDN Niosomes prepared as per numerical optimization

Span 60 (A)	Cholesterol (B)	Drug (C)	Response	%EE (R1)	Size (nm) (R2)	Desirability
7.882	2.178	1.25	Predicted	92.81	119.86	0.900
7.882	2.178	1.25	Observed	89.3±4.29	124.5±3.74	-
-	-	-	% Error	3.78	3.87	-

Final optimized formulation of VDN Niosomes was Drug: Lipid in 1:8 ratio and Span 60: cholesterol in 7.882:2.178 ratio as per numerical optimization of combined D-optimal design.

6.15.8 Graphical optimization to generate control space

Figure 6.53 indicates the control space obtained after applying one sided tolerance interval at alpha level of 0.05. For R1 the lower constraint was 75% EE and for R2 upper constraint was fixed to 200 nm size. Working inside the control space or ± 5% change in the composition provided by control space won't affect the desired response.

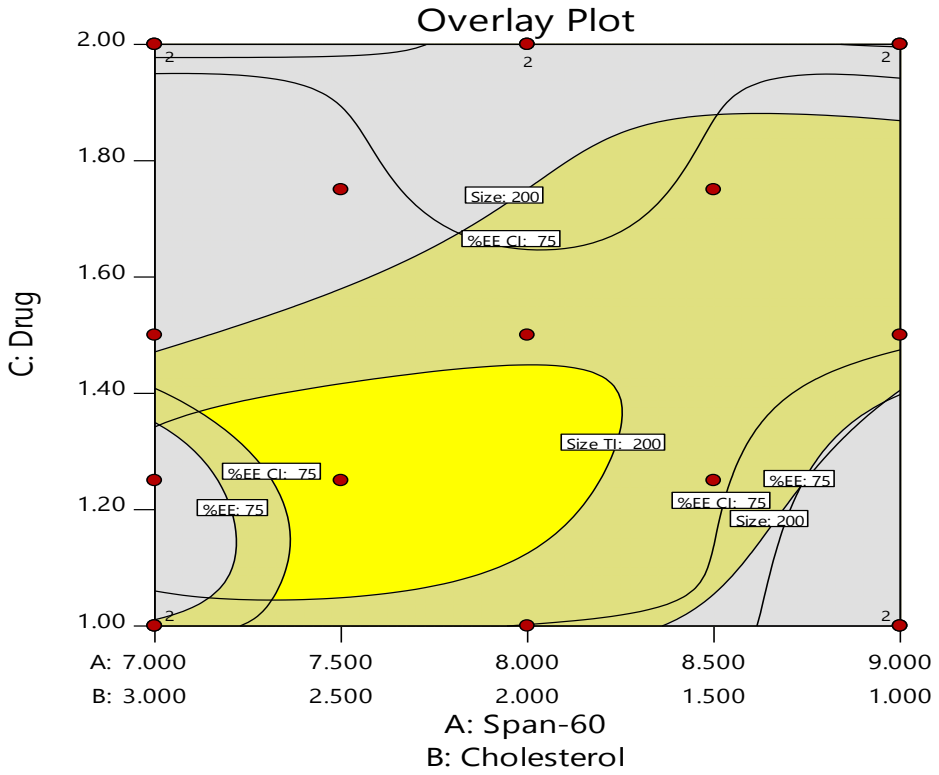

Figure 6.53 Overlay plot showing control space for VDN Niosomes

6.16 Optimization of Cryoprotectant for Lyophilization of ILO and VDN Niosomes

Freeze-drying has been the most utilized drying method for nanoparticulate formulations as this technique is a promising way to increase the chemical and physical stability over extended period of time. Transformation of the niosomes like nanoparticulate suspension into solid form

prevents Ostwlad ripening. Hence, it is expected that lyophilized solid powder will have better chemical and physical stability than aqueous dispersions [62]. Cryoprotectants decrease the osmotic activity of water and crystallization as well during freezing steps. It favors the glassy state of the frozen samples by acting as "space holders" between niosomes to prevent contact. Moreover, by interacting with polar head groups of surfactants of niosomes it serves as a "pseudo hydration shell". Hence, it is expected that niosomes size would increase after lyophilization, because niosomes tend to aggregate during lyophilization. If the aggregated niosomes do not separate during re-dispersion, then mean diameter of niosomes will be increased.

Cryoprotectant, present at niosomes surface, protects the niosomes from aggregation and make sure the re-dispersion requires a minimum of energy, being attributed to the formation of a steric barrier between the niosomes during lyophilization [63].

Table 6.31 depicts the effect of mannitol concentration on the size of ILO and VDN niosomes after reconstituting the lyophilized powder with double distilled water. The results showed that mannitol at 1:4 w/w was effective cryoprotectant in preventing niosomes from aggregation during lyophilization process. At lower concentration of mannitol, formulations had poor re-dispersity whereas, at higher concentration of 1:5 w/w, 30 sec bath sonication was required to re-disperse.

Table 6.33 Mean diameter (nm) measured by DLS technique

	ILO niosomes	VDN niosomes
Before lyophilization	112.1±7.26	124.5±3.74
After lyophilization		
Niosomes: mannitol ratio		
1:2	394.8±13.40	489.1±12.39
1:3	179.8±9.38	242.0±15.39
1:4	137.9±11.38	142.4±10.20
1:5	163.2±8.49	151.6±13.29

6.17 Characterization of ILO and VDN Niosomes

6.17.1 Bilayer thickness measurement

As shown in figure 6.54 and figure 6.55, scattering intensity was recorded for ILO niosomes and VDN niosomes using SANS technique. Absence of Bragg's peak in both the images indicates large uni-lamellar structure of niosomes [64]. After fitting the data using core shell model (spherical core with bilayer shell) using SASfit software (Version: 0.94.8), the average thickness of the bilayer was found to be 4.2 nm and 4.3 nm for ILO niosomes and VDN niosomes respectively, whereas for blank niosomes the bilayer thickness was found to be 2.4 and 2.7 nm respectively (Figure 6.56 and Figure 6.57) Hence, increase in thickness of bilayer for drug loaded formulations indicated encapsulation of drug inside the bilayer.

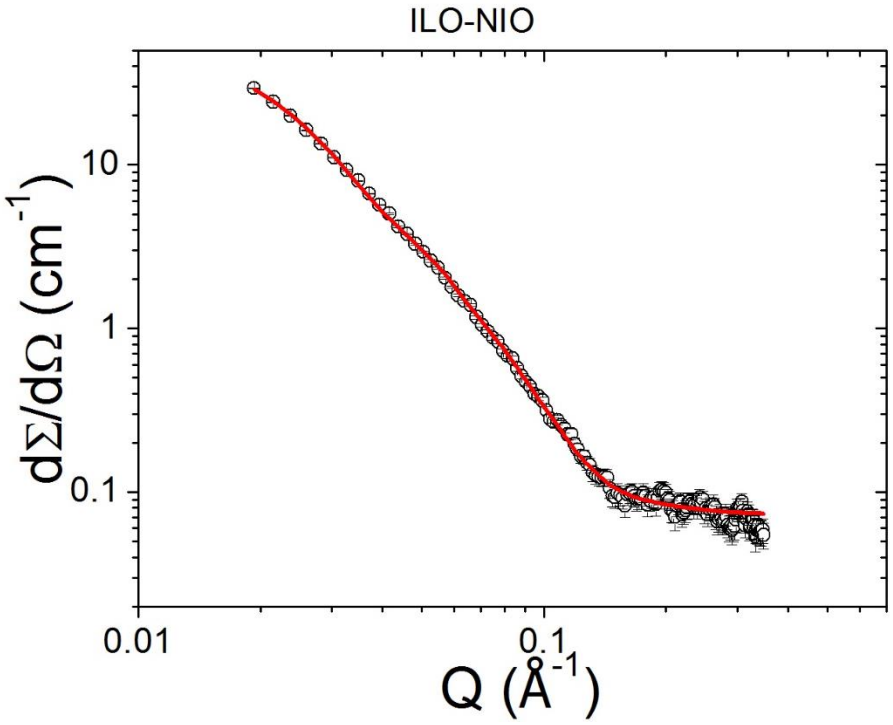

Figure 6.54 Bilayer thickness measurement of ILO niosomes using SANS

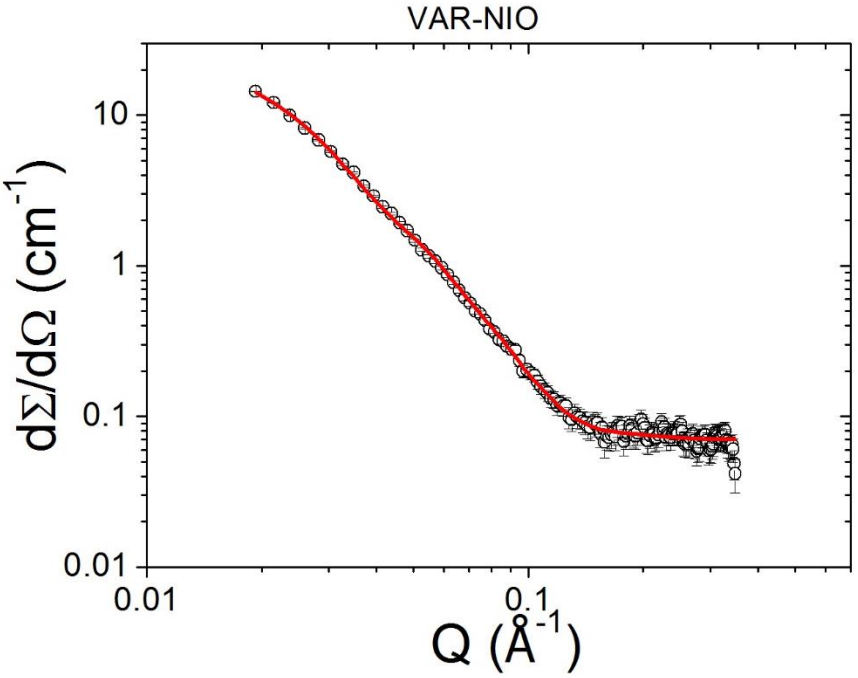

Figure 6.55 Bilayer thickness measurement of VDN niosomes using SANS

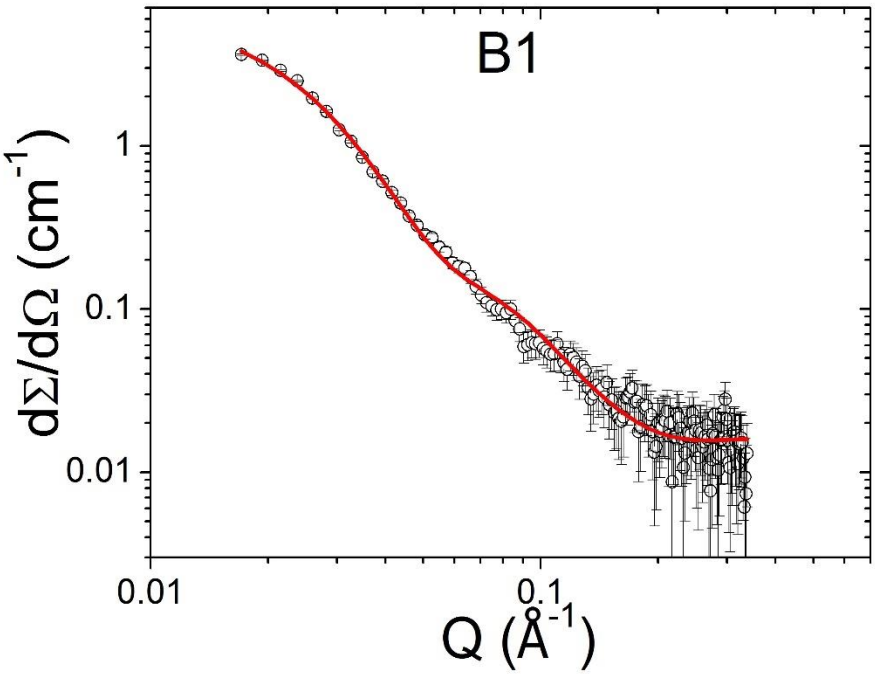

Figure 6.56 Bilayer thickness of blank niosomes prepared as per ILO Niosomes optimized formula

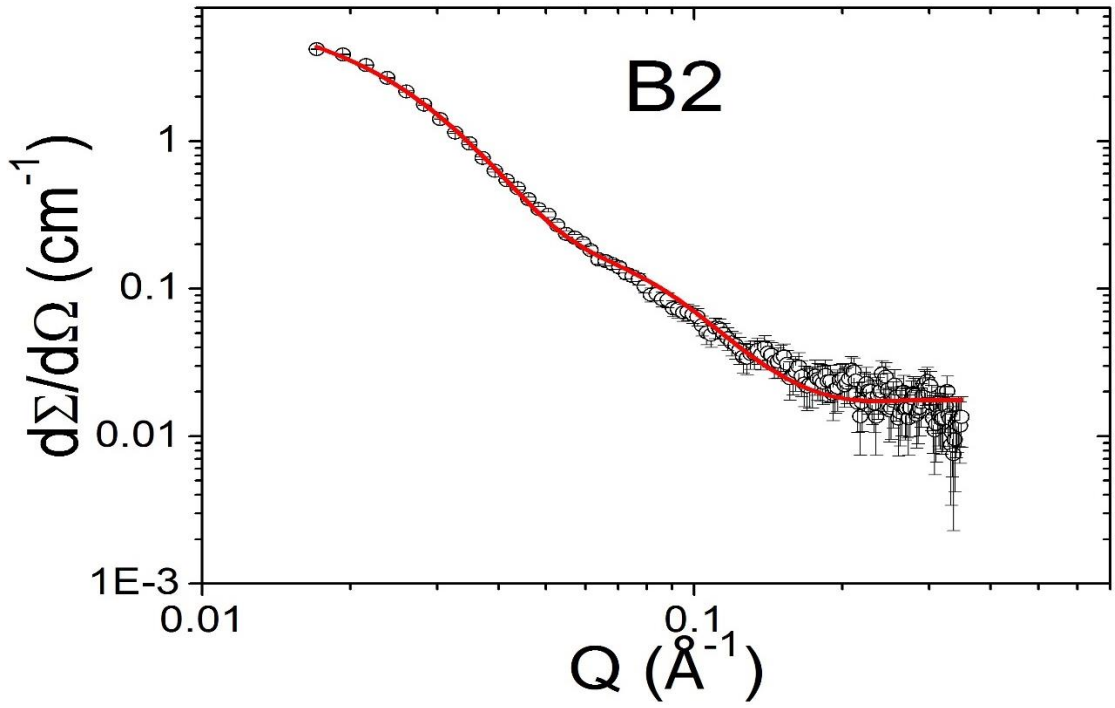

Figure 6.57 Bilayer thickness of blank niosomes prepared as per VDN Niosomes optimized formula

6.17.2 Surface Morphology

Cryo-TEM is a preferred technique for imaging of niosomes in their intact state [65]. Figure 6.57 depicts the cryo-TEM image of the optimized formulation, in which niosomes were found to be of spherical shape. Formulated niosomes had a mean diameter of around 112.1±7.26 nm for ILO niosomes and 124.5±3.74 nm for VDN niosomes when measured using zetasizer which was also confirmed by cryo-TEM image. The size observed in cryo-TEM was found to be nearly 100 nm.

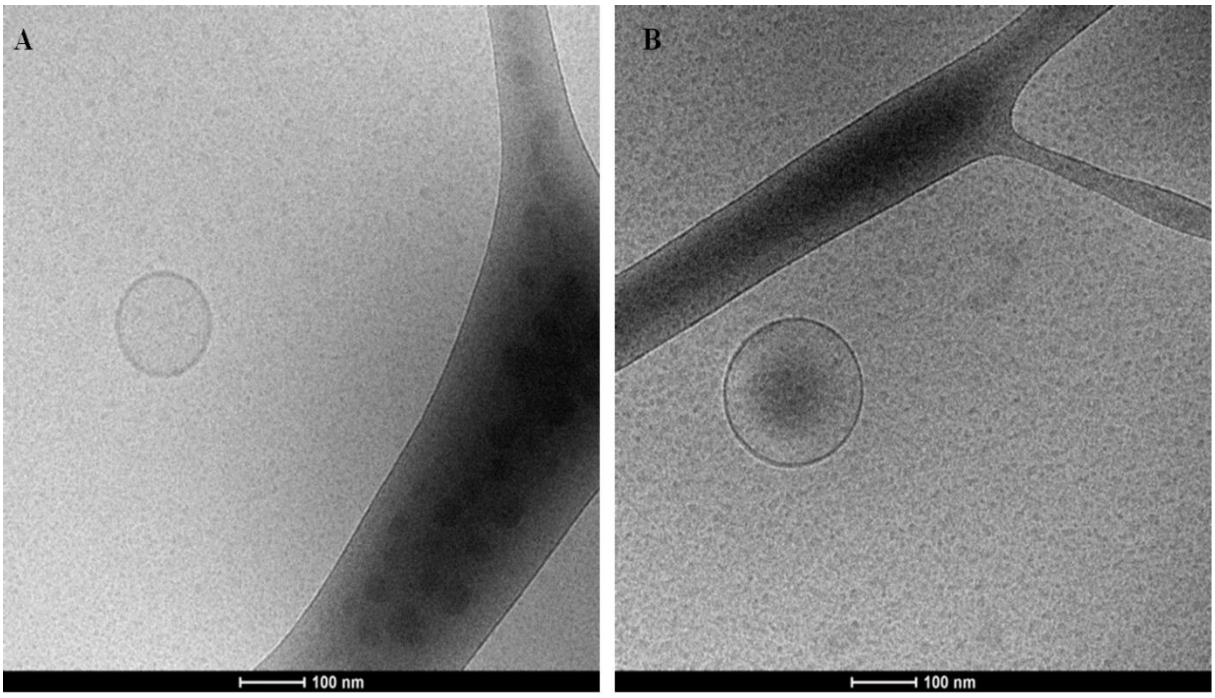

Figure 6.58 Cryo-TEM images of A) ILO niosomes and B) VDN niosomes

6.17.3 DSC study

DSC thermograms given in Figure 6.58 demonstrated that ILO, VDN, cholesterol, and Span 60 exhibited sharp melting peaks at 122.04, 200.43, 149.28 and 56.96°C. The melting points of each component was similar to reported data. In both the thermograms of ILO niosomes and VDN niosomes, there was only an endothermic peak of Span 60 at 65.65°C. This indicates that Span 60 preserved its crystal structure while forming an ordered bilayer structure of niosomes with other excipients [66]. The ILO and VDN's peak were absent in the thermogram of ILO niosomes and VDN niosomes respectively. This shows that ILO or VDN was in amorphous structure and molecularly dispersed in niosomes. Regarding the chemical structures of the materials, ILO has seven hydrogen bond acceptor count whereas VDN has five hydrogen bond donor count and ten hydrogen bond acceptor count. Hence, it is expected that the drugs will easily form hydrogen bond with Span 60. These bonds prevent transitions between the amorphous and crystal forms during storage, therefore enhancing the stability of the system [67].

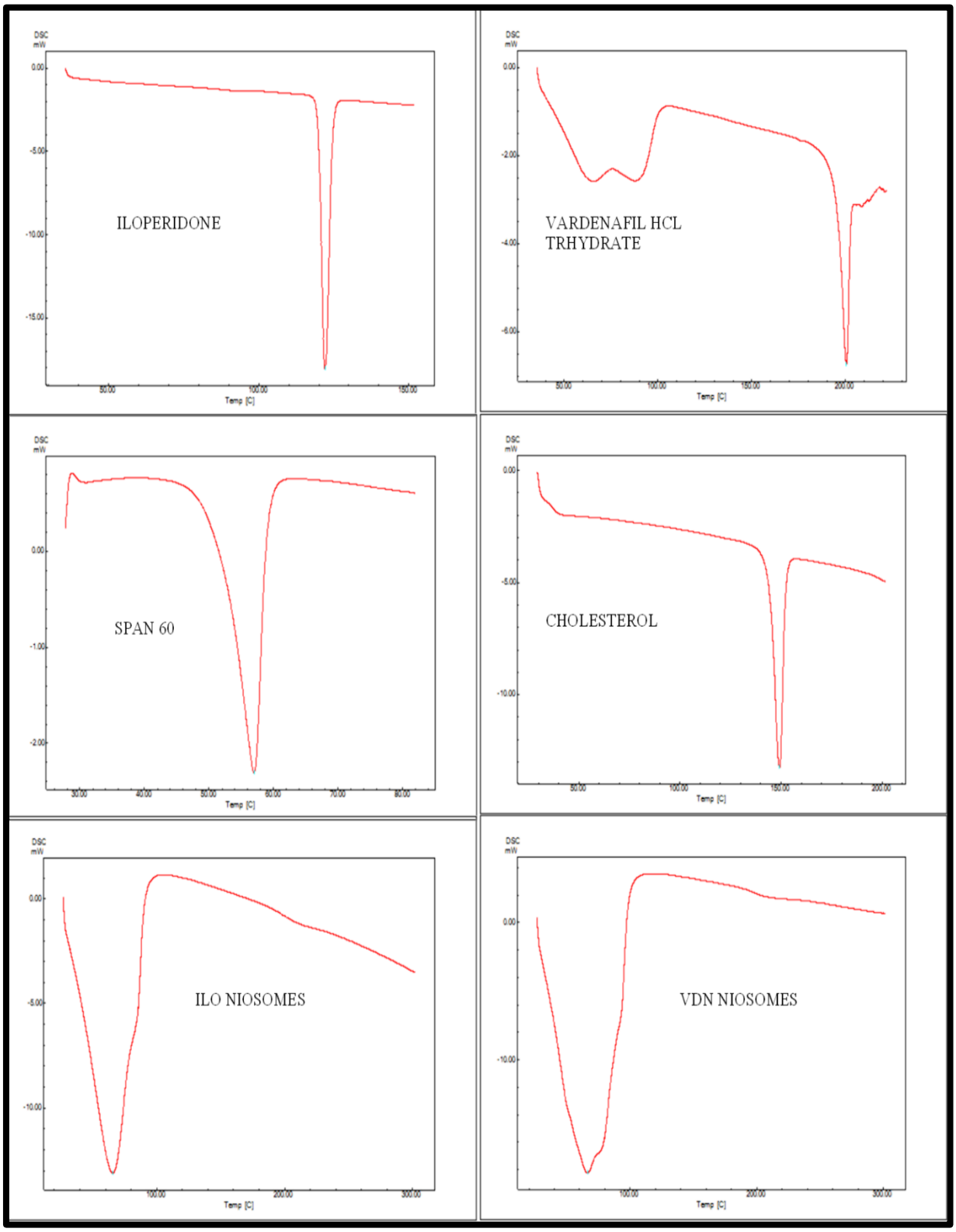

Figure 6.59 DSC study for niosomes

6.17.4 Drug Excipient Compatibility Study

FTIR of ILO, VDN and mixture of drug with excipients suggested that there was no interaction between the drug and excipients used. The FTIR characteristic peaks of ILO and VDN is shown in table 6.32. Similar peaks were obtained from FTIR scan of niosomal formulations, which confirmed the compatibility of drug with excipients in the formulation (Figure 6.59).

Table 6.34 FTIR characteristic peaks of ILO and VDN

ILOPERIDONE		VARDENAFIL	
Characteristic Peak (cm-1)	Group Present	Characteristic Peak (cm-1)	Group Present
3000 – 3100	Aromatic C-H stretch	3000 – 3100	Aromatic C-H stretch
1699	C=O stretch	1699	C=O stretch
1507	N-O stretch	1050	C=S stretch
1000 – 1320	C-O stretch	1000 – 1320	C-O stretch
1000 – 1400	C-F stretch	3300 – 3500	N-H stretch
675 – 900	C-H oop	675 – 900	C-H oop

A. ILO Drug

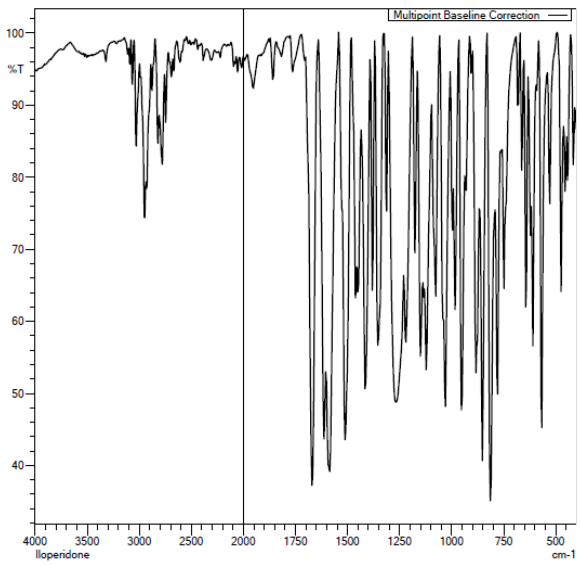

B. VDN Drug

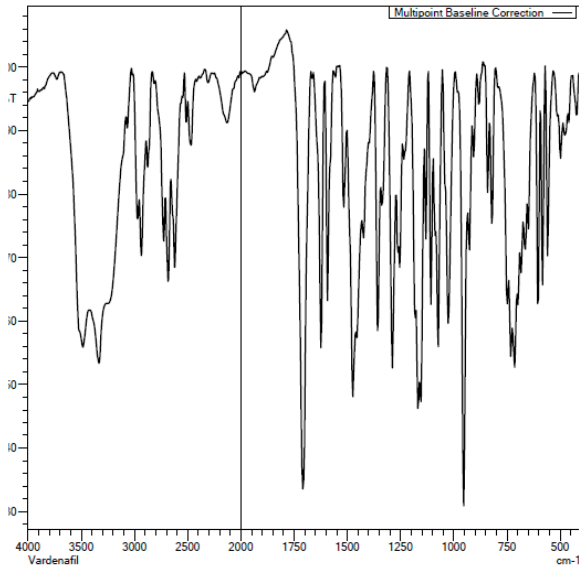

C. Cholesterol

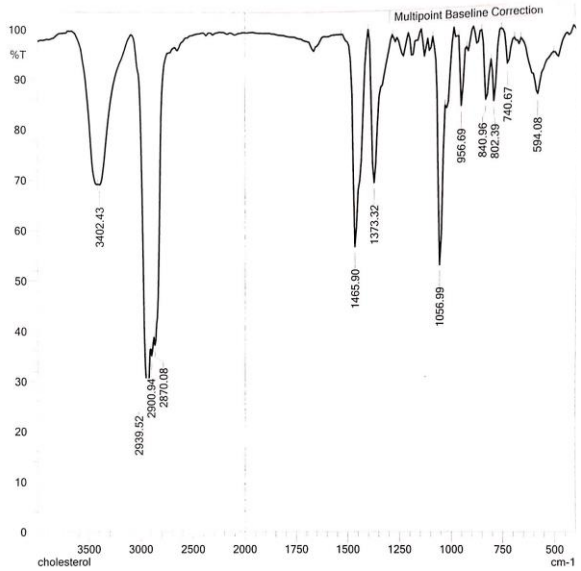

D. Span 60

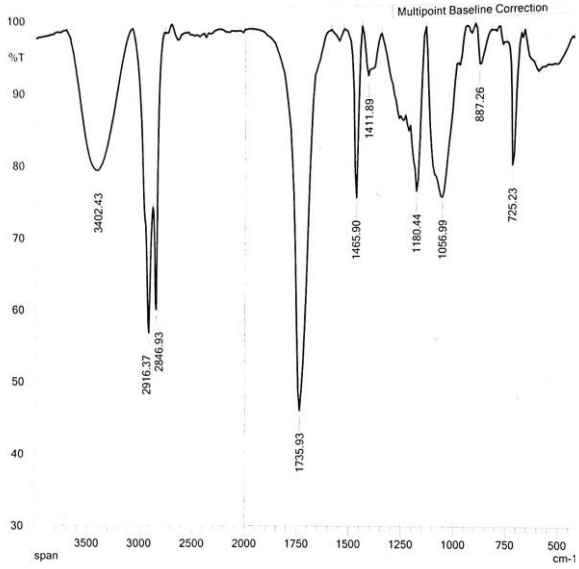

E. ILO Niosomes

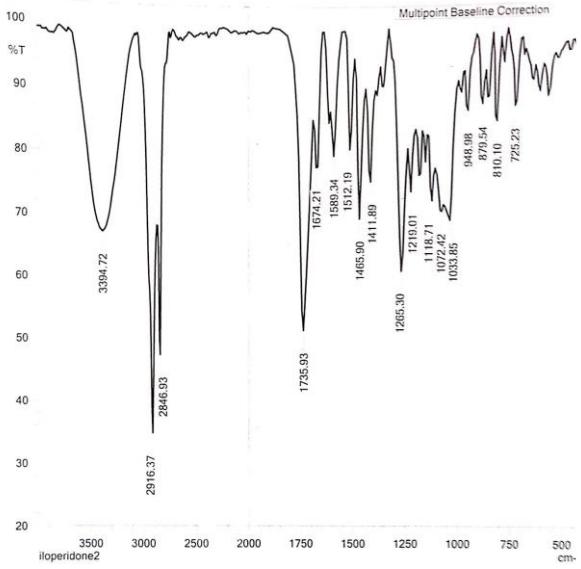

F. VDN Niosomes

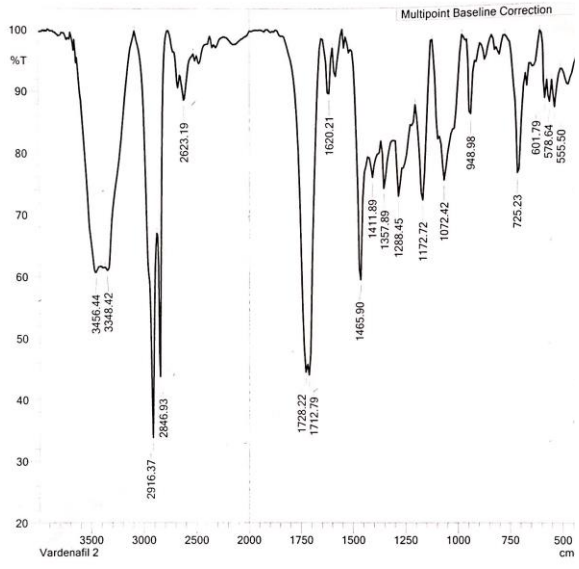

Figure 6.60 FTIR Spectra for Drug-Excipient Compatibility

6.17.5 *In vitro* Drug Release

The drug release is an important quality control tool for the dosage forms. The diffusion study of ILO and VDN from Niosomes formulations is presented in Figure 6.61.

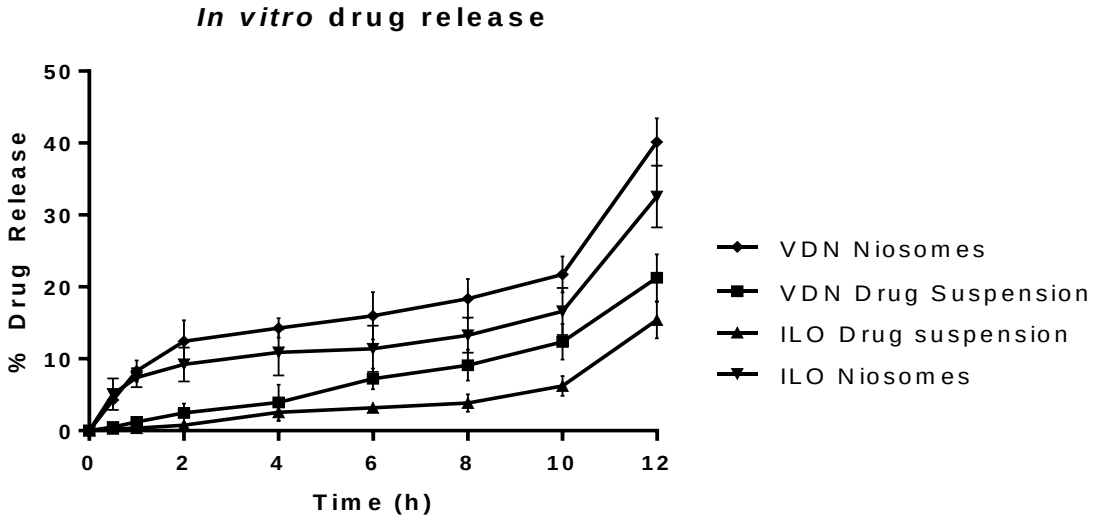

Figure 6.61 In vitro drug release of ILO and VDN Niosomes

The amount of drug released at the end of 12 h from niosomes is depicted in figure 6.61. ILO and VDN are highly lipophilic drugs and does not ionize in physiological pH range; thus, the partitioning of ILO and VDN molecules to the bilayer lipidic membranes of niosomes might have sustained release of the drug from niosomes [67]. Compared to drug suspension, the drug release from niosomes is more. This is owing to solubilization of drug in the bilayer. Increased solubility of drug led to increased diffusion rate than suspended drug.

6.17.6 *Ex vivo* Drug Release

From *ex vivo* diffusion study of the drug suspension and niosomes, it was observed that drug diffusion across the intestinal barrier from the niosomes was faster than drug suspension. Reasonably, it might be due to increased solubilization and permeation of nano-sized niosomal formulation compared to drug suspension [66]. Within 12 h, 34.15±3.29% and 38.49±4.28% drug diffused from ILO niosomes and VDN Niosomes respectively. On the other hand, only 19.06±3.59 % ILO and 21.94±4.82% VDN drug diffusion was observed from respective drug suspension (Figure 6.62). This may be due to the rate limiting step of dissolution of drug itself.

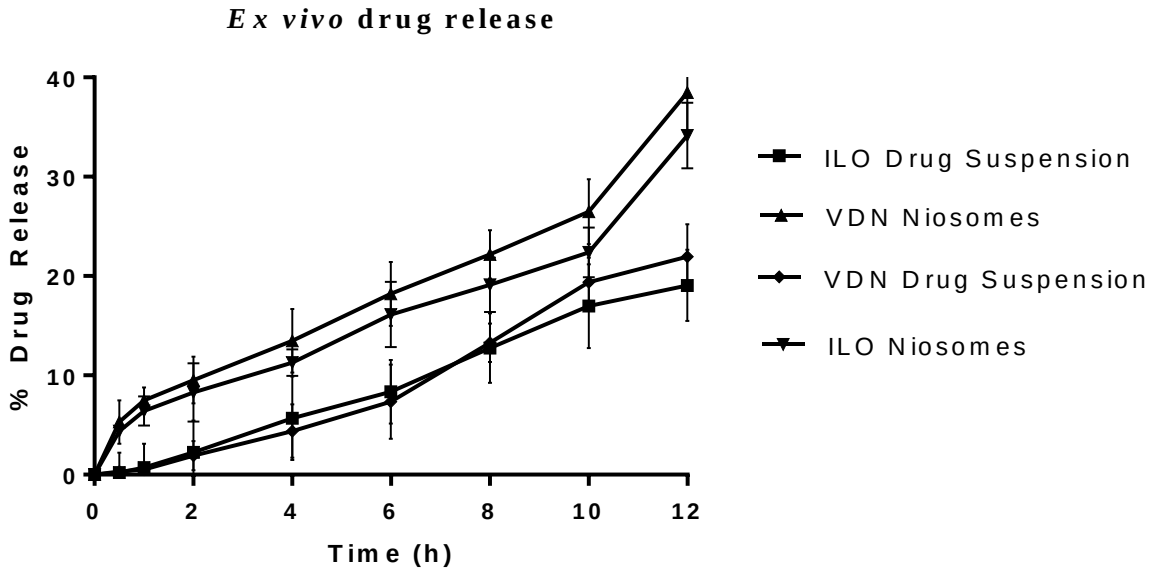

Figure 6.62 *Ex vivo* drug release of Niosomes

These results suggest that the physicochemical characteristics of the niosomes improved diffusion through the mucosa. The niosomes permeation might be associated with a non-specific diffusion process driven by a concentration gradient. Additionally, nano size of the formulation might have increased drug solubility and the permeation rate.

Enhancement ratio (Er) was found to be 1.3993 for ILO Niosomes and 1.4017 for VDN Niosomes, clearly indicated enhancement in permeation by incorporation of ILO and VDN in Niosomes, which is expected to enhance its absorption and bioavailability.

6.17.7 Stability – Niosomes

Stability study of any formulation is necessary as it reflects whether the desirable properties of the formulation are retained on storage. The desirable properties for niosomes include integrity of bilayer and size distribution of particles. Upon storage, niosomes are susceptible to many physical changes i.e. niosomes may undergo fusion and aggregation leading to increase in particle size of niosomes. Also, there may occur loss of integrity of niosomes and subsequently leakage of encapsulated drug may take place.

As per the ICH guideline Q1A (R2) and Q1C, stability studies should be performed on a drug product intended for storage at room temperature for long term and accelerated conditions.

Hence, samples of ILO SMEDDS were stored at 5±3°C and 25±2°C - 60±5% RH conditions. After the predefined time intervals of 1, 2, 3 and 6 months, niosomes samples were analyzed for physico-chemical stability. The results of the evaluations carried out are shown in table 6.35. No significant change in particle size and drug content was observed at the end of 6 months stability study.

Table 6.35 Stability study results of Niosomes

Niosomes	ILO Niosomes		VDN Niosomes	
Time (months)	Long term study (5±3°C)			
	Particle size (nm)	Drug content (%)	Particle size (nm)	Drug content (%)
Initial	112.1±7.2	98.24±3.2	124.5±3.7	97.93±2.6
1	115.3±4.7	96.37±3.6	119.2±6.6	96.47±4.3
2	127.4±7.8	97.62±4.2	125.2±4.1	96.38±2.2
3	124.3±4.7	95.86±2.6	128.9±5.4	96.24±3.5
6	125.2±6.6	95.06±1.5	134.3±3.1	95.27±5.4
	Accelerated study (25±2°C - 60±5%RH)			
1	128.3±6.2	96.12±3.6	127.2±5.4	96.35±3.7
2	132.4±4.9	95.29±5.3	134.2±6.7	97.23±2.9
3	127.3±6.7	95.04±3.4	131.9±5.3	96.45±4.4
6	136.2±7.4	95.36±2.6	139.5±6.4	95.98±3.8

6.18 References

1. Dokania, S., & Joshi, A. K. (2015). Self-microemulsifying drug delivery system (SMEDDS) – challenges and road ahead. *Drug Delivery, 22*(6), 675-690, doi:10.3109/10717544.2014.896058.
2. Mundada, V., Patel, M., & Sawant, K. (2016). Submicron Emulsions and Their Applications in Oral Delivery. *Critical Reviews™ in Therapeutic Drug Carrier Systems, 33*(3), 265-308, doi:10.1615/CritRevTherDrugCarrierSyst.2016017218.
3. Date, A. A., & Nagarsenker, M. S. (2007). Design and evaluation of self-nanoemulsifying drug delivery systems (SNEDDS) for cefpodoxime proxetil. *International Journal of Pharmaceutics, 329*(1), 166-172, doi:10.1016/j.ijpharm.2006.08.038.
4. Prajapati, S. T., Joshi, H. A., & Patel, C. N. (2013). Preparation and Characterization of Self-Microemulsifying Drug Delivery System of Olmesartan Medoxomil for Bioavailability Improvement. *Journal of Pharmaceutics*, 1-9, doi:10.1155/2013/728425.
5. Kiss, L., Walter, F. R., Bocsik, A., Veszelka, S., Ózsvári, B., Puskás, L. G., et al. Kinetic Analysis of the Toxicity of Pharmaceutical Excipients Cremophor EL and RH40 on Endothelial and Epithelial Cells. *Journal of Pharmaceutical Sciences, 102*(4), 1173-1181, doi:10.1002/jps.23458.
6. Azeem, A., Rizwan, M., Ahmad, F. J., Iqbal, Z., Khar, R. K., Aqil, M., et al. (2009). Nanoemulsion Components Screening and Selection: a Technical Note. *AAPS PharmSciTech, 10*(1), 69-76, doi:10.1208/s12249-008-9178-x.
7. Resende, K. X., Corrêa, M. A., Oliveira, A. G. d., & Scarpa, M. V. (2008). Effect of cosurfactant on the supramolecular structure and physicochemical properties of non-ionic biocompatible microemulsions. *Revista Brasileira de Ciências Farmacêuticas, 44*, 35-42.
8. Patel, K., Patil, A., Mehta, M., Gota, V., & Vavia, P. (2013). Medium Chain Triglyceride (MCT) Rich, Paclitaxel Loaded Self Nanoemulsifying Preconcentrate (PSNP): A Safe and Efficacious Alternative to Taxol®. *Journal of Biomedical Nanotechnology, 9*(12), 1996-2006, doi:10.1166/jbn.2013.1710.
9. Javed, A., Saima, A., Kanchan, K., & Showkat, M. (2013). Construction of Pseudoternary Phase Diagram and its Evaluation: Development of Self-dispersible Oral Formulation. *Interantional Journal of Drug Development and Research, 5*(2), 84-90.
10. Myers, R. H., Montgomery, D. C., & Anderson-Cook, C. M. (2016). Response surface methodology: process and product optimization using designed experiments. In (pp. 1-12). USA: John Wiley & Sons.
11. Ranjit, K. (2010). Multicollinearity: Causes, Effects and Remedies. (pp. 1-14).
12. Worldwide, M. I. (2011). Dynamic light scattering, Common terms defined. *Inform white paper. Malwern Instruments Limited*, 1-6.
13. Agatonovic-Kustrin, S., & Beresford, R. (2000). Basic concepts of artificial neural network (ANN) modeling and its application in pharmaceutical research. *Journal of pharmaceutical and biomedical analysis, 22*(5), 717-727.
14. Medarević, D. P., Kleinebudde, P., Djuriš, J., Djurić, Z., & Ibrić, S. (2016). Combined application of mixture experimental design and artificial neural networks in the solid dispersion development. *Drug development and industrial pharmacy, 42*(3), 389-402.

15. Hashad, R. A., Ishak, R. A., Fahmy, S., Mansour, S., & Geneidi, A. S. (2016). Chitosan-tripolyphosphate nanoparticles: Optimization of formulation parameters for improving process yield at a novel pH using artificial neural networks. *International journal of biological macromolecules, 86*, 50-58.
16. Alam, F. M., McNaught, K. R., & Ringrose, T. J. (2004). A comparison of experimental designs in the development of a neural network simulation metamodel. *Simulation Modelling Practice and Theory, 12*(7), 559-578.
17. Arulsudar, N., Subramanian, N., & Murthy, R. (2005). Comparison of artificial neural network and multiple linear regression in the optimization of formulation parameters of leuprolide acetate loaded liposomes. *J Pharm Pharm Sci, 8*(2), 243-258.
18. Bouanani, F., Bendedouch, D., Teixeira, J., Marx, L., & Hemery, P. (2012). Characterization of a miniemulsion by DLS and SANS. *Colloids and Surfaces A: Physicochemical and Engineering Aspects, 404*, 47-51, doi:https://doi.org/10.1016/j.colsurfa.2012.04.011.
19. Hegde, R. R., Kumar, S., Aswal, V. K., Verma, A., Bhattacharya, S. S., & Ghosh, A. (2014). Small-Angle Neutron Scattering Study of Nonionic Surfactant Micelles and Phase Transitions in w/o Microemulsion. *Journal of Dispersion Science and Technology, 35*(6), 783-788, doi:10.1080/01932691.2013.813393.
20. Shu, F., Ramakrishnan, V., & Schoenborn, B. P. (2000). Enhanced visibility of hydrogen atoms by neutron crystallography on fully deuterated myoglobin. *Proceedings of the National Academy of Sciences of the United States of America, 97*(8), 3872-3877.
21. Talmon, Y. (2007). Seeing Giant Micelles by Cryogenic-Temperature Transmission Electron Microscopy (Cryo-TEM). In R. Zana, & E. W. Kaler (Eds.), *Giant micelles: properties and applications* (Vol. 140, pp. 163-178). London: CRC Press.
22. Singh, G., & Pai, R. S. (2015). Trans-resveratrol self-nano-emulsifying drug delivery system (SNEDDS) with enhanced bioavailability potential: optimization, pharmacokinetics and in situ single pass intestinal perfusion (SPIP) studies. *Drug Delivery, 22*(4), 522-530, doi:10.3109/10717544.2014.885616.
23. Hupfeld, S., Evjen, T. J., Myhren, F., & Thøgersen, H. (2017). Liquid phospholipid-containing compositions for the preparation of pharmaceuticals. Google Patents.
24. Chhabra, R. P. (2010). Non-Newtonian fluids: an introduction. In *Rheology of complex fluids* (pp. 3-34): Springer.
25. Bandivadekar, M., Pancholi, S., Kaul-Ghanekar, R., Choudhari, A., & Koppikar, S. (2013). Single non-ionic surfactant based self-nanoemulsifying drug delivery systems: formulation, characterization, cytotoxicity and permeability enhancement study. *Drug development and industrial pharmacy, 39*(5), 696-703, doi:10.3109/03639045.2012.687745.
26. Patel, K., Sarma, V., & Vavia, P. (2013). Design and evaluation of Lumefantrine–Oleic acid self nanoemulsifying ionic complex for enhanced dissolution. *DARU Journal of Pharmaceutical Sciences, 21*(1), 1-10.
27. Avdeef, A. (2012). Transport Model. In *Absorption and drug development: solubility, permeability, and charge state* (pp. 12-30): John Wiley & Sons.
28. Kiela, P. R., & Ghishan, F. K. (2016). Physiology of Intestinal Absorption and Secretion. *Best practice & research. Clinical gastroenterology, 30*(2), 145-159, doi:10.1016/j.bpg.2016.02.007.

29. Gupta, M., Kovar, A., & Meibohm, B. (2005). The Clinical Pharmacokinetics of Phosphodiesterase-5 Inhibitors for Erectile Dysfunction. *The Journal of Clinical Pharmacology, 45*(9), 987-1003, doi:10.1177/0091270005276847.
30. Young, J. M. (2002). Vardenafil. *Expert Opinion on Investigational Drugs, 11*(10), 1487-1496, doi:10.1517/13543784.11.10.1487.
31. Negi, L. M., Tariq, M., & Talegaonkar, S. (2013). Nano scale self-emulsifying oil based carrier system for improved oral bioavailability of camptothecin derivative by P-Glycoprotein modulation. *Colloids and Surfaces B: Biointerfaces, 111*, 346-353, doi:https://doi.org/10.1016/j.colsurfb.2013.06.001.
32. Date, A. A., & Nagarsenker, M. (2007). Design and evaluation of self-nanoemulsifying drug delivery systems (SNEDDS) for cefpodoxime proxetil. *International Journal of Pharmaceutics, 329*(1), 166-172.
33. Eriksson, L., Johansson, E., & Wikström, C. (1998). Mixture design—design generation, PLS analysis, and model usage. *Chemometrics and Intelligent Laboratory Systems, 43*(1-2), 1-24.
34. Jones, B., & Goos, P. (2012). I-optimal versus D-optimal split-plot response surface designs. *Journal of Quality Technology, 44*(2), 85-101, doi:10.1080/00224065.2012.11917886.
35. Yoo, W., Mayberry, R., Bae, S., Singh, K., He, Q., & Lillard, J. W. (2014). A Study of Effects of MultiCollinearity in the Multivariable Analysis. *International journal of applied science and technology, 4*(5), 9-19.
36. Costa Nuno, R., & Lourenço, J. (2016). Multiresponse problems: desirability and other optimization approaches. *Journal of Chemometrics, 30*(12), 702-714, doi:10.1002/cem.2848.
37. Sawant, K., Pandey, A., & Patel, S. (2016). Aripiprazole loaded poly (caprolactone) nanoparticles: Optimization and in vivo pharmacokinetics. *Materials Science and Engineering: C, 66*, 230-243.
38. Zeng, L., Xin, X., & Zhang, Y. (2017). Development and characterization of promising Cremophor EL-stabilized o/w nanoemulsions containing short-chain alcohols as a cosurfactant. [10.1039/C6RA27096D]. *RSC Advances, 7*(32), 19815-19827, doi:10.1039/C6RA27096D.
39. Hodaei, D., Baradaran, B., Valizadeh, H., Mohammadnezhad, L., & Zakeri-Milani, P. (2014). The effect of tween excipients on expression and activity of P-glycoprotein in Caco-2 cells. *Pharmind (die pharmazeutische industrie), 75*, 1-12.
40. Chu, B., & Liu, T. (2000). Characterization of Nanoparticles by Scattering Techniques. *Journal of Nanoparticle Research, 2*(1), 29-41, doi:10.1023/A:1010001822699.
41. How to Determine HLB of an Emulsifier (1976). In *The HLB SYSTEM a time-saving guide to emulsifier selection* (pp. 20-21): ICI Americas Inc.
42. Matsaridou, I., Barmpalexis, P., Salis, A., & Nikolakakis, I. (2012). The Influence of Surfactant HLB and Oil/Surfactant Ratio on the Formation and Properties of Self-emulsifying Pellets and Microemulsion Reconstitution. *AAPS PharmSciTech, 13*(4), 1319-1330, doi:10.1208/s12249-012-9855-7.
43. Tran, T., Rades, T., & Müllertz, A. (2017). Formulation of self-nanoemulsifying drug delivery systems containing monoacyl phosphatidylcholine and Kolliphor® RH40

using experimental design. *Asian Journal of Pharmaceutical Sciences*, 1-10, doi:10.1016/j.ajps.2017.09.006.

44. Attwood, D., & Florence, A. (2012). Aspects of surfactant toxicity. In *Surfactant systems: their chemistry, pharmacy and biology* (pp. 614-697). USA: Springer Science & Business Media.
45. Zidan, A. S., Mokhtar Ibrahim, M., & Megrab, N. A. E. (2017). Optimization of methotrexate loaded niosomes by Box–Behnken design: an understanding of solvent effect and formulation variability. *Drug development and industrial pharmacy, 43*(9), 1450-1459, doi:10.1080/03639045.2017.1318907.
46. Kumar, G. P., & Rajeshwarrao, P. (2011). Nonionic surfactant vesicular systems for effective drug delivery—an overview. *Acta Pharmaceutica Sinica B, 1*(4), 208-219, doi:10.1016/j.apsb.2011.09.002.
47. Kazi, K. M., Mandal, A. S., Biswas, N., Guha, A., Chatterjee, S., Behera, M., et al. (2010). Niosome: A future of targeted drug delivery systems. *Journal of Advanced Pharmaceutical Technology & Research, 1*(4), 374-380, doi:10.4103/0110-5558.76435.
48. Bnyan, R., Khan, I., Ehtezazi, T., Saleem, I., Gordon, S., O'Neill, F., et al. (2018). Surfactant Effects on Lipid-Based Vesicles Properties. *Journal of Pharmaceutical Sciences, 107*(5), 1237-1246, doi:10.1016/j.xphs.2018.01.005.
49. Pandey, A. P., More, M. P., Karande, K. P., Chitalkar, R. V., Patil, P. O., & Deshmukh, P. K. (2017). Optimization of desolvation process for fabrication of lactoferrin nanoparticles using quality by design approach. *Artificial Cells, Nanomedicine, and Biotechnology, 45*(6), 1101-1114, doi:10.1080/21691401.2016.1202259.
50. Mundada, P. K., Sawant, K. K., & Mundada, V. P. (2017). Formulation and optimization of controlled release powder for reconstitution for metoprolol succinate multi unit particulate formulation using risk based QbD approach. *Journal of Drug Delivery Science and Technology, 41*, 462-474, doi:10.1016/j.jddst.2017.09.001.
51. Cullis, P. R., Fenske, D. B., & Hope, M. J. (1996). Physical properties and functional roles of lipids in membranes. *New comprehensive biochemistry, 31*, 1-33.
52. Na, J. Y., Kang, B., Sin, D. H., Cho, K., & Park, Y. D. (2015). Understanding Solidification of Polythiophene Thin Films during Spin-Coating: Effects of Spin-Coating Time and Processing Additives. *Scientific Reports, 5*, 1-14, doi:10.1038/srep13288.
53. Guidance for Industry: Q3C–Tables and List (2012). Food and Drug Administration, USA.
54. Venema, F. R., & Weringa, W. D. (1988). The interactions of phospholipid vesicles with some anti-inflammatory agents. *Journal of Colloid and Interface Science, 125*(2), 484-492, doi:10.1016/0021-9797(88)90013-6.
55. Maryana, W., Rachmawati, H., & Mudhakir, D. (2016). Formation of Phytosome Containing Silymarin Using Thin Layer-Hydration Technique Aimed for Oral Delivery. *Materials Today: Proceedings, 3*(3), 855-866, doi:10.1016/0021-9797(88)90013-6.
56. Taurozzi, J. S., Hackley, V. A., & Wiesner, M. R. (2012). Preparation of nanoparticle dispersions from powdered material using ultrasonic disruption. *NIST special publication, 1200*(2), 1200-1202, doi:10.6028/NIST.SP.1200-2.
57. Richardson, E. S., Pitt, W. G., & Woodbury, D. J. (2007). The Role of Cavitation in Liposome Formation. *Biophysical Journal, 93*(12), 4100-4107, doi:10.1529/biophysj.107.104042.

58. Raffy, S., & Teissié, J. (1999). Control of Lipid Membrane Stability by Cholesterol Content. *Biophysical Journal, 76*(4), 2072-2080, doi:10.1016/S0006-3495(99)77363-7.
59. Shaker, S., Gardouh, A. R., & Ghorab, M. M. (2017). Factors affecting liposomes particle size prepared by ethanol injection method. *Research in Pharmaceutical Sciences, 12*(5), 346-352, doi:10.4103/1735-5362.213979.
60. Gandhi, M., Misra, A., & Mashru, R. (2018). Lipoplex Delivery System for P11 Gene: A Risk Based Quality by Design Approach. *Sciol Genetic Science, 1*(1), 22-40.
61. Slater, S. J., Ho, C., Taddeo, F. J., Kelly, M. B., & Stubbs, C. D. (1993). Contribution of hydrogen bonding to lipid-lipid interactions in membranes and the role of lipid order: Effects of cholesterol, increased phospholipid unsaturation, and ethanol. *Biochemistry, 32*(14), 3714-3721, doi:10.1021/bi00065a025.
62. Joshi, G., Kumar, A., & Sawant, K. (2014). Enhanced bioavailability and intestinal uptake of Gemcitabine HCl loaded PLGA nanoparticles after oral delivery. *European Journal of Pharmaceutical Sciences, 60*, 80-89, doi:https://doi.org/10.1016/j.ejps.2014.04.014.
63. Joshi, G., Kumar, A., & Sawant, K. (2016). Bioavailability enhancement, Caco-2 cells uptake and intestinal transport of orally administered lopinavir-loaded PLGA nanoparticles. *Drug Delivery, 23*(9), 3492-3504, doi:10.1080/10717544.2016.1199605.
64. Heftberger, P., Kollmitzer, B., Heberle, F. A., Pan, J., Rappolt, M., Amenitsch, H., et al. (2014). Global small-angle X-ray scattering data analysis for multilamellar vesicles: the evolution of the scattering density profile model. *Journal of Applied Crystallography, 47*(Pt 1), 173-180, doi:10.1107/S1600576713029798.
65. Gandhi, M., Pandya, T., Gandhi, R., Patel, S., Mashru, R., Misra, A., et al. (2015). Inhalable liposomal dry powder of gemcitabine-HCl: Formulation, in vitro characterization and in vivo studies. *International Journal of Pharmaceutics, 496*(2), 886-895, doi:https://doi.org/10.1016/j.ijpharm.2015.10.020.
66. Bansal, S., Aggarwal, G., Chandel, P., & Harikumar, S. L. (2013). Design and development of cefdinir niosomes for oral delivery. *Journal of Pharmacy & Bioallied Sciences, 5*(4), 318-325, doi:10.4103/0975-7406.120080.
67. Sezgin-Bayindir, Z., & Yuksel, N. (2012). Investigation of Formulation Variables and Excipient Interaction on the Production of Niosomes. *AAPS PharmSciTech, 13*(3), 826-835, doi:10.1208/s12249-012-9805-4.